NPS-ME-96-002

NAVAL POSTGRADUATE SCHOOL
Monterey, California

**Simplified Finite Element Modeling of Stiffened
Cylinders Subjected to Underwater Explosion**

by

Richard E. Cunningham
Young W. Kwon

February 1996

DTIC QUALITY INSPECTED 4

Approved for public release; distribution is unlimited.

Prepared for: Naval Surface Warfare Center
Protection & Weapons Effects Department
Code 67
Carderock Division
Bethesda, MD 20084

NAVAL POSTGRADUATE SCHOOL
Monterey, California 93943

Rear Admiral Marsha J. Evans
Superintendent

This report was prepared for and fully funded by both the Naval Surface Warfare Center, Bethesda, MD 20084 and the Naval Postgraduate School, Monterey, Ca 93943.

This report was prrepared by:

R.E. Cunningham
LT, USN

Y.W. Kwon
Associate professor of Mechanical Engineering

Reviewed by:

T.R. McNelley
Chairman
Dept. of Mechanical Eng.

Released by:

G.E. Schacher
Dean of Research (Acting)

REPORT DOCUMENTATION PAGE		Form Approved OMB No. 0704-0188

Public reporting burden for this collection of information is estimated to average 1 hour per response, including the time for reviewing instruction, searching existing data sources, gathering and maintaining the data needed, and completing and reviewing the collection of information. Send comments regarding this burden estimate or any other aspect of this collection of information, including suggestions for reducing this burden, to Washington Headquarters Services, Directorate for Information Operations and Reports, 1215 Jefferson Davis Highway, Suite 1204, Arlington, VA 22202-4302, and to the Office of Management and Budget, Paperwork Reduction Project (0704-0188) Washington DC 20503.

1. AGENCY USE ONLY *(Leave blank)*	2. REPORT DATE February 29, 1996	3. REPORT TYPE AND DATES COVERED Progress Report from May 1, 1995 to February 29, 1996
4. TITLE AND SUBTITLE SIMPLIFIED FINITE ELEMENT MODELING OF STIFFENED CYLINDERS SUBJECTED TO UNDERWATER EXPLOSION		5. FUNDING NUMBERS
6. AUTHOR(S): Cunningham, Richard E. , and Kwon, Young W.		
7. PERFORMING ORGANIZATION NAME(S) AND ADDRESS(ES) Naval Postgraduate School Monterey, CA 93943-5000		8. PERFORMING ORGANIZATION REPORT NUMBER NPS-ME-96-002
9. SPONSORING/MONITORING AGENCY NAME(S) AND ADDRESS(ES) Protection & Weapons Effects Department, Code 67 Carderock Division Naval Surface Warfare Center Bethesda, MD 20084		10. SPONSORING/MONITORING AGENCY REPORT NUMBER
11. SUPPLEMENTARY NOTES The views expressed in this report are those of the authors and do not reflect the official policy or position of the Department of Defense or the U.S. Government.		
12a. DISTRIBUTION/AVAILABILITY STATEMENT Approved for public release; distribution is unlimited.		12b. DISTRIBUTION CODE

13. ABSTRACT *(maximum 200 words)*

Simplified finite element modeling of a stiffened cylinder subjected to underwater explosion was investigated. The use of smearing the stiffeners onto the base structure as well as beam modeling using SOR (Surface of Revolution) beam elements were used in the simplification process. The dynamic response and overall global deformation were then compared between the fully discretized stiffened cylinder model and simplified models. The study first examined the effectiveness of smearing stiffeners onto a flat plate. The smearing of stiffeners onto a cylindrical shell orthotropically was then examined. Next, beam modeling of both unstiffened and stiffened cylinders was investigated. Finally, an integrated beam/shell model of a stiffened cylinder was developed. These models were subjected to the same underwater explosive loading for numerical study. The analysis showed that when comparing the dynamic responses caused by underwater explosions between the discrete model, the beam model, and the beam/shell model of a stiffened or unstiffened cylinder, globally similar results could be produced.

14. SUBJECT TERMS Underwater Explosion, Finite Element Method, Smearing Technique	15. NUMBER OF PAGES 117
	16. PRICE CODE

17. SECURITY CLASSIFI-CATION OF REPORT Unclassified	18. SECURITY CLASSIFI-CATION OF THIS PAGE Unclassified	19. SECURITY CLASSIFICA-TION OF ABSTRACT Unclassified	20. LIMITATION OF ABSTRACT UL

NSN 7540-01-280-5500

Standard Form 298 (Rev. 2-89)
Prescribed by ANSI Std. 239-18 298-102

i

ii

ABSTRACT

Simplified finite element modeling of a stiffened cylinder subjected to underwater explosion was investigated. The use of smearing the stiffeners onto the base structure as well as beam modeling using SOR (Surface of Revolution) beam elements were used in the model simplification process. The dynamic response and overall global deformation were then compared between the fully discretized stiffened cylinder model and the simplified models. The study first examined the effectiveness of smearing stiffeners onto a flat plate. The smearing of stiffeners onto a cylindrical shell orthotropically was then examined. Next, beam modeling of both unstiffened and stiffened cylinders was investigated. Finally an integrated beam/shell model of a stiffened cylinder was developed. These models were subjected to the same underwater explosive loading for numerical study. The analysis showed that when comparing the dynamic responses caused by underwater explosions between the discrete model, the beam model, and the beam/shell model of a stiffened cylinder, globally similar results could be produced.

TABLE OF CONTENTS

ACKNOWLEDGEMENTS

I. INTRODUCTION

Detailed finite element modeling of a submerged structure including internal structures subjected to underwater explosion is costly. The cost can be equated in both computational time and more importantly manpower. As a result, a simple, but still accurate model of a structure was investigated. The objective of the study was to develop an efficient means of representing the stiffened cylinder while still providing accurate dynamic response predictions to underwater explosion. Past work at the Naval Postgraduate School focused on comparison of numerical modeling to the physical testing. Cylindrical models have been previously subjected to various types of underwater explosions and their results have been closely approximated by the computer code. Fox, Kwon, and Shin [Ref. 1] and Chisum [Ref. 2] have all demonstrated that the finite element and boundary element programs closely approximate experimental results. Their research work clearly indicates that limited numerical modeling can be conducted without the need to physically build the actual structure for experimental testing.

The studies [Ref. 1, 2] did not explore modeling cylindrical shells with internal structures. This type of modeling involves adding internal equipment and structures to the outer shell, which dramatically increases the degrees of freedom of the problem. This directly correlates to a long computational time for solutions. This study will examine two means by which a simplified model and discrete model can be numerically tested to produce similar dynamic responses due to an underwater explosion. The first technique models the stiffened cylinder with SOR(Surface of Revolution) beam elements and the

1

second technique involves smearing the stiffeners onto the cylindrical shell structure.

Using a material smearing technique is prevalent in composites where smearing material properties reduces the complexity of the structure when subjected to various forms of loading. Raftenberg [Ref. 3] demonstrated that smearing in structures required that the structure be entirely axiymetric or have regions which varied circumferentially about its axis of symmetry with rapid periodicity. The smearing technique was used for static loading only. Pitarresi, Caletka, Caldwell , and Smith used a similar finite element material-smearing technique to dynamically test a printed circuit board with favorable results [Ref. 4]. Both studies dramatically reduced both complexity and computational time with their simplification methods.

The finite element and boundary element programs utilized for providing the numerical analysis for this study are called USA/DYNA3D. VEC/DYNA3D is a finite element analysis code developed by Lawrence Livermore National Laboratory [Ref. 5]. The Underwater Shock Analysis, USA [Ref. 6] is a boundary element code that is based on the Doubly Asymptotic Approximation (DAA) which was developed by Geers [Ref. 7]. The linkage between the two codes was developed in 1991 and has provided acceptable results of dynamic responses of cylindrical shells.

One of the applications of the USA code developed by Deruntz [Ref. 6] allows the beam to be modeled with SOR (Surface of Revolution) elements. The SOR element approximates a beam element with a surface of revolution element. The SOR element contains a number of sub-elements around the circumference of each surface of revolution element. The SOR branch interpolates sub-elements using a circumferential harmonic

function which ultimately reduces the number of surface of revolution degrees of freedom.

The original discrete model of the cylinder analyzed in this study was provided by Protection & Weapons Effects Department, Code 67 Carderock Division of the Naval Surface Warfare Center and is provided in Figure 1. This cylinder is called the ONR cylinder and is a test vehicle which is currently being planned for a series of underwater explosions. This study will first examine the effects of smearing stiffeners onto a flat plate. Next, the discrete model will be modeled without internal stiffeners with Belytschko-Lin-Tsay 4 node shell elements due to its computational efficiency in DYNA3D program. The unstiffened model will be modeled as a beam with SOR elements and an integrated beam(SOR)/shell model will be developed. All three models will be subjected to simulated underwater explosions and their responses will be analyzed and discussed.

The discrete model with internal stiffeners will then be modeled. Based on the study of smearing stiffeners onto a flat plate, the ONR stiffeners are smeared onto the shell of the cylinder orthotropically. Beam model with SOR elements will be developed as well as integrated beam/shell model. The internal stiffeners will be incorporated into beam model by adjusting section properties of beam. The discrete and two simplified models will be numerically analyzed by applying the explosive charge first at the symmetric point of all three models. Detailed analysis will be provided at beam/shell interface as well as endplates and deep frame stiffeners to compare discrete model to simplified models. The three models will then be exposed to an off-center charge and analysis will be performed as previously noted.
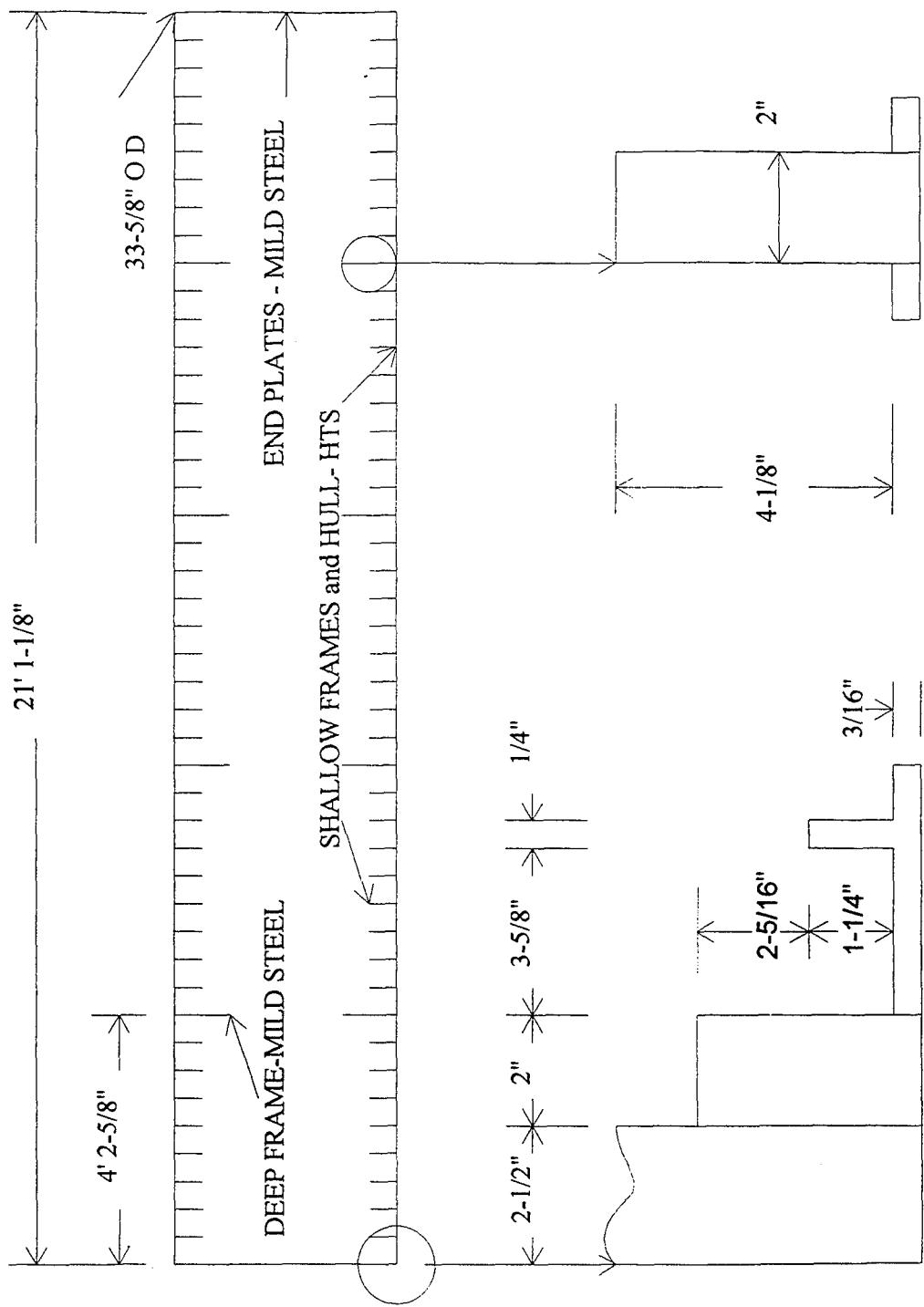
**Figure 1. Naval Warfare Surface Center's ONR Cylinder**

II. UNDERWATER EXPLOSION CHARACTERISTICS

The underwater explosion testing that is performed by USA computer code provides the user many options. For this study, however, the same options and explosion characteristics were used so that an accurate comparison between the discrete or full model and simplified models could be made. All models developed in this study were subjected to an underwater shock wave modeled as a spherical wave with a peak amplitude of 2585 psi and a decay constant of 0.3493 msec. This approximation to the actual shock wave uses an exponential pressure relationship and is good for pressure greater than about 1/3 of the peak value [Ref. 8]. This peak pressure pulse is generated using 60 lbs charge of HBX-1 explosive at a 10 foot depth and a standoff distance of 27.2 feet. The attack geometry is provided in Figure 2. The pressure profile is provided in Figure 3 for a reference.

The 10 foot underwater depth was selected in order to fall within the gas bubble radius of 15.8 feet. This allows the gas bubble to vent to the surface and not migrate to the surface of the cylindrical surface. If the bubble were not to vent to the surface then a significant amount of explosive energy would be subjected to the structure(approximately 47%) [Ref. 8]. This was done in order to eliminate the effects of bubble pulse on the simulations perfomed in this study. Free surface effects were also ignored in this study.
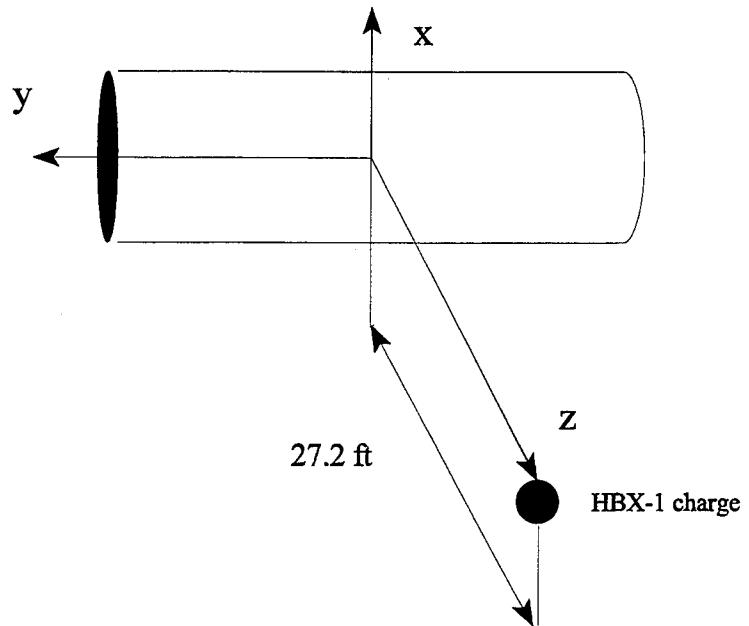
Figure 2. Attack Geometry
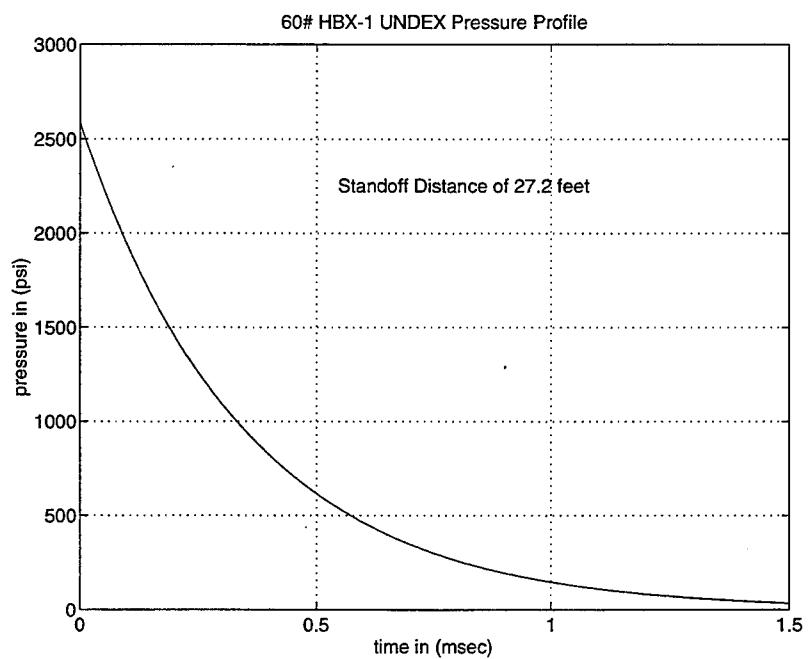
Figure 3. Pressure Profile for HBX-1 60 Pound Charge

6

III. FLAT PLATE SMEARING

The first area of model simplification that was studied involved examining the effects of smearing stiffeners onto a flat plate. The aim of the study was to find an optimal way to smear the stiffeners without affecting the global dynamic response of the flat plate. From this study, the objective was to use these results for finding an efficient means of smearing the stiffeners onto the cylindrical shell.

The plates used in this study were either clamped or simply supported at the edges and were subjected to a unit step pressure load of 1000psi. All plates examined were 88" x 88" with a stiffener spacing of 4 inches. The stiffeners are 1.25" thick and 0.25" wide and were modeled in both directions. A comparison between the discrete and smeared models was accomplished using VEC/DYNA3D finite element programs. The discrete model had the stiffeners fully modeled to the base plate whereas the smeared model had the stiffeners smeared onto the base plate. The smeared value was simply an adjustment in the material property of the base material. The adjustment is mad within the material definition portion of INGRID. The smeared value was obtained using a well known formula derived from Timoshenko and Woinowsky-Kreiger [Ref. 9]:

$$E' = E + \frac{12\ EI_s\ (1-v^2)}{ah^3}$$

where

E'= fictitious smeared elastic modulus
E = elastic modulus of plate and stiffener
I_s = moment of inertia of the stiffener
a = spacing between two stiffeners
h = thickness of the plate
v = Poison's ratio

The density of the base material was also adjusted to take into account the mass of the stiffeners.

The discrete model of a 0.1875" thick plate with clamped edges was generated and subjected to the unit step pressure loading. Figure 4 is the dynamic response of the discrete model at 0.5 msec. The transverse deformation plot is magnified by a scale factor of 10 for clearer visualization of the deformation. Next the smeared value was computed for a 0.1875 " thick plate with the given parameters for the stiffeners. The smeared model was subjected to the same pressure loading and Figure 5 shows the deformation of the smeared model. The fictitious smearing value was approximately 85 times larger than the original material's elastic modulus (E'≅ 85*E).

This modeling shows the case where the stiffeners dominated the overall response of the original structure. Notice that when comparing the two results, it was observed that the discrete model had a much larger deformation gradient near edges of the plate. The area near the edges of the discrete model governs the global deformation of the structure and for discussion purposes will be called the critically deformed area. The glaring difference in global deformation between the discrete and smeared models can be accounted for by the low stiffness of the discrete model base plate. In other words, the original discrete model has 1/85 of the globally smeared model's stiffness in the base plate. As a result, stiffeners in the

8
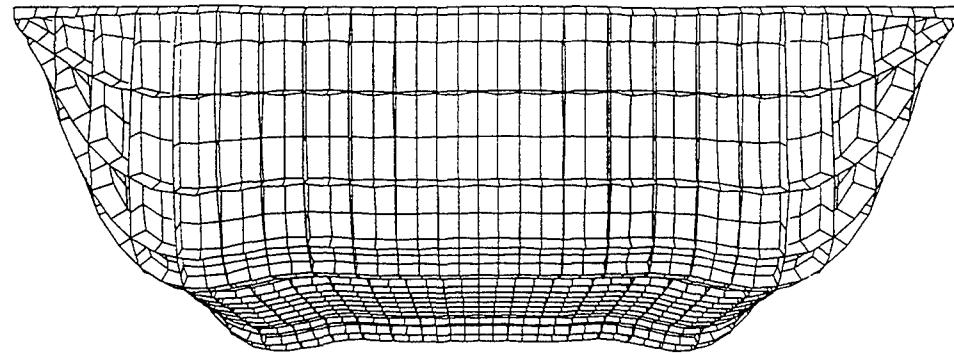
Figure 4. Global Deformation Plot of Discrete Model of 0.1875" Plate With Clamped Edges, Magnified by a factor of 10, taken at 0.5msec
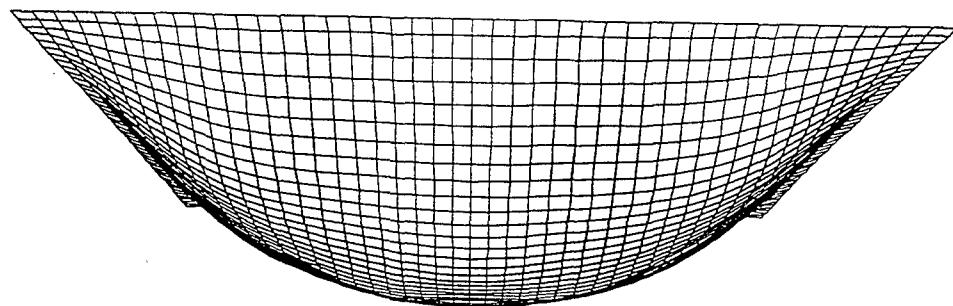

Figure 5. Globally Smeared Model of 0.1875" Plate With Clamped Edges Magnified by a factor of 10, taken at 0.5msec

9

mid-section of the discrete model's base plate are less constrained from the side edge constraints. This produces a very large gradient near the edges of the base plate and a minimum gradient at the mid-section of the plate. The contrapositive of this analysis is that the smeared plate is uniformly constrained in both directions therefore the globally smeared plate has a uniform deformation gradient over the entire plate.

The most effective way of simplifying the discrete model and obtaining the proper deformation gradient at the critically deformed area is to smear locally. That is, leave the discrete stiffeners modeled around the edges of the plate in the critically deformed area, however locally smear the remaining stiffeners onto the base plate as in the globally smeared model using the same smearing value as in the globally smeared model. Figure 6 shows the dynamic response of the locally smeared versus the discrete model. The local smearing did not affect the critically deformed area. As a result the dynamic response of the locally smeared plate was in excellent agreement with the discrete model.

A second study of the same stiffened plate was undertaken using simply supported boundary conditions at the plate edges. The dynamic responses produced similar results to what was observed for the clamped plate modeling. The simply supported 0.1875" thick plate models (discrete and globally smeared) are provided in Figure 7. The responses completed supported the analysis of the clamped plate.

Next, a study was conducted to analyze the case where the ratio of fictitious elastic modulus to original elastic modulus is lowered. By increasing the plate thickness to 1", the ratio was reduced to 2 ($E \cong 2E$). This time, the results were expected to show excellent agreement between the discrete and globally smeared models due to the increased stiffness

10
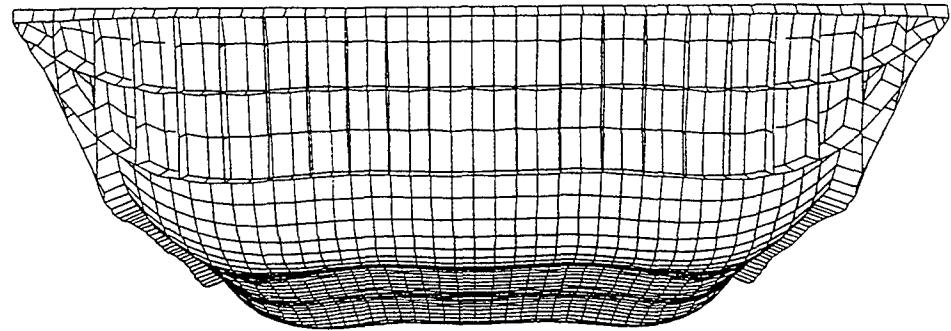
6a) Locally Smeared Model
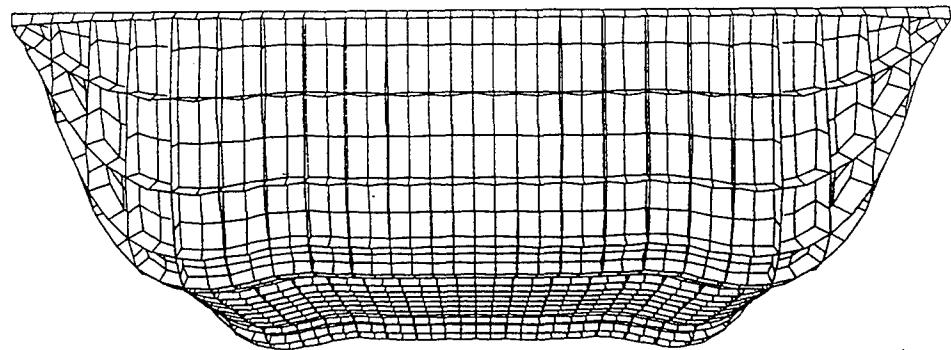
6b) Discrete Model

Figure 6a,b. Comparison of Locally Smeared model of 0.1875" Plate versus Discrete Model of 0.1875" Plate. Both With Clamped Edges and with magnification factor of 10, taken at 0.5 msec

11
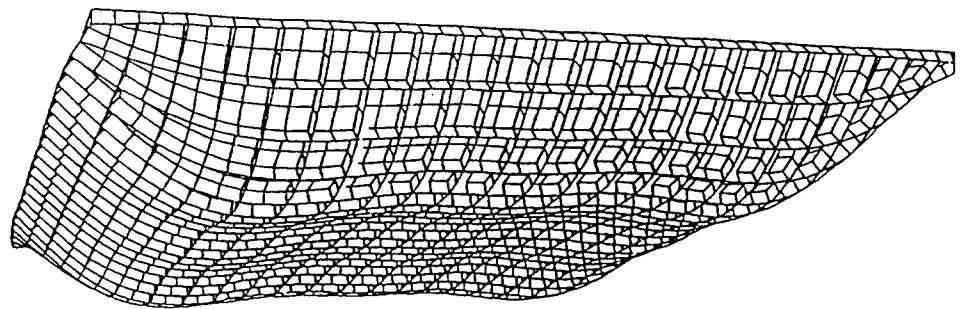
(a) Discrete Model with Simply Supported Edges
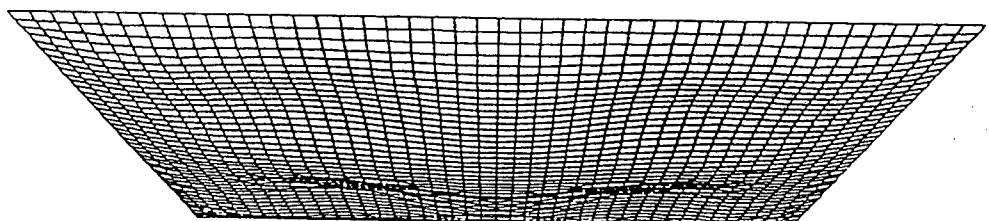
(b) Globally Smeared Model

Figure 7.   0.1875" Plates With Simply Supported Edges: (a) Discrete Model (b) Globally Smeared Model. Both with 10X magnification , at 0.5 msec

in the base plate.   Again the discrete model was generated and subjected to the same unit step pressure loading. Figure 8 shows the result of the 1" discrete plate model versus the globally smeared model with both models having clamped edges. Figure 9 compares both discrete and globally smeared 1" plates with simply supported edges.   As predicted the responses were very close to each other for both sets of boundary conditions.

Based on the study conducted on smearing flat plates, the smearing technique directly supported the well known and established formula derived in Ref. 9. The present study provided an additional criteria for determining the proper approach to smearing stiffeners onto a base structure based on the original plate's thickness and elastic modulus. If the ratio between fictitious elastic modulus and original elastic modulus is too high erroneous solutions will be obtained if global smearing is undertaken. If the ratio is small, then global smearing is an effective means for simplifying the structure.
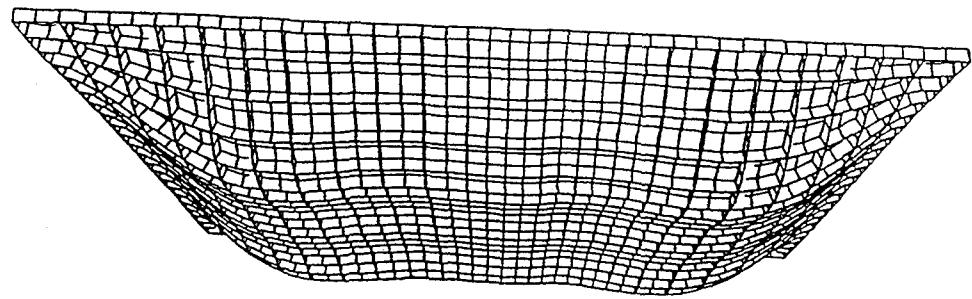
(a) 1" Discrete Model With Clamped Edges
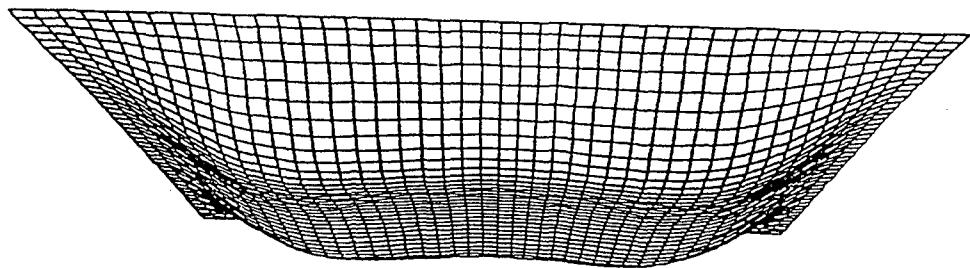
(b) Globally Smeared 1" Plate Model

Figure 8. 1" Plates With Clamped Edges: (a) Discrete Model (b) Globally Smeared Model. Both with 10X magnification factor and taken at 0.5msec.

14
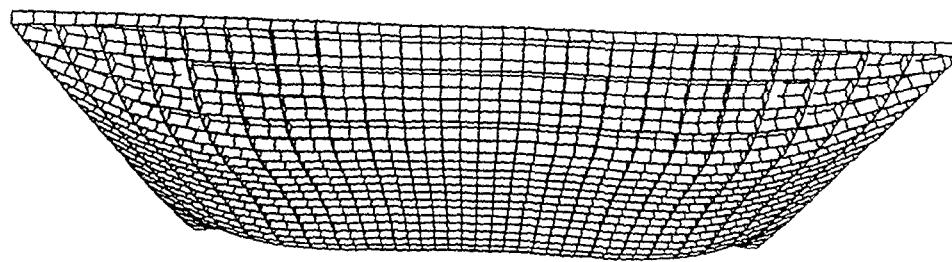
(a) Discrete Model With Simply Supported Edges
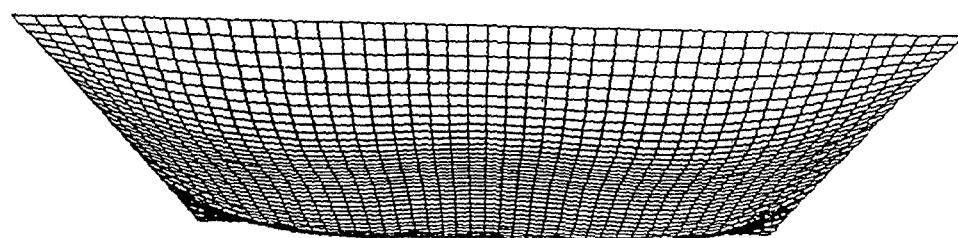

(b) Globally Smeared Model

Figure 9. 1" Plates With simply Supported Edges: (a) Discrete Model (b)Globally Smeared Model. Both at 10X magnification factor and at time 0.5 msec

15

IV. MODELING OF UNSTIFFENED ONR CYLINDER

When first considering the task of simplifying a stiffened cylinder, a detailed study was undertaken to investigate simplification techniques in general. Two techniques were investigated in order to model onto the external shell the internal structures such as stiffeners. The technique previously investigated studied smearing the stiffeners onto the base structure. This knowledge will be used when investigating orthotropically smearing the stiffeners onto the cylindrical shell later in this report. The second simplification technique involves using SOR elements to effectively model the cylindrical shell and internal structures. This section of the work details how to model an unstiffened cylinder with SOR elements. The SOR beam model will be developed and compared to the unstiffened shell. Finally, an integrated SOR beam/shell model of the unstiffened cylinder will be generated and all three models will be subjected to the same explosive testing.

A. DISCRETE UNSTIFFENED ONR CYLINDER MODEL

The three-dimensional model is shown in Figure 10. Its dimensions conform to those depicted on Figure 1 except for no internal stiffeners. This particular model uses HY-100 steel for the shell and mild steel for the endplates. Both materials for modeling purposes were considered an isotropic elastic material. Material properties used for this model are provided in Table 1.

		Mild Steel	HY-100
Density	(lbm/ft^3)	490.0	490.0
Poisson's Ratio		0.3	0.3
Yield Strength	(ksi)	32.0	108.0
Young's Modulus	(psi)	2.9x10^7	2.9x10^7
Tangential Hardening Modulus	(psi)	5.1x10^4	5.02x10^4

**Table 1. Material Properties for ONR Cylinder**
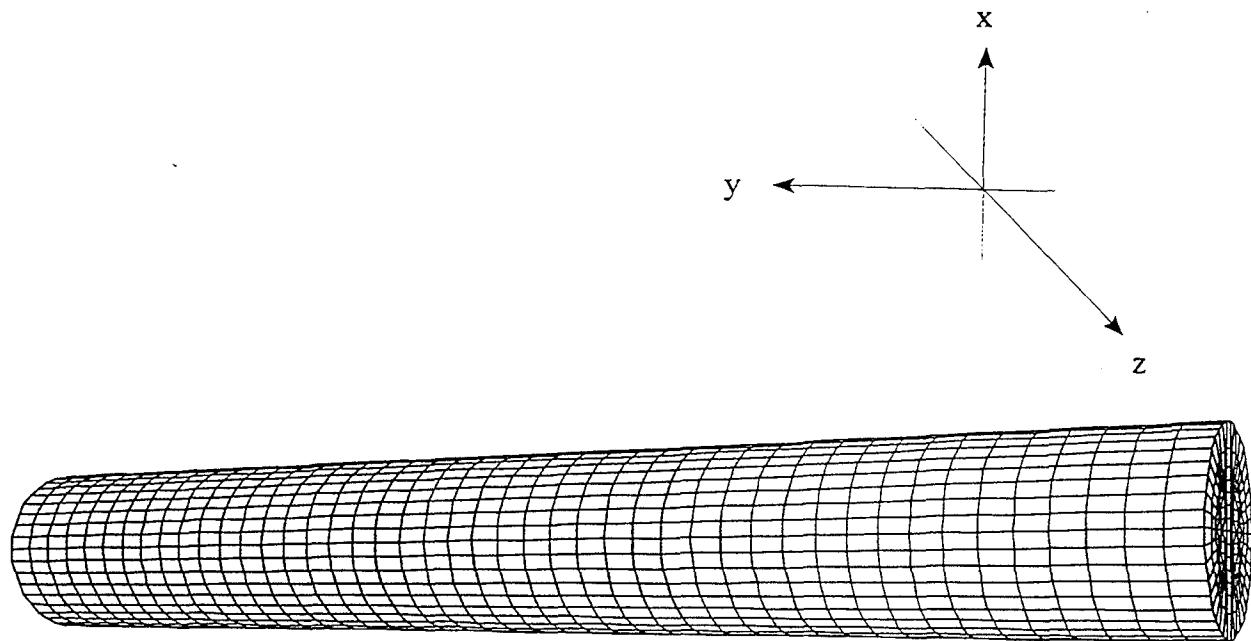
Figure 10. ONR Cylinder Modeled Without Internal Stiffeners

Although the model shown is a full model, a half model of the cylinder was used in the numerical analysis to take advantage of symmetry condition. The yz-plane was the symmetric plane from Figure 10. Even with a half cylinder model, there are 20 elements around the half circumference and 45 elements in the axial direction with an element length of 5.625 inches. The element length represents the spacing between the shallow frame stiffeners.

The discrete model was subjected to an underwater shock with USA/DYNA3D programs with shot geometry shown on Figure 2. The major response of the cylinder to the shock is in the yz-plane. Since there was a boundary condition imposed on yz-plane, there is no global motion in the x-axis. As a result, only global deformation responses in the z-direction are compared in Figure 11 at discrete states of time. The plots are magnified by a factor of 50 for improved visual ease. At early time, the deformation appears symmetric except for slight pinching near endplates. The endplates behave similarly to the clamped edges on the flat plates in that a large deformation gradient forms around each endplate.

Another way to analyze the dynamic response is to plot the displacement, velocity and acceleration at desired points on the cylinder. A comparison of the axial displacement, velocity and acceleration will indicate the cylinder's accordion motion. Plots in the z-direction indicate the whipping motion of the cylinder. These time history plots will be presented later in this chapter to compare the discrete model's response to the simplified model's dynamic response.
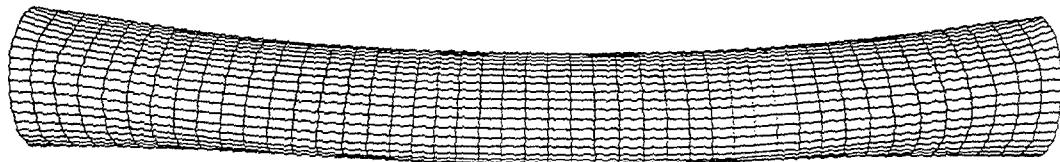
11a) State time of 0.5 msec
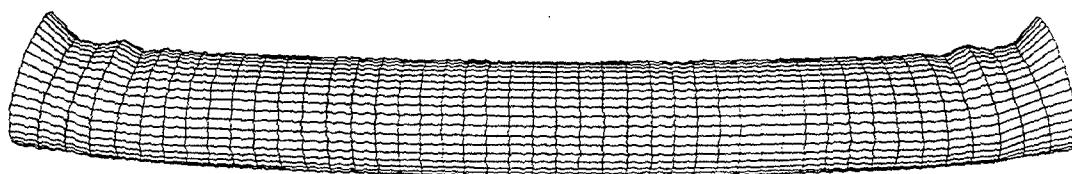
11b) State time of 1.0 *msec*
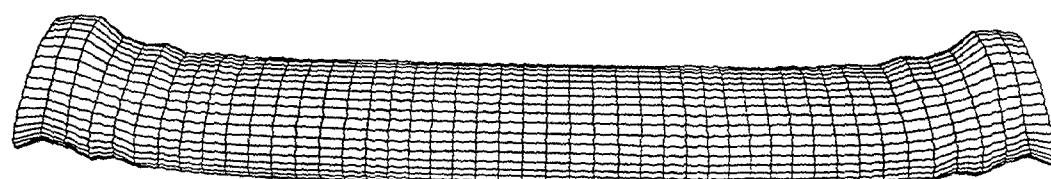
11c) State time of 1.5 msec

Figure 11a,b,c. Deformation Results of Unstiffened ONR Cylinder Model
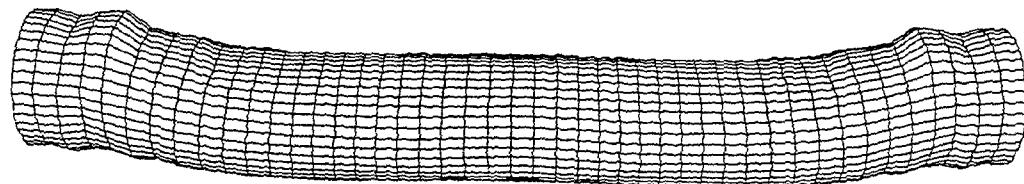
11d) State time of 2.0 msec
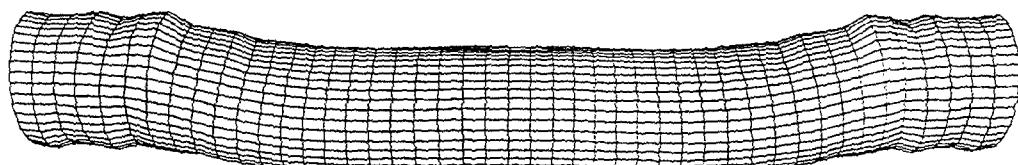
11e) State time of 2.5 msec
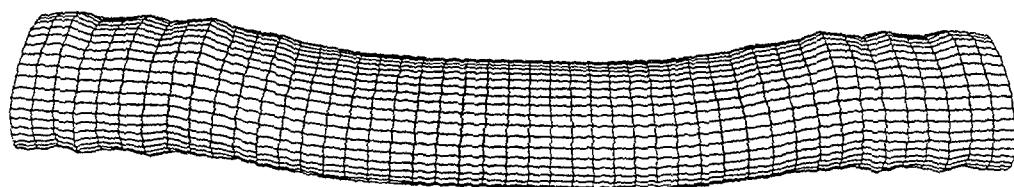
11f) State time of 3.0 msec

Figure 11d,e,f.   Deformation Results For Unstiffened ONR Cylinder Model (cont.)

21

B.   SOR BEAM MODEL

The SOR beam element formulation is based on approximating the shell's curvature with surfaces of revolution. This type of approximation has extensive applications for modeling containers, tanks, domes and has been done for a long period of time [Ref. 9]. A small displacement of a point on the surface of revolution can be resolved into two components. One of the components is in the direction tangent to the curvature of the surface about its SOR axis. The other component is in the direction of the normal to the beam surface. The displacement about the surfaces of revolution are estimated by applying a sine and cosine harmonic function for approximating the response on the surfaces of revolution. The harmonic function is then incorporated into the double asymptotic approximation procedure for estimating the fluid structure interaction in an infinite medium. As previously noted, Deruntz [Ref. 6] developed an application to USA codes that assigns a harmonic function to each of the SOR elements or branches. The harmonic function will describe the SOR fluid degrees of freedom and more closely predict the responses to the underwater explosive testing. During this study, the beam was modeled with separate sine and cosine functions, however it was proven that a more accurate numerical result was obtained when both sine and cosine function was used for modeling the beam with SOR elements. The net result was that the unstiffened and stiffened cylinder could be effectively modeled as a beam using the SOR element technique.

The SOR beam model was modeled with the same number of finite elements (45) that was used to model the discrete cylinder along its axis. The model is shown in Figure 12 and was subjected to explosive testing. The beam had the same material properties as the

22

cylinder's shell and its cross-sectional area and moments of inertia were computed using the cylinder's dimensions. That is, the cross-section area of the SOR beam is

$$A = \frac{\pi}{4}(d_o^2 - d_i^2)$$

where d_o and d_i are the outside and inside diameters, respectively. Similarly the second moment of inertia and polar moment of inertia of the cross-section are

$$I = \frac{\pi}{64}(d_o^4 - d_i^4)$$

and

$$J = \frac{\pi}{32}(d_o^4 - d_i^4)$$
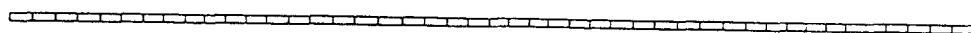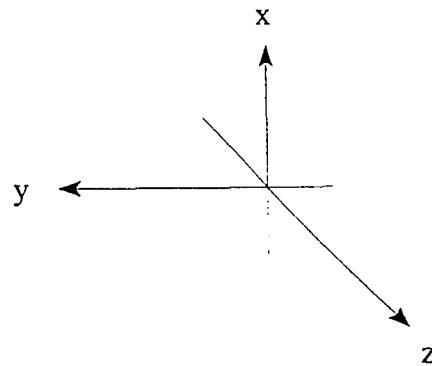
Figure 12. SOR Beam Model With 45 Elements

The global deformation of the beam model was plotted for state times 0.5 msec to 3.0 msec and is shown in Figure 13. The plots are magnified by a factor of 50 for enhanced visual recognition. There is an appearance of some crumpling or wrinkling at a few peaks with an increase in time. The deformation gradient at the ends are not as distinct as with the cylinder, however the overall shape and curvature is in excellent agreement with the discrete model. The displacement, velocity, and acceleration time histories were also generated and will be discussed later in the chapter.
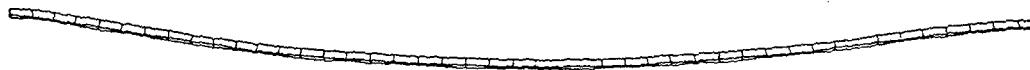
13a) State time of 0.5 msec
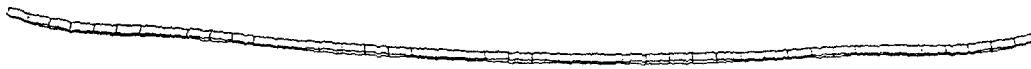
13b) State time of 1.0 msec
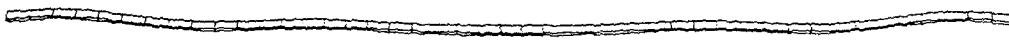
13c) State time of 1.5 msec
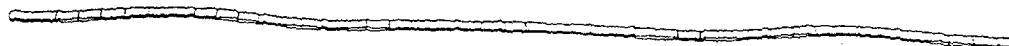
13d) State time of 2.0 msec
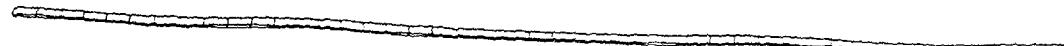
13e) State time of 2.5 msec
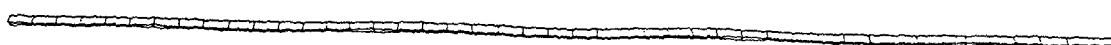
13f) State time of 3.0 msec

Figure 13a,b,c,d,e,f.   Deformation Plots for SOR Beam Model with
                         50X magnification factor

25

C.   INTEGRATED SOR BEAM/SHELL MODEL

A third study was undertaken to simplify the original unstiffened cylinder by integrating SOR beam elements with shell elements. This type of model would not only reduce the size of the discrete model but would now be sufficiently small enough to allow for additional internal structures to be added to the shell section of the beam/shell model. The same harmonic functions for the SOR elements were used and the shell elements were generated in the same manner as in the discrete model. The success of this model solely depended on developing the proper interface between SOR beam and shell elements that would produce accurate dynamic response to the explosions. The first consideration for the interface between both types of elements was using internal beams to connect SOR elements to shell elements. This consideration proved to be totally ineffective because there was entirely too much local deformation at the beam/shell interface.

The next type of interface explored was the use of a dry endplate with thickness equal to the thickness of the shell. More favorable dynamic responses were obtained, however there were sizeable differences in the axial motions of the model. This type of model is represented in Figure 14. The model is shown as a full model, even though a half model was used to reduce computational time and take advantage of symmetry conditions.

1.   Variation of Material Properties for Beam/Shell Interface

A sensitivity study was undertaken by changing the material property of the dry endplate being used as the interface. Both the thickness of the plate and Young's modulus were adjusted in order to observe changes in the deformation, both axially and in the transverse or z-direction. The transverse or whipping motion of the model was not affected
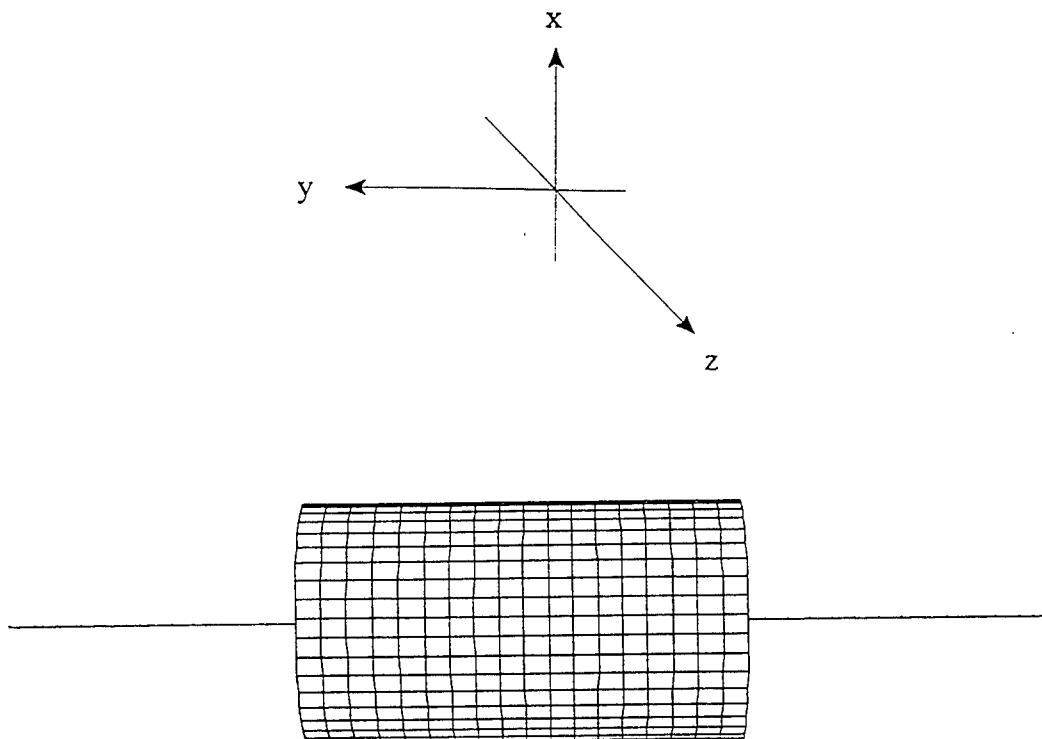
Figure 14.   Integrated SOR Beam/Shell Model with Dry Endplate Used as Interface

by large changes in the material properties for the endplate. The axially direction, however was affected by changes in either endplate thickness or Young's modulus.

It was noted that the dynamic responses were more sensitive to changes in endplate thickness.   Only when Young's modulus was adjusted in a large amount, there was a noticeable change in the dynamic response of the entire model.   After performing numerous

27

numerical studies using the dry endplate, it was determined that the dry endplate produced favorable results for the modeling the integrated SOR beam/shell model. Furthermore, the endplate's material properties can be approximated by the following formula:

$$\frac{3* P* a^4}{4* E* t^3} \leq \delta$$

where:

P= max incident pressure(psi)
a= radius of plate
E= Young's modulus
t= thickness of plate
δ = tolerance of axial displacement for the endplate

The formula was simplified from the exact solution for the deflection of a circular plate loaded at the center [Ref. 9]. Results from application of the formula have produced an integrated model that has very similar whipping motion responses and slight differences in axial direction responses. The reasons for slight differences in axial direction responses can be attributed to approximating the shell with SOR elements. Although SOR elements produce good whipping motions, the axial motions are slightly off because the shell elements not only bend axially but also bend in the radial direction causing differences in the overall result. The SOR beam model did not adjust locally for the mass of the endplates which also causes differences in the axial direction. Locally smearing the properties of the endplates will be examined in the discussion on stiffened beam/shell models.

Figure 15 shows a comparison of the SOR/shell model with a 3/16" thick dry endplate. Figure 15a shows the model's global deformation at 0.5 msec after the shock has

28

hit the structure and before the interface endplate's material properties were adjusted. Figure 15b shows the global deformation after the endplate's material property was adjusted. Notice that the unadjusted model has a noticeable amount of axial deformation at the endplate as compared to the adjusted model which shows very little axial deformation at endplate. The tolerance for the adjusted model was set at .01 inch. Using a small tolerance ensures that there will be very little deflection of the dry endplate which improves the overall global deformation of the model. Also, the small tolerance ensures a smooth transition of deformation at the interface. There is some pinching of the shell caused by the rigidity of the dry endplate, however it will be seen later in this chapter that the overall global deformation and dynamic responses at the beam/shell interface are in good agreement with the discrete model. This type of model also provides for a smooth transition of the dynamic responses from beam to shell at the interface region.
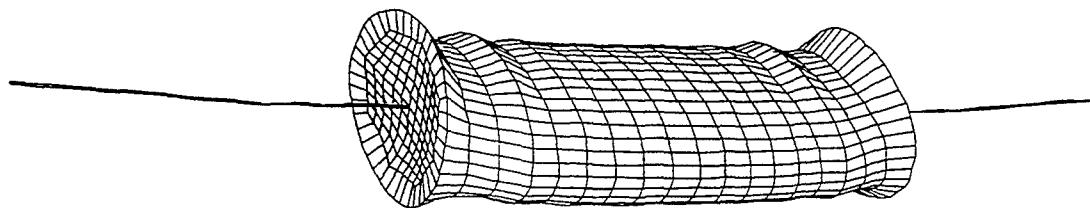
15a) 3/16" Thick Endplate- No Adjustment to Material Properties 50 X Magnification Factor , state time of 0.5 msec
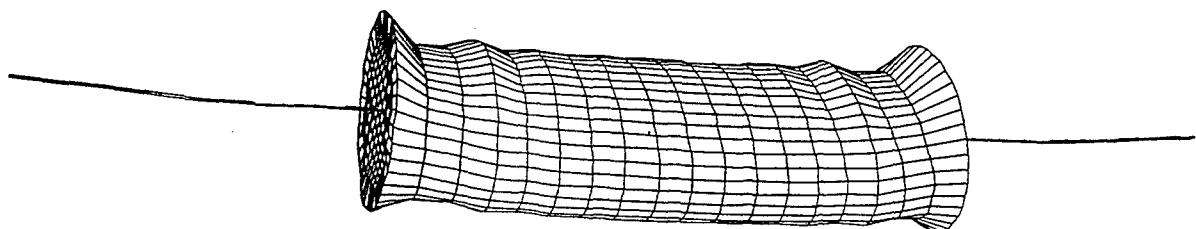
15b) 3/16" Thick Endplate, Material Property Adjusted, 50 X Magnification Factor, state time 0.5 msec

Figure 15a,b. Global Deformation Plots for SOR Beam/Shell Model:

The beam/shell model with adjusted material properties provides very similar deformation results when compared to the discrete model, however there is one disadvantage to this type of modeling. Adjusting the elastic modulus causes a longer computation time due to the increased stiffness in each element. The time step size used in the explicit finite element computer program is computed by the following formula:

$$\Delta t = \frac{SL}{\sqrt{\dfrac{E}{\rho}}}$$

where:

S= safety factor (use number less than 1)
L=length of smallest element in any direction
E= Young's modulus
ρ= material density

By selecting a larger Young's modulus, the overall time step is decreased which increased the overall computational time.

After formulating the proper way to integrate SOR beam/shell elements, a study was done to find a dry endplate that would produce accurate results but reduce the computational time. A thicker endplate was first examined since it would help reduce the ratio of Young's modulus to material density. The Young's modulus for the 1/2" thick endplate was calculated using the endplate formula. A 1/2" thick dry endplate was selected for the integrated SOR/shell model since this produced an adjusted Young' modulus of about 100 times less than the 3/16" thick endplate's Young's modulus. Both models were subjected to the same explosive testing with the charge location at the symmetric point on the shell.

31

Figures 16-18 compare the axial displacements, velocities and accelerations between the 3/16" and 1/2" thick endplate models. There is exceptional agreement with all three plots, however there is a slight difference in magnitude and frequency which can be accounted for by different masses of the endplates. The 1/2" thick plate produced slightly larger displacements in the axially direction. Figures 19-21 compares the z-direction or whipping motion responses of the two models. There is very tight agreement between both models for the displacement, velocity, and acceleration. This clearly suggests that the estimation of the material property of the endplates is a very effective tool for integrating the SOR Beam/Shell model. Even though a thicker endplate was used the overall time step was (9.027×10^{-8}) which is 30 times less than the original time step of (2.5×10^{-6}). Further optimization of this problem would produce a dry endplate of about 1.75" that would have a time step of about 80% of the original time step. Because DYNA3D code allows a material choice option for modeling a material as a rigid body, the time step problem can be eliminated. This material option will now be discussed.
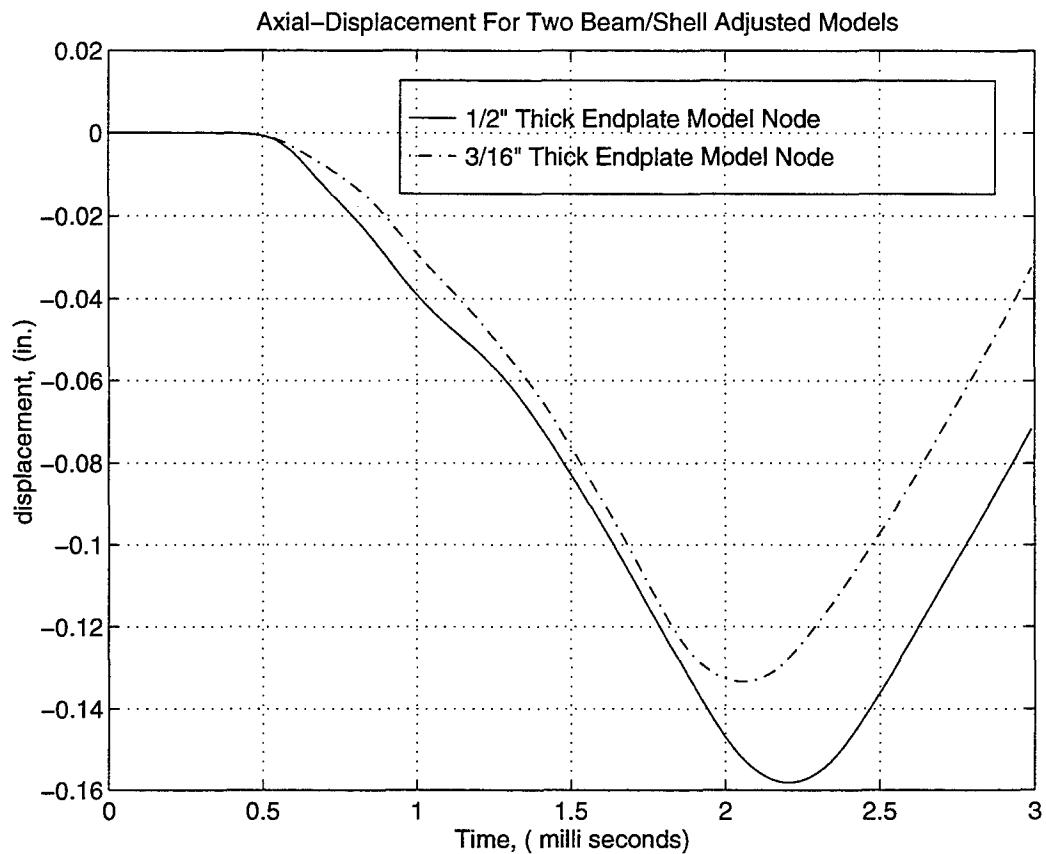
Figure 16. Axial Displacement of Two Integrated SOR Beam/Shell Models Both With Material Property Adjustment to Endplates

33
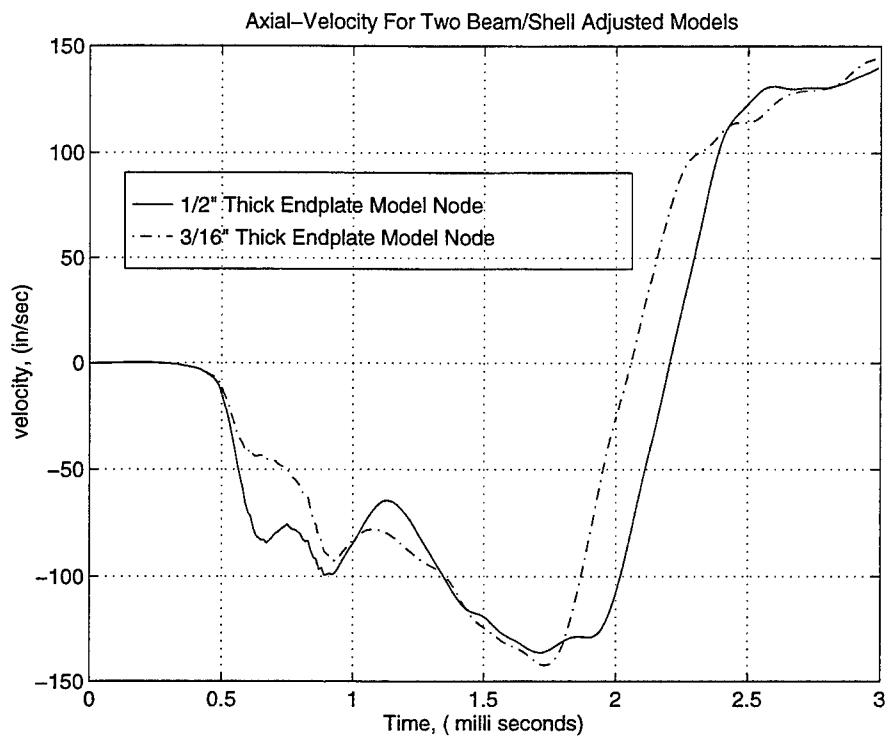
Figure 17. Axial Velocity Response for Two Integrated SOR Beam/Shell Models
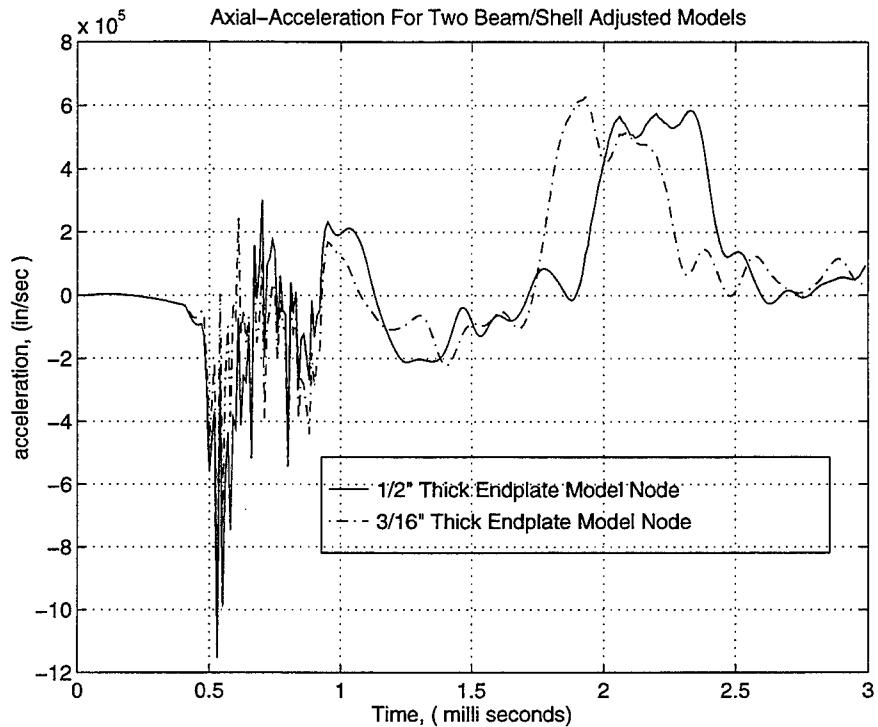
Figure 18. Axial Acceleration Response for Two Integrated SOR Beam/Shell Models

34
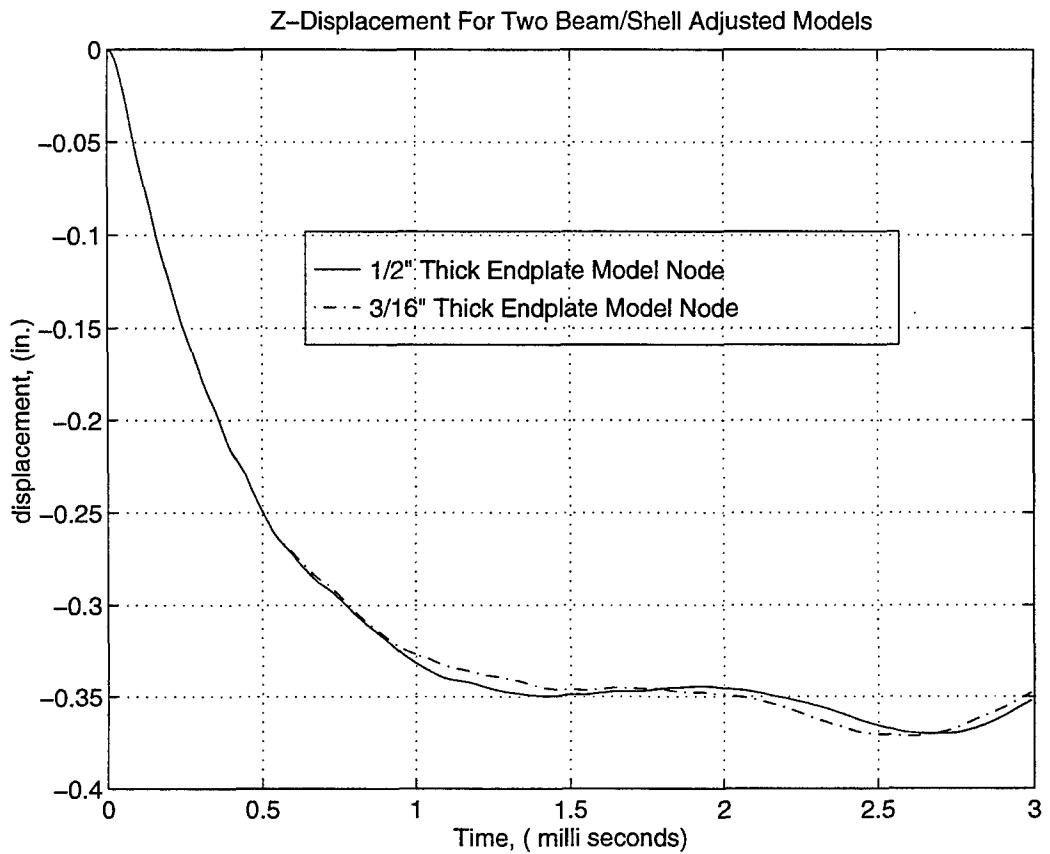
Figure 19. Whipping Displacement Response for Two Integrated Models
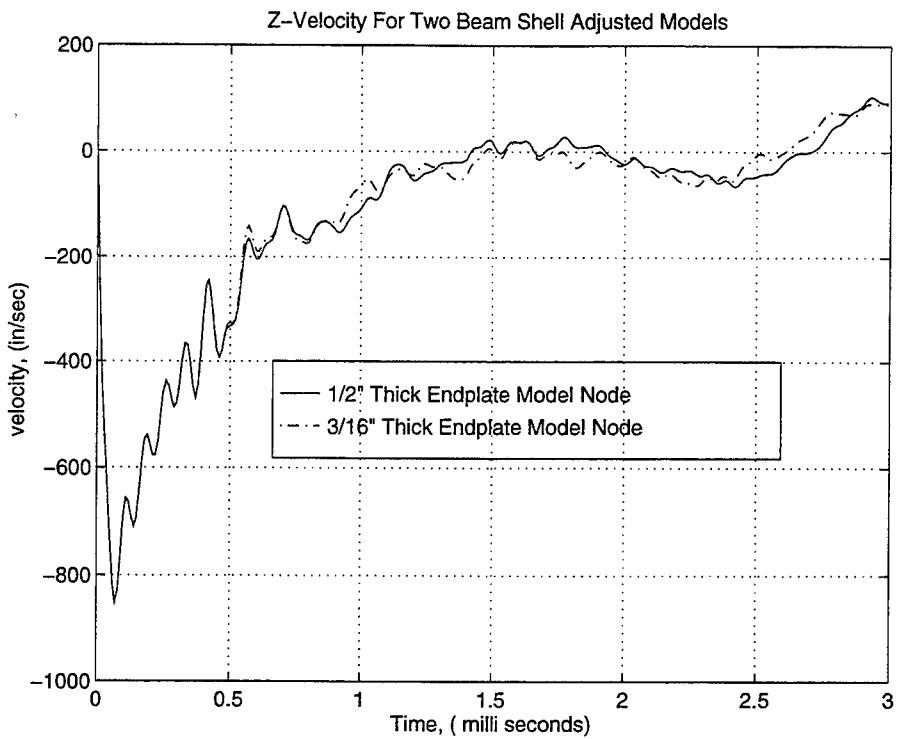
Figure 20. Whipping Velocity Response for Two Integrated Models
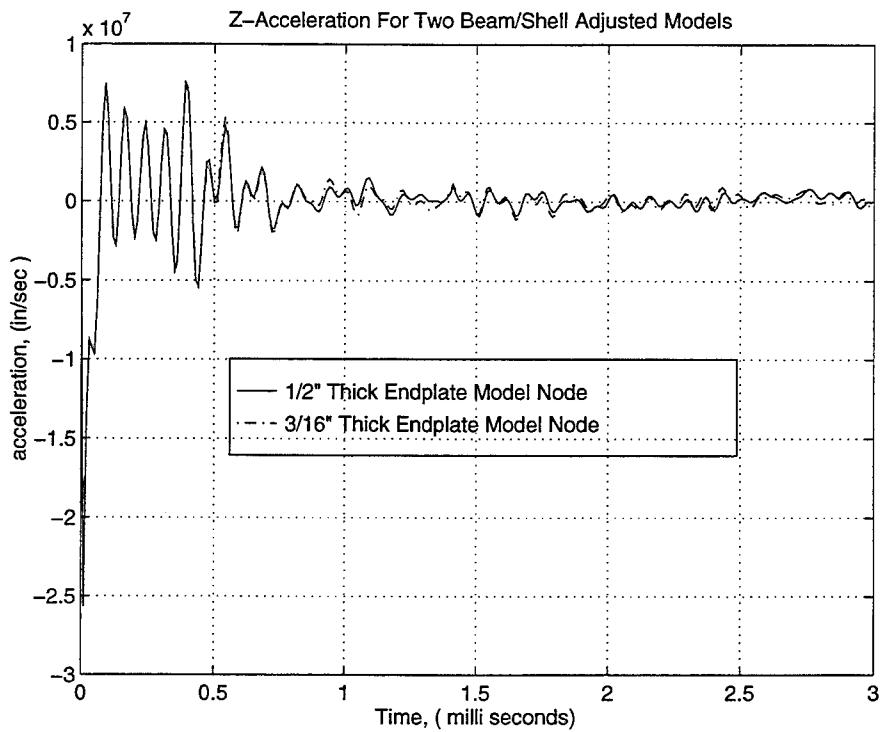
Figure 21. Whipping Acceleration Response for Two Integrated Models

36

The rigid body material option on DYNA3D is built into the computer code and only requires three material property inputs (E, ρ, v). The thickness of the endplate was first selected at 3/16" and then varied to see how well this material option would predict the dynamic responses. It is recommended that the thickness of the endplate be very close to the thickness of the cylindrical shell or too much local deformation will occur at the interface area due to the increased mass distribution of the thicker endplate. The structure created with this material option will then behave as a rigid body dynamically when subjected to any type of loading. The SOR beam/shell model was redesigned using this material option and tested. Figure 22 shows the global deformation plots for the model using the rigid body material option. As with the previous modeling of the beam/shell interface, the rigid body model produces pinching at the endplate interface. Figure 23 shows a comparison plot between the adjusted 3/16" thick endplate model and the beam/shell model with the rigid body endplate at 0.5 msec. Both models were in excellent agreement with each other. The big advantage of using this material option is that the original values of Young's modulus and density can be used which in return does not affect the original time step. This significantly reduces the overall computational time of the model and makes it a viable choice for simplifying the cylindrical shell.
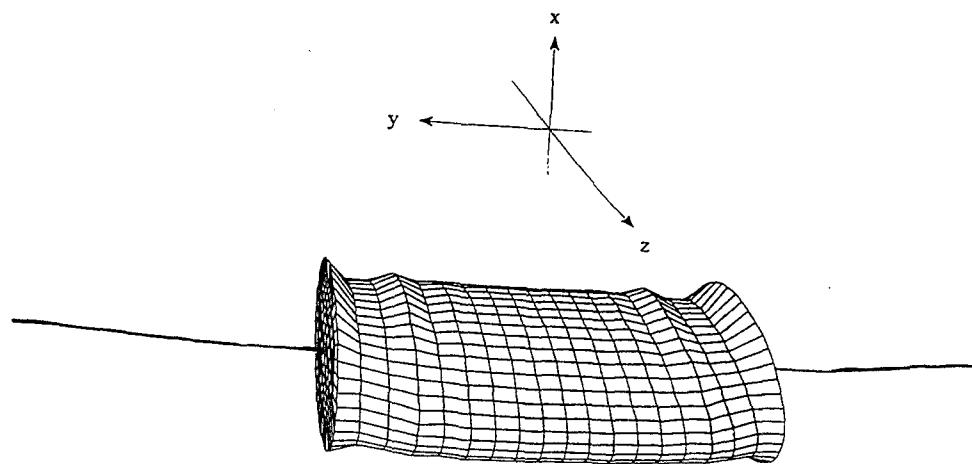
Figure 22a) State time of 0.5 msec
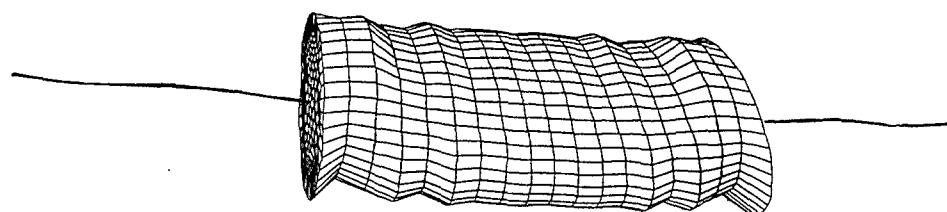
Figure 22b) State time of 1.0 msec
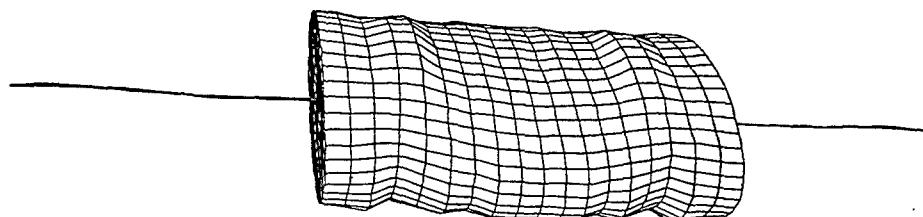
Figure 22c) State time of 1.5 msec

Figure 22a,b,c. Deformation Results for Integrated SOR Beam/Shell Model Using Rigid Body Material Option with DYNA3D
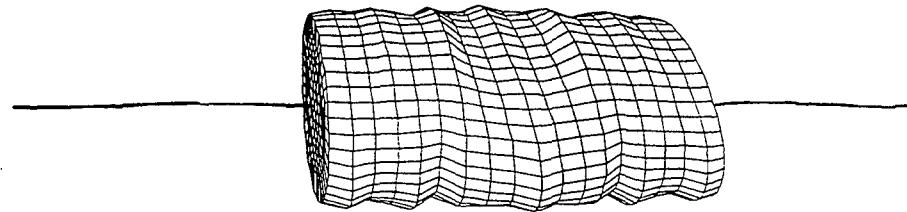
Figure 22d) State time of 2.0 msec
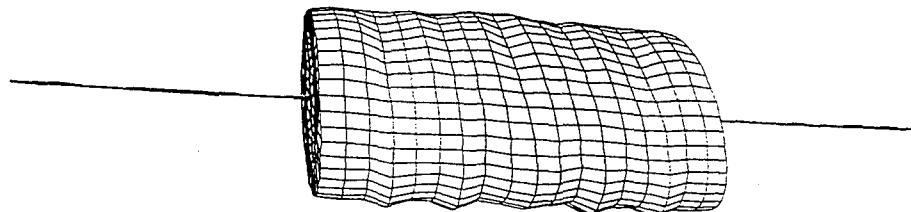
Figure 22e) State time of 2.5 msec
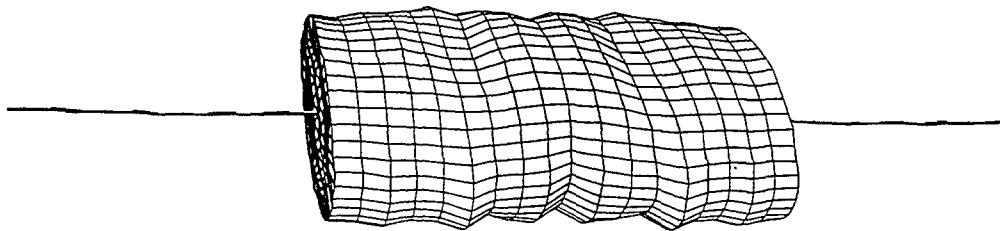
Figure 22f) State time of 3.0 msec

Figure 22d,e,f. Deformation Results for Integrated SOR Beam/Shell Model (cont.)
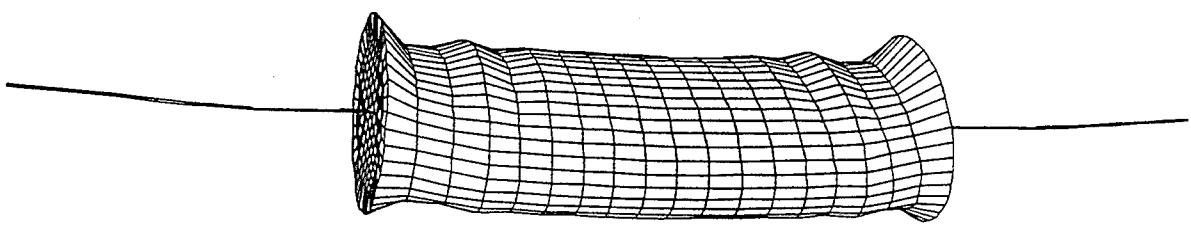
Figure 23a) Deformation Plot of 3/16" Thick Endplate for SOR Beam/shell Model
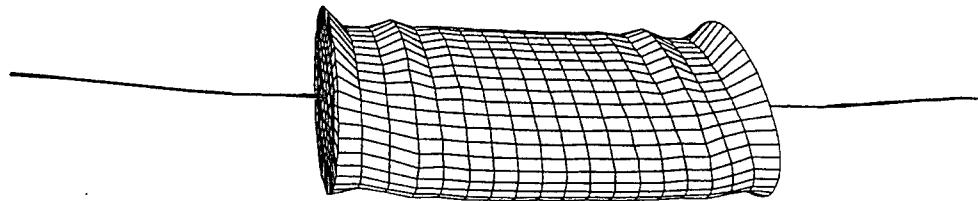
Figure 23b) Deformation Results of Rigid Body Endplate for SOR Beam/shell Model

Figure 23 a,b. Deformation Results for 3/16" Thick Endplate SOR Beam/shell Model Versus Rigid Body Endplate SOR Beam/shell Model of Unstiffened ONR Cylinder

D.   COMPARISON OF DISCRETE TO SIMPLIFIED MODELS

This section will compare the results of the explosive testing on the discrete unstiffened model to those of the simplified SOR beam and integrated SOR beam/shell models. Comparisons will be done by plotting the displacement, velocity and acceleration in both the axial and transverse(z) directions for all three models at selected points. The z-direction or whipping motion response will be examined at the center point nearest to the charge. The axial or accordion motion responses will be monitored at the left endplate for all three models.

For the cylinder, the center point nearest to the charge (so-called side shell node) and at the top of the cylinder at the center (called top shell node) and center point away from charge (called back side node) could be selected for comparison. Because the cylinder has both global and local deformations at the three nodal points, the locations are expected to have different responses. Depending on which motion is dominant, the difference may be large or small. If the global response is dominant over the local response, the three points will have a similar response. Otherwise, the three points will have quite different responses. In the z-direction, the global response dominanted over the local response. This can be clearly seen in Figure 24 which compares the three shell nodal points to the same beam nodal point on the simplified SOR beam model. Notice how the responses are very similar and that the top and back side shell nodes have a slight delay before the deformation occurs. This is due to the shock wave progressing through the cylinder where it hits the front side node first due to its closer location to the charge. Except for the delay, the responses are quite similar in shape and magnitude. When comparing all three models from now on, only the front side

41

shell node will be plotted.
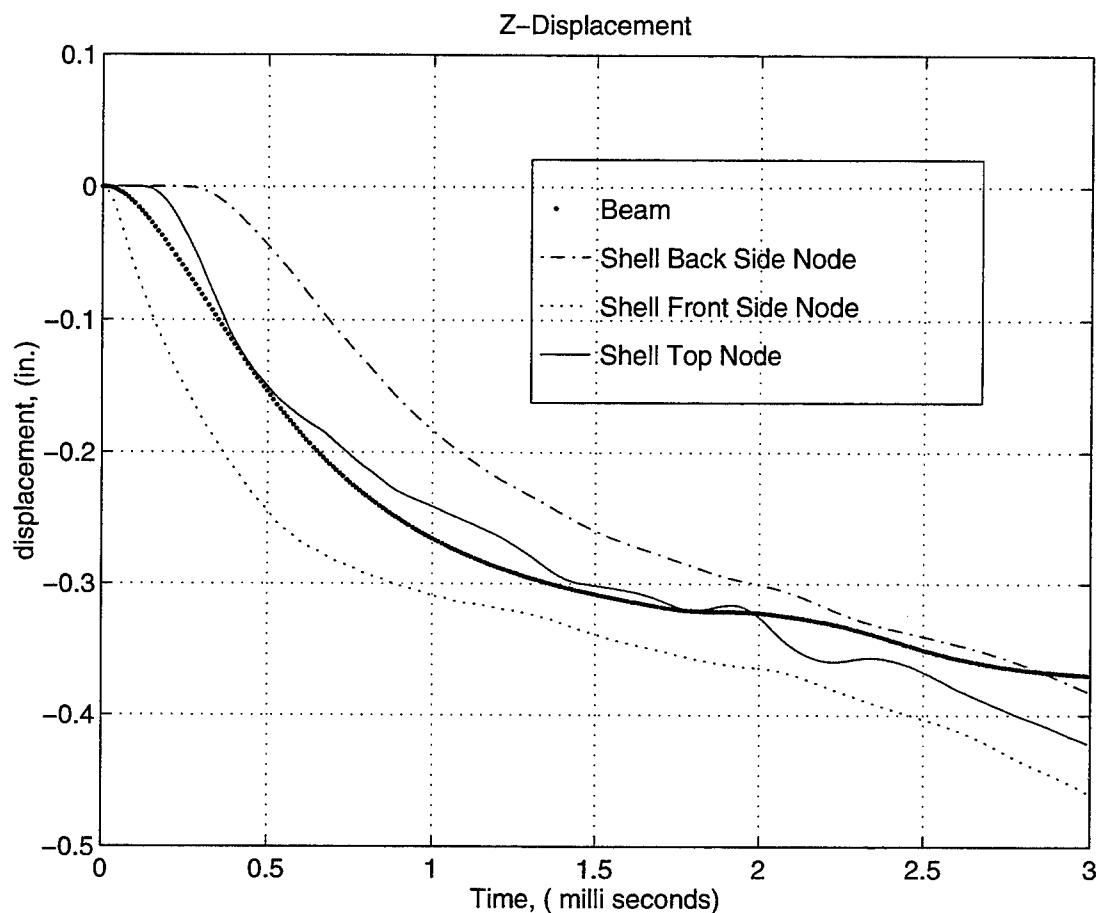
Figure 24. Whipping Displacement Plot Showing Comparison of Shell Node Response for Unstiffened Shell versus SOR Beam Model

The axial displacement, velocity, and acceleration time history plots for the discrete and two simplified models are provided in Figures 25-27. The beam/shell model was modeled with the rigid body material option using a 3/16" thick endplate for more accurate results and a quicker computational time. There is however noticeable differences between all three models for all three responses. An explanation for the differences is that the SOR beam model will not have the same local nodal point response as the same point on the cylinder. The local response in the axial direction is more dominant than the global response. The beam/shell model and the beam model did not account locally for the mass of the endplate which causes some error in the axial direction. If the magnitude of the local responses are examined, there is about a 45% difference between shell and beam model displacements. Figure 28 shows the global deformation plot at 0.5 msec for all three models. The overall global deformation is in good agreement except for local deformation at the beam/shell interface.

Figures 29-31 provide the whipping responses for all three models at the location of the closest point to the charge. These plots show excellent agreement between all three models with the error less than 10%. The SOR approximation predicts responses better in the transverse direction than in the axial direction.
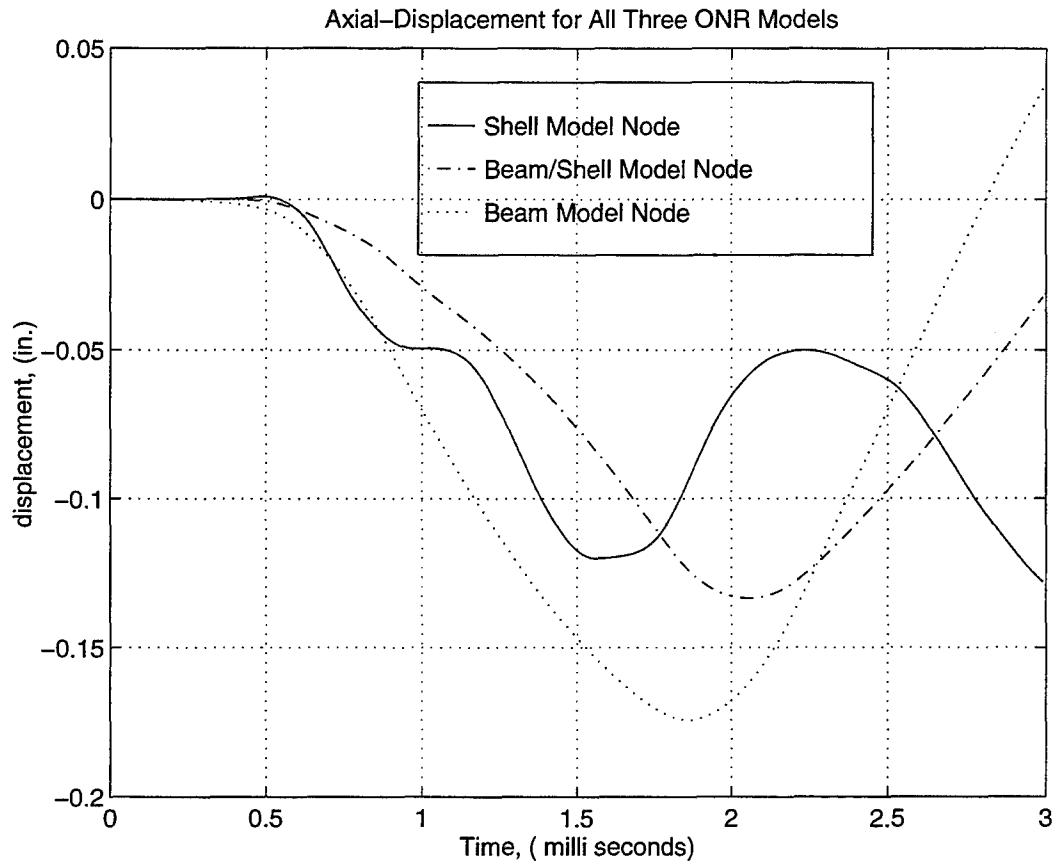
Figure 25. Axial Displacement for All Three Models

44
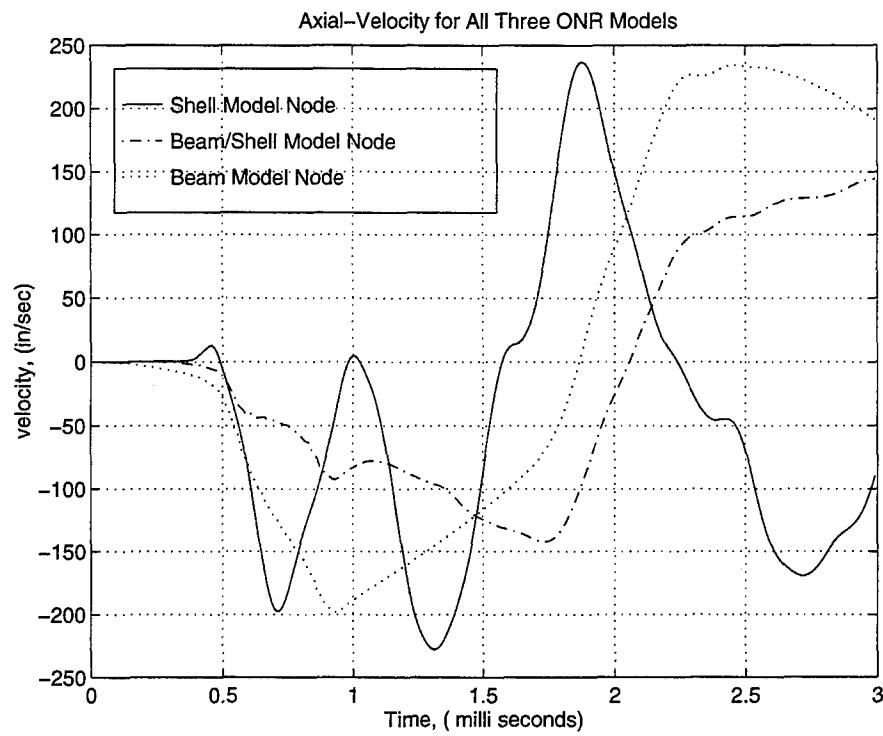
Figure 26. Axial Velocity for All Three Models
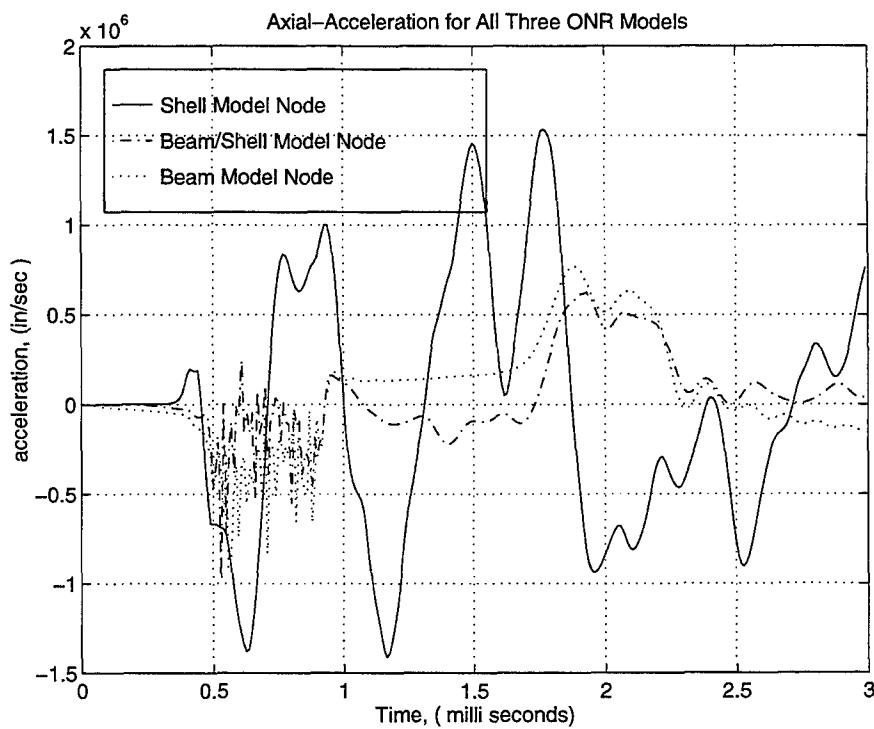
Figure 27. Axial Acceleration Plot for All Three Models

45
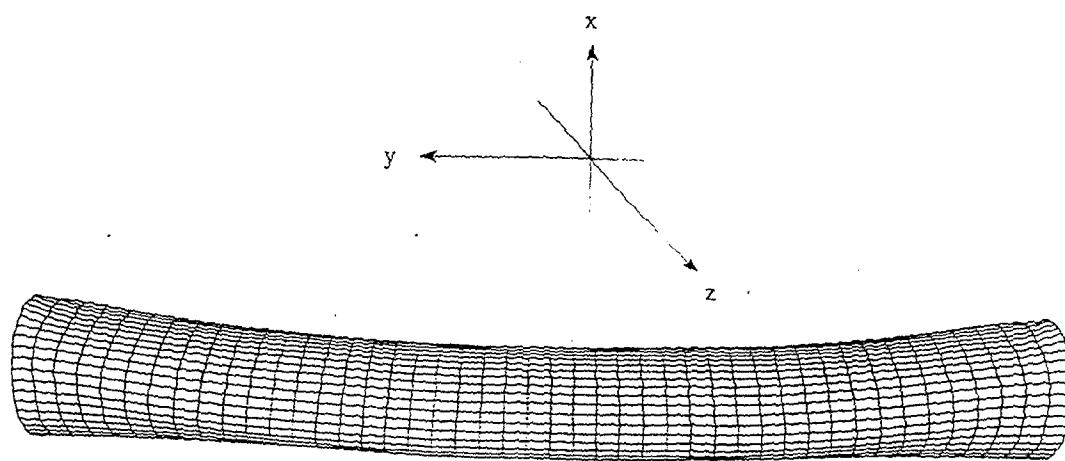
28a) Global Deformation for Unstiffened Cylinder

28b) Global Deformation for SOR Beam Model
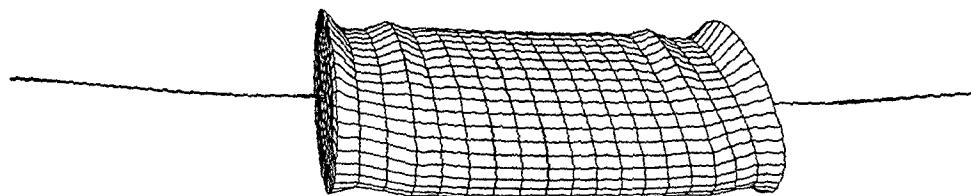
28c) Global Deformation Result For SOR Beam/Shell Model

Figure 28a,b,c. Global Deformation Plots for All Three Models at 0.5msec with 50X Magnification Factor
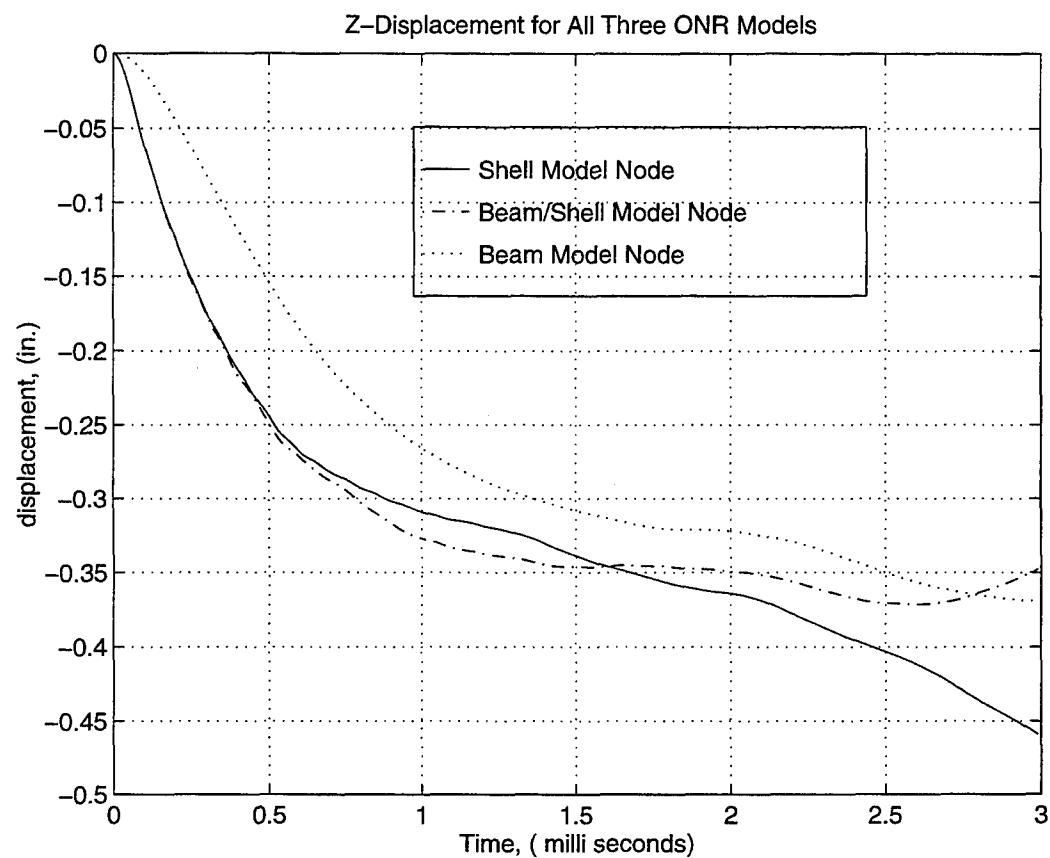
Figure 29. Whipping Displacement for All Three Models
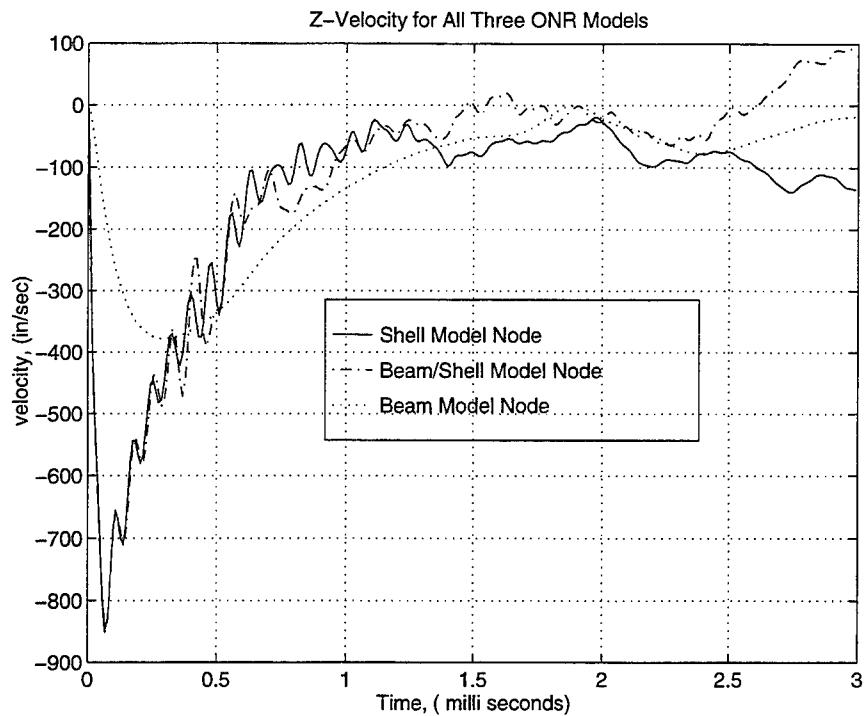
Figure 30. Whipping Velocity Plot for All Three Models
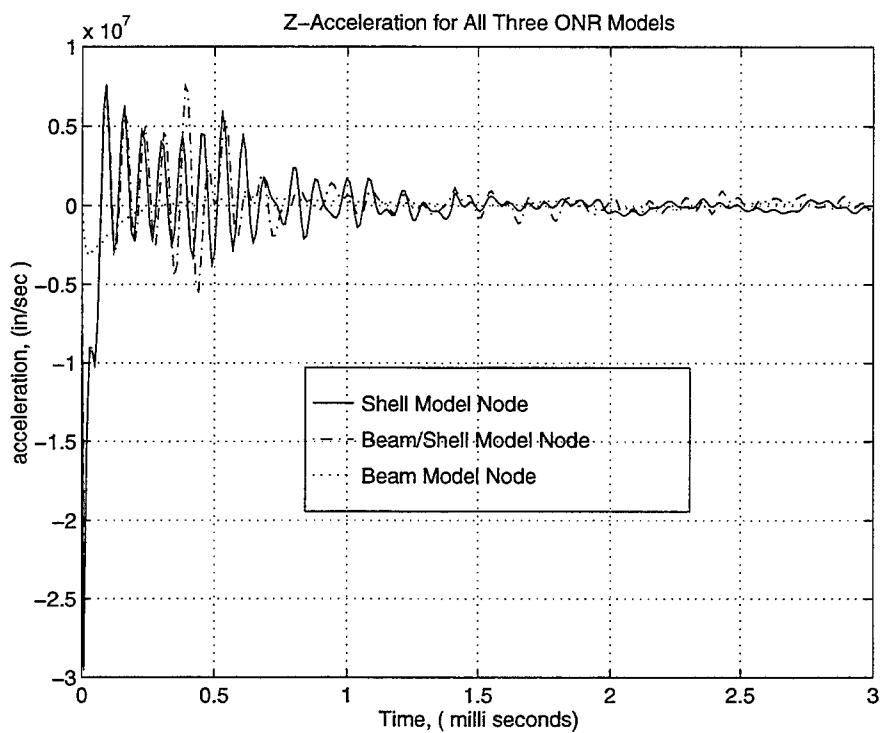
Figure 31. Whipping Accelearation Plot for All Three Models

48

And finally, Table 2 is provided to compare the size of the model with the overall computational time for each model. The SOR beam/shell model data is for the rigid body material option for modeling the beam/shell interface. Clearly, one must make a decision as to whether to use SOR beam elements or original shell elements. Clearly the accuracy lies in using shell elements, however if a section of the cylinder model requires isolation for detailed internal modeling, then the beam/shell model can be used to simplify the design and to reduce computational time. The next part of the study will examine modeling the ONR stiffnened cylinder.

	Unstiffened ONR Cylinder	SOR Beam Model	Integrated Beam/shell Model
Number of Nodes	1140	47	534
Number of Wet Elements	1080	45	360
Computational Time (sec)	1968	6.44	742

Table 2. Comparison Data For all Three Models of Unstiffened ONR Cylinder

49

V. MODELING OF STIFFENED ONR CYLINDER

In this section the simplification of the ONR cylinder is investigated. The original

ONR cylinder with stiffeners will be modeled first. Next, the stiffener smearing technique

will be used to model the cylinder with orthotropic shell elements. The SOR beam model

will be generated next and finally, the integrated SOR beam/shell model will be generated.

The original material used for all four models is as specified in Table 1. Only the smearing

values will be different. This section will conclude with a comparison of the displacement,

velocity and acceleration responses for the models subjected to both a symmetric and off-

center shock wave.

A.   DISCRETE STIFFENED ONR CYLINDER

The three-dimensional model is shown in Figure 32. As with the unstiffened model,

a full model is depicted even though a half model was analyzed due to symmetry conditions.

Both the unstiffened and stiffened models contain 1080 wet shell elements, however with

the stiffeners, the total amount of elements for the stiffened model is 2064. The term wet

means exposed to the shock wave pressure. This type of model involves longer

computational time to complete the computation of the response to the shock wave due to

the increased number of wet elements. It is because of both the computational time and

design effort that a simpler model is needed.

The stiffened or discretized model was subjected to both symmetric and off-center

shock waves. As with the unstiffened model, there was no global deformation observed in
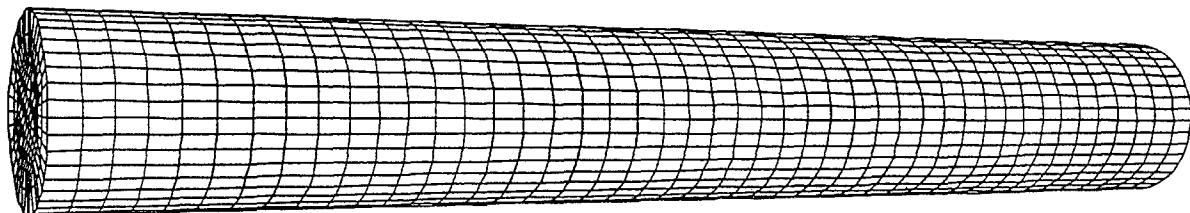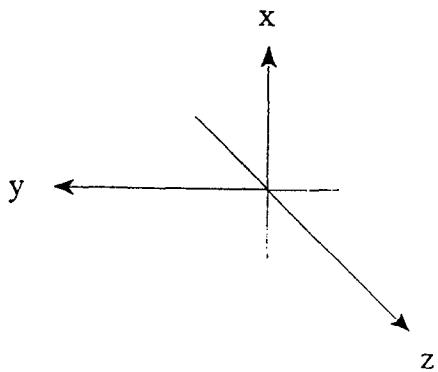
Figure 32. ONR Full Cylinder Model with Internal Stiffeners

the x-axis (see Figure 32). The global deformation responses are provided in Figure 33 at

discrete states of time. The plots are again magnified at a scale factor of 50 for viewer

enhancement. The deformation analysis indicates that there is a large local deformation

gradient at the locations of the deep frames and endplates. The gradient smoothed out as the

shock wave progresses through the cylinder and by 3 msec, there is very little pinching effect

caused by the deep frames. Displacement, velocity, and acceleration plots will be presented

later in this section.
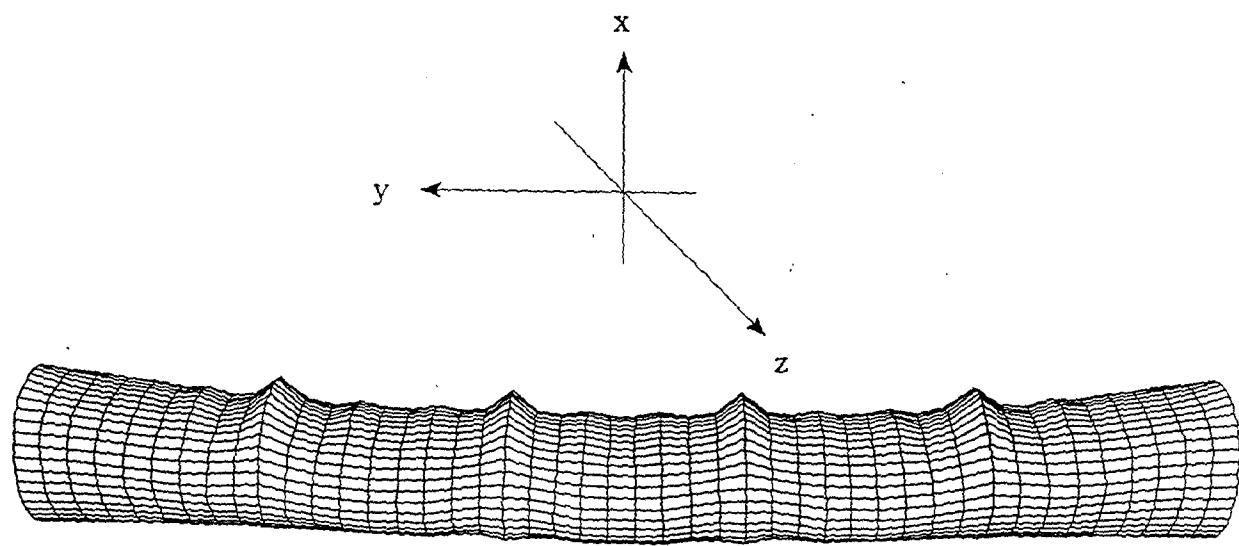
Figure 33a)   State time of 0.5 msec
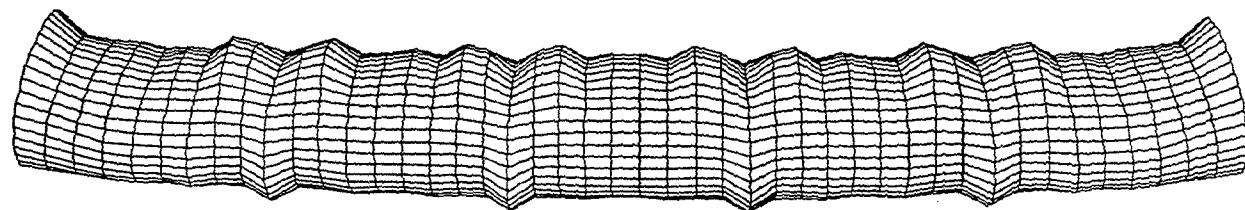
Figure 33b)   State time of 1.0 msec
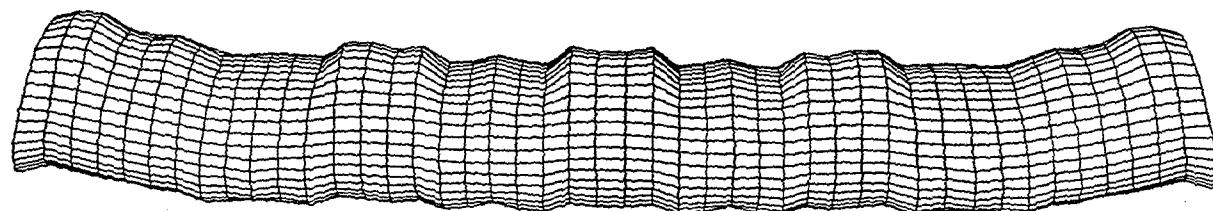
Figure 33c)   State time of 1.5 msec

Figure 33a,b,c. Deformation Results of Stiffened ONR Cylinder Model

53
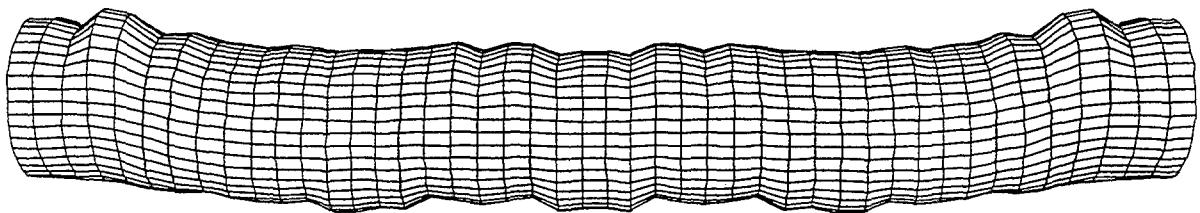
Figure 33d) State time of 2.0 msec
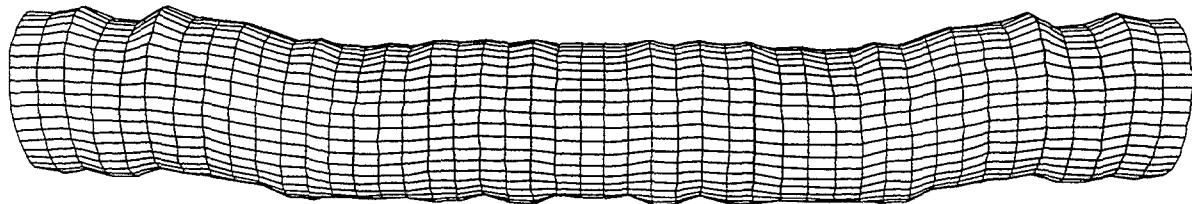
Figure 33e) State time of 2.5 msec
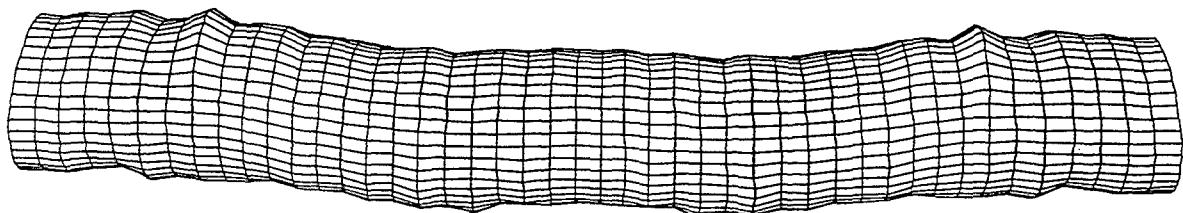
Figure 33f) State time of 3.0 msec

Figure 33d,e,f Deformation Results of Stiffened ONR Cylinder (cont.)

54

B.   ORTHOTROPICALLY SMEARED ONR CYLINDER MODEL

The first simplification model of the stiffened ONR cylinder investigated was the orthotropically smeared ONR cylinder. This type of simplification attempts to properly model the cylinder as one unit with homogenized properties. Once the effective or smeared properties are computed, the cylinder can be subjected to the underwater explosion and the results analyzed. The DYNA3D code allows the user to select an orthotropic elastic material. The material selection requires 9 properties in order to complete the material matrix. The six properties would represent the smeared properties of the original ONR cylinder. The first three properties were the Poisson's ratio for all three material axes. The material axis corresponds to the axis shown in Figure 1. All three of these values were assumed to be the same value of the original material or 0.3.

Next the values for the Young's modulus were developed. The value for smeared Young's modulus in the axial direction (y-direction) is simply the discrete value for the original material since ring stiffeners do not contribute much in the longitudinal direction. To determine the smeared elastic modulus values in the radial (x or z-direction) and tangential direction (x or z-direction), the assumption was made that the radial stiffness of the shell is significantly less important than the tangential stiffness. The tangential stiffness in other words directly affects the bending stiffness of the cylinder. This assumption is also stated by Timoshenko and Woinowsky-Kreiger [Ref. 9]. Therefore the smeared value in the tangential direction would be set equal to the radial direction smeared value ($E_{\theta'} = E_{r}$). To calculate this smearing value for the radial and tangential direction, the 2-dimensional static smearing technique developed in [Ref. 9] was used. This smearing value would be

used in the three-dimensional representation of the stiffened ONR cylinder. The smearing

value for both directions was computed by the following formula [Ref. 9] :

$$E' = E + [\frac{12(1- v^2)}{h^3}] \frac{E_s I_s}{a}$$

where:

$E' = E_{\theta'} = E_{r'}$
E= discrete or original Young's modulus for cylinder
v= Poisson's ratio
h= thickness of cylinder
E_s = Young's modulus for stiffeners
I_s = moment of inertia of the stiffener

The remaining three values are for the elastic shear modulii for all three planes. The values

for G_{xy}' and G_{yz}' were assumed equal to each other due to the same reasoning for the elastic

modulus. The value for these two planes was found by using the following formula [Ref. 9]:

$$G_{xy}' = G_{yz}' = \frac{E}{2(1+v)}$$

where

E= elastic modulus of original cylinder
v= Poisson's ratio for original cylinder

The value for the elastic shear modulus G_{xz}' was found using the following expression

[Ref.9]::

$$G_{xz}' = G + \frac{G_s}{2a}$$

where

G= original elastic shear modulus of cylinder
G_S = shear modulus of stiffeners
a= spacing between stiffeners

Besides ensuring that the proper stiffness smeared values are inserted into the smeared model, the effective mass distribution must also be accounted for. The effective mass distribution for the smeared model was calculated by using the formula:

$$\rho' = \frac{M}{V}$$

where:

ρ' = smeared mass density value
M = total mass including cylinder and stiffeners to be smeared
V= volume of cylindrical shell without stiffeners

Due to the large thickness of the deep frame stiffener, the deep frames were discretely modeled in the smeared ONR cylinder model. The model is presented in Figure 34 with the axis as shown. Table 3 summarizes the inputs for the orthotropic model. This model was then subjected to the underwater explosive testing for both symmetric and off-center shot geometries. The overall global deformation plots for the symmetric shot geometry is provided in Figure 35 at a magnified scale factor of 50. There is slight pinching around deep frames at the earlier state times but the deformation gradient around each of the deep frames is less than the original discrete model. As will be seen in futures ection in this chapter, the overall dynamic reponses of this model are in close agreement with the discrete model.
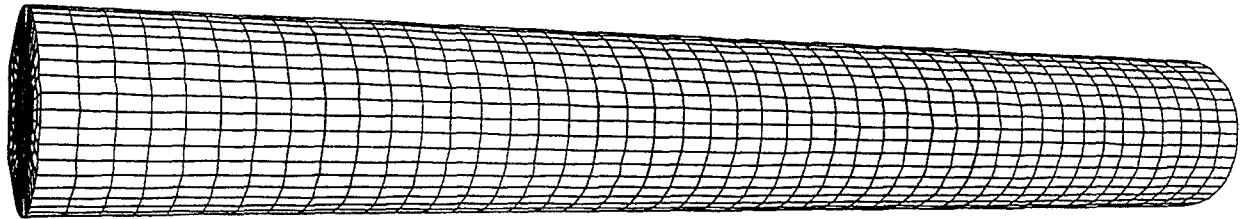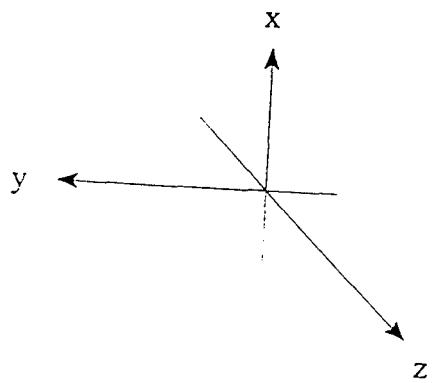
Figure 34. Orthotropically Smeared Model of ONR Stiffened Cylinder

ν(xz, yz, xy)	0.3	0.3	0.3
E (psi) (E_{xx}, E_{yy}, E_{zz})	17.813×10^8	same	2.9×10^6
G(psi) (xz, yz, xy)	12.145×10^6	11.154×10^6	11.154×10^6

Table 3. Material Properties for Orthotropic Smeared ONR Cylinder

The use of the orthotropic smeared technique produces results similar to the study on the flat plate where local smearing was used around the clamped edges. In both cases, local smearing reduced the deformation gradient and produced effective global deformation results. One of the disadvantages of using the orthotropic smeared model is more lengthy computation times due to explicit time integration scheme. Although the model was reduced from 2064 nodes to 1124 nodes, the amount of wet elements remains the same. Since smearing also involves increasing the Young's modulus, the overall critical time step is decreased from the original isotriopic model's time step. These factors cause a very lengthy computational time.
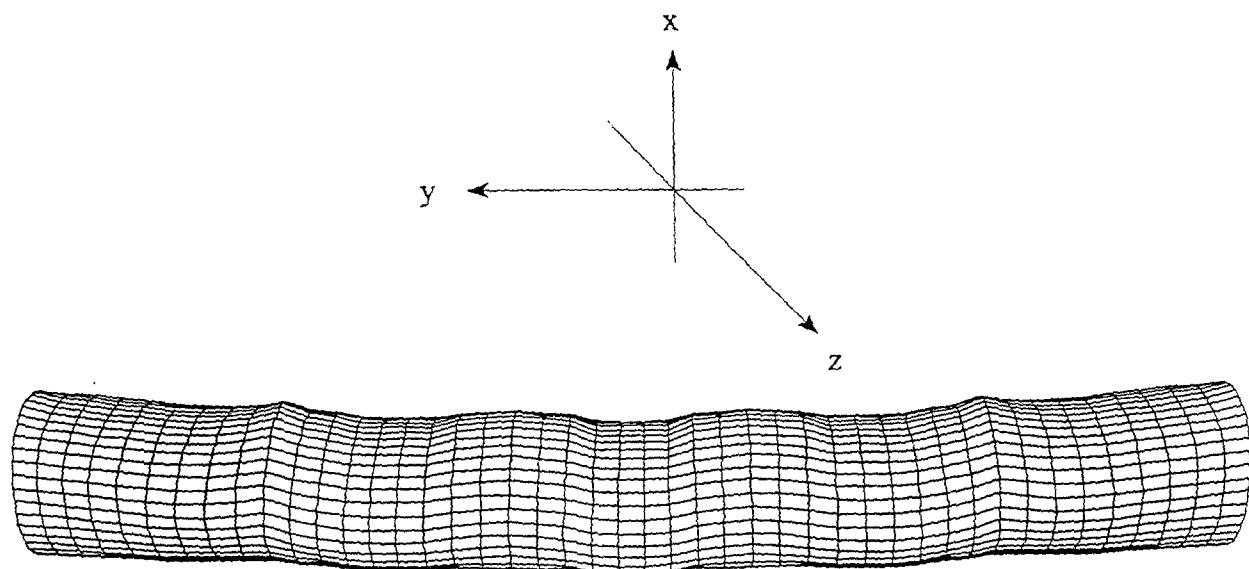
Figure 35a)   State time of 0.5 msec
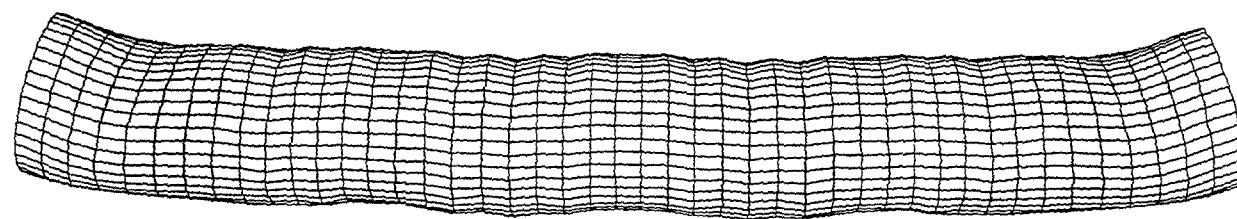
Figure 35b)   State time of 1.0 msec
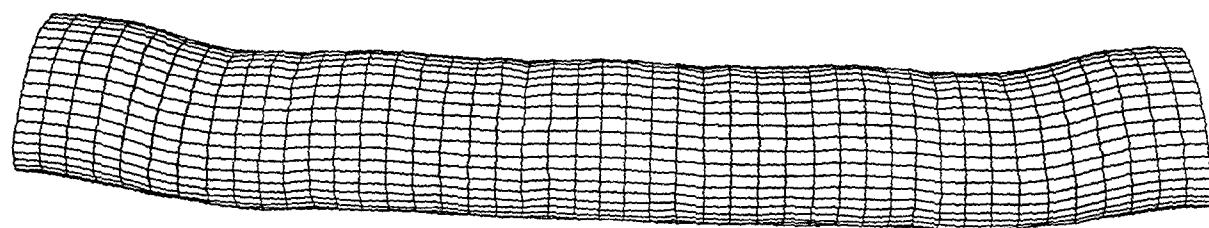
Figure 35c)   State time of 1.5 msec

**Figure 35a,b,c. Deformation Results of Orthotropically Smeared ONR Cylinder Model**

60
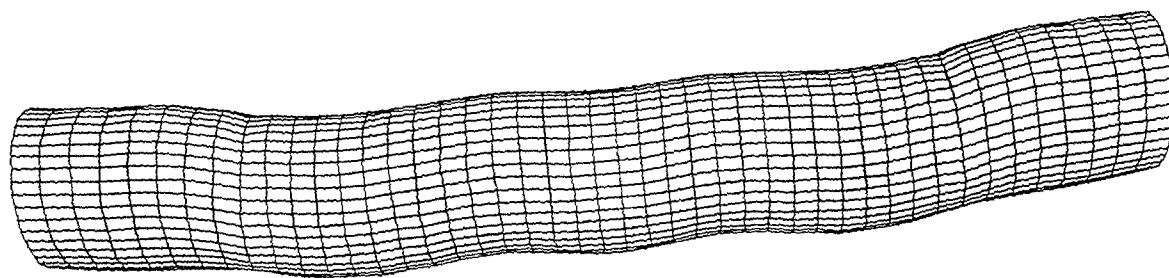
Figure 35d) State time of 2.0 msec
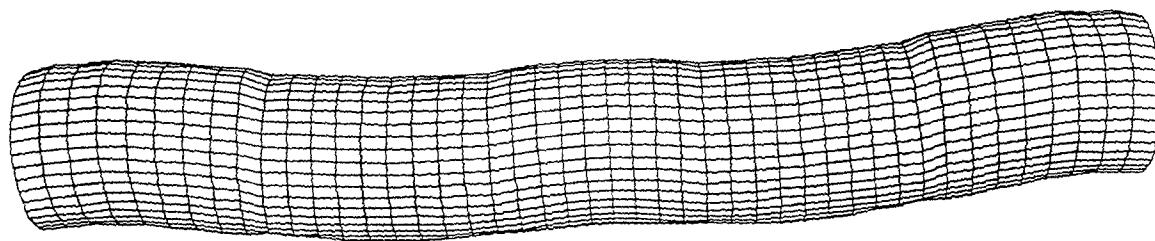
Figure 35e) State time of 2.5 msec
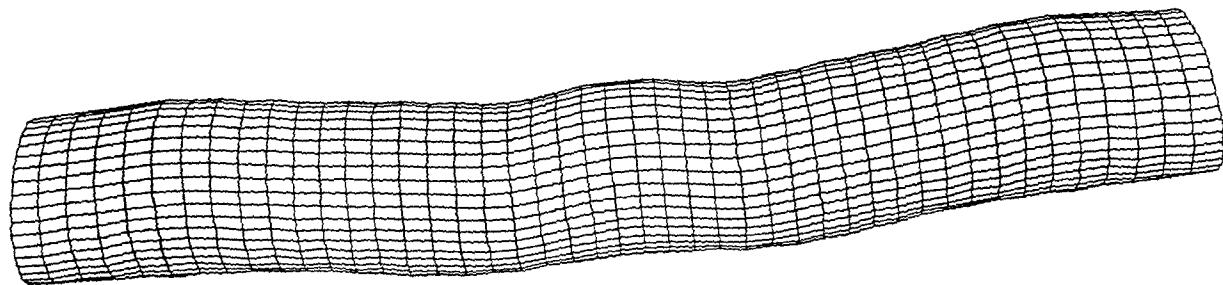
Figure 35f) State time of 3.0 msec

Figure 35d,e,f. Deformation Results of Orthotropically Smeared ONR Cylinder (cont.)

61

C. SOR BEAM MODEL

The SOR beam model for the stiffened ONR cylinder is developed in the same procedure as the unstiffened SOR beam model. However, the effective stiffness and mass distribution of the stiffened model must be incorporated into the SOR beam model. This will ensure that the beam model will have the equivalent fluid structure interaction as compared with the stiffened ONR cylinder. The same harmonic function will be used in computing the fluid mass matrix for the SOR beam model. Both symmetric and off-center shot geometry will be used for analyzing the model.

There are 45 SOR beam elements used to model the cylinder along its longitudinal direction. In order to obtain the equivalent stiffness, the cross-sectional areas and moments of inertia were adjusted. The cross-section area of the stiffened SOR beam model is:

$$A = \frac{\pi}{4}(d_o^2 - d_i^2)$$

where d_o and d_i are the outside and inside diameters respectively. This value is the same for both stiffened and unstiffened models. However, the second moment of inertia and polar moment of inertia of the stiffened cylinder differed from the unstiffened cylinder because the stiffeners were considered. The values were computed as follows:

$$I = [\frac{\pi}{4}(d_o^4 - d_i^4)]_{cylinder} + [\frac{\pi}{4}(d_o^4 - d_i^4)]_{deepframe} + [\frac{\pi}{4}(d_o^4 - d_i^4)]_{shallowframe}$$

62

$$J = 2 * I$$

The mass distribution value was the same as the orthotropically smeared mass value. Figure 36 shows the SOR beam model of the stiffened ONR cylinder. The model was subjected to shock wave and the deformation plots were made and shown in Figure 37. The deformation has a similar shape to the discrete model, however closer examination revealed that the deformation was in fact less than the discrete model. This was due to not taking into account the local effects of the deep frames and endplates. Since the mass distribution and cross-sectional properties of the model only accounted for the shallow frames, the model doe not properly show the local mass density and equivalent stiffness of the endplates and deep frames.
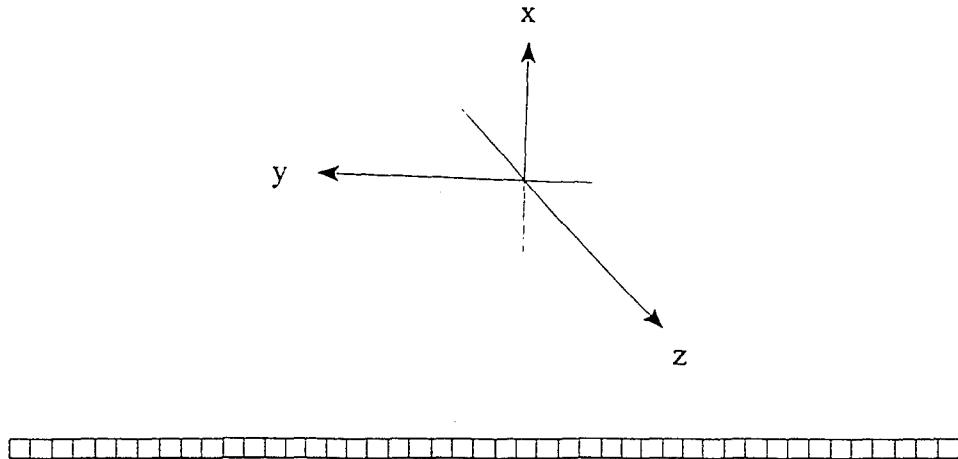
Figure 36. SOR Beam Model of Stiffened ONR Cylinder
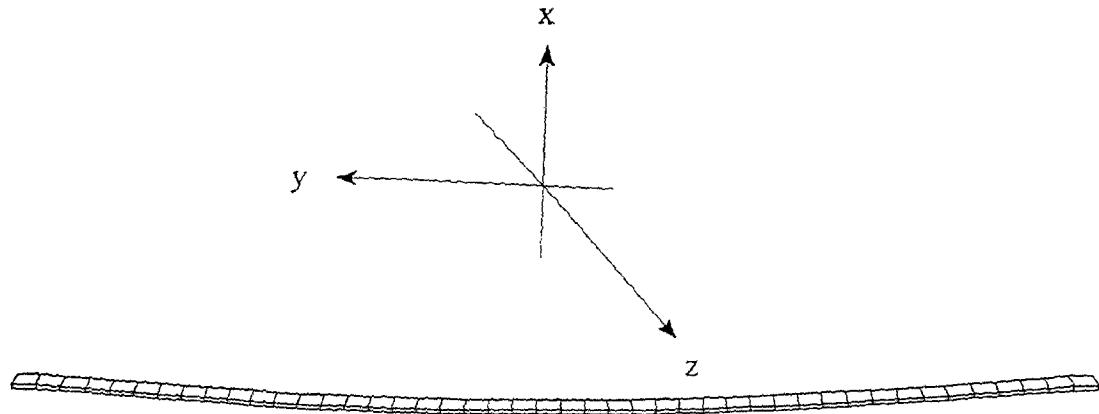
Figure 37a)   State time of 0.5 msec
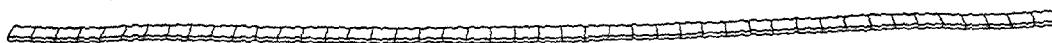
Figure 37b)   State time of 1.0 msec
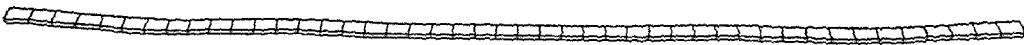
Figure 37c)   State time of 1.5 msec

Figure 37a,b,c. Deformation Results of SOR Beam Model of ONR Cylinder Model

64
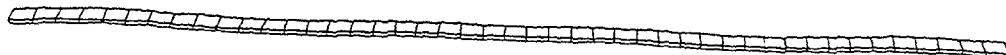
Figure 37d) State time of 2.0 msec
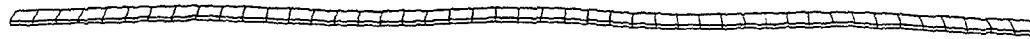
Figure 37e) State time of 2.5 msec
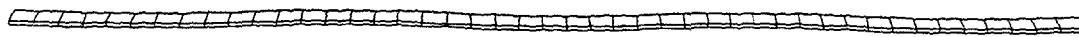
Figure 37f) State time of 3.0 msec

Figure 37 d,e,f. Deformation Results for SOR Beam Model of ONR Cylinder (cont.)

65

To correct the mass distribution and equivalent stiffness of the SOR beam model, the mass density of the deep frames and endplates were inputted at their respective element location in the DYNA3D program. The cross sectional properties were also adjusted locally for the deep frames and endplates. Additionally, the element length for the deep frame section was reduced to two inches which corresponds with the original cylinder dimensions. This allowed for a more accurate local smearing of both mass density and cross-sectional properties for the deep frames. The adjusted SOR Beam model now contains 49 elements and is shown in Figure 38. The global deformation plots are presented in Figure 39. The deformation plots show an improvement from the globally mass smeared 45 SOR beam element model. Figures 40-42 show the axial dynamic responses at the left endplate which support using local smearing of the mass density for deep frames and endplates. Detailed comparisons between discrete and SOR beam model will be presented later in this report. The computational time using the SOR beam model is approximately 1/20 of the discrete model's computational time.
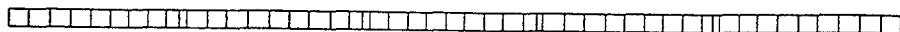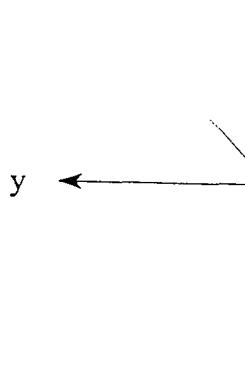
Figure 38. SOR Beam Model With Local Mass Density Smearing

66
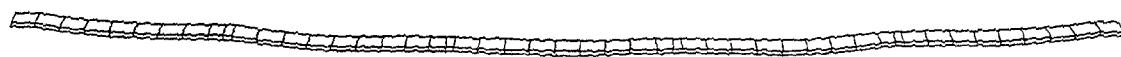
Figure 39a) State time of 0.5 msec
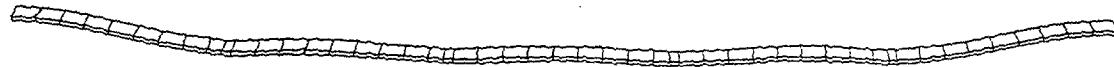
Figure 39b) State time of 1.0 msec
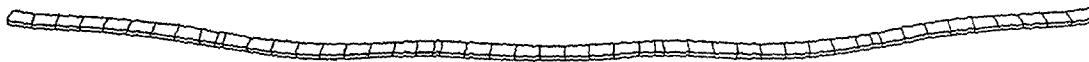
Figure 39c) State time of 1.56 msec

Figure 39a,b,c. Deformation Results For SOR Beam Model With Local Mass Density Smearing of Endplates and Deep Frames

67
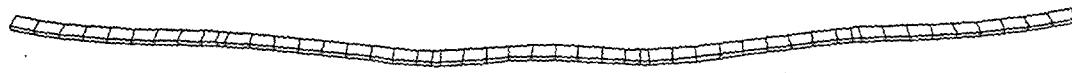
Figure 39d) State time of 2.0 msec

Figure 39e) State time of 2.5 msec
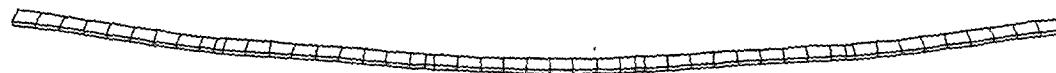
Figure 39f) State time of 3.0 msec

Figure 39d,e,f. Deformation Results for SOR Beam Model With Local Mass Density Smearing of Deep Frames and Endplates (cont.)
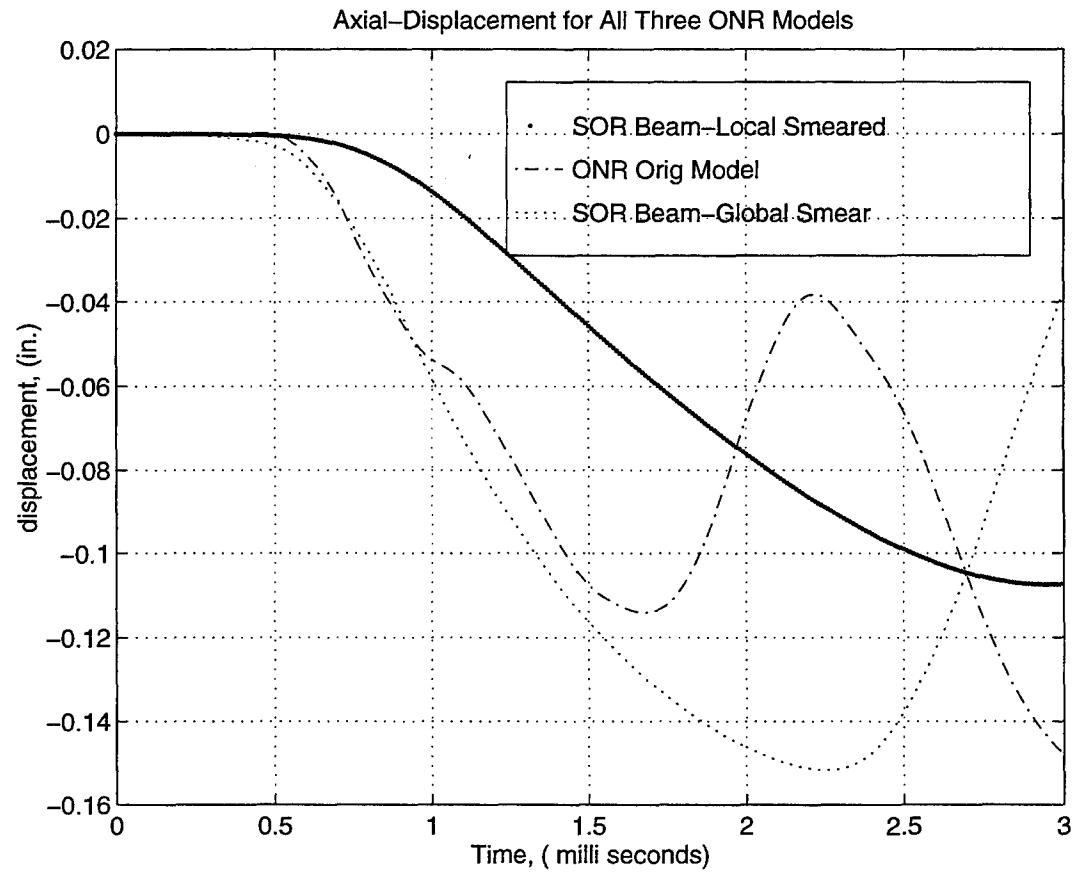
Figure 40. Axial Displacement Response Comparing Local to Global Mass Density Smearing of SOR Beam Model

69
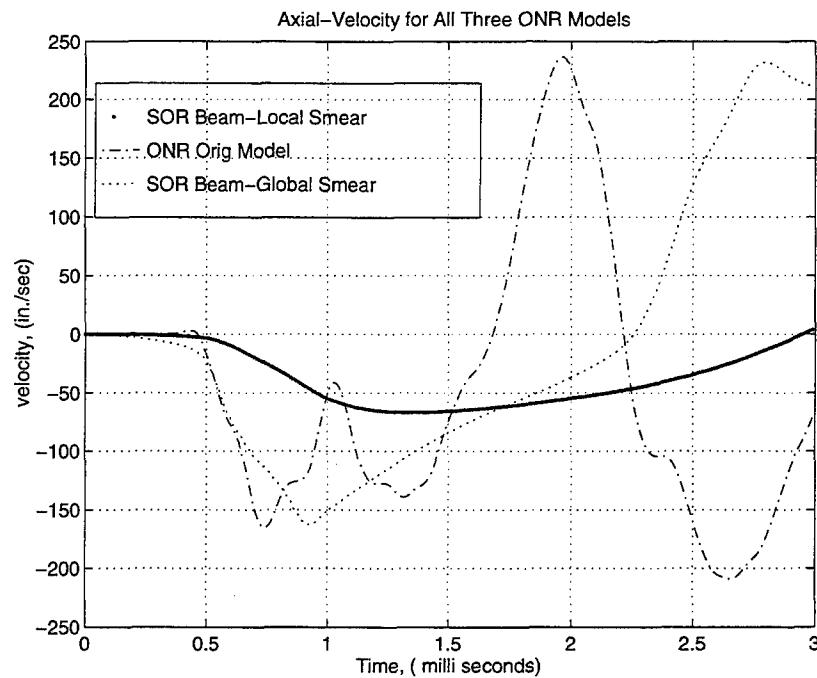
Figure 41. Axial Velocity Response Comparing Local to Global Mass Density Smearing of SOR Beam Model
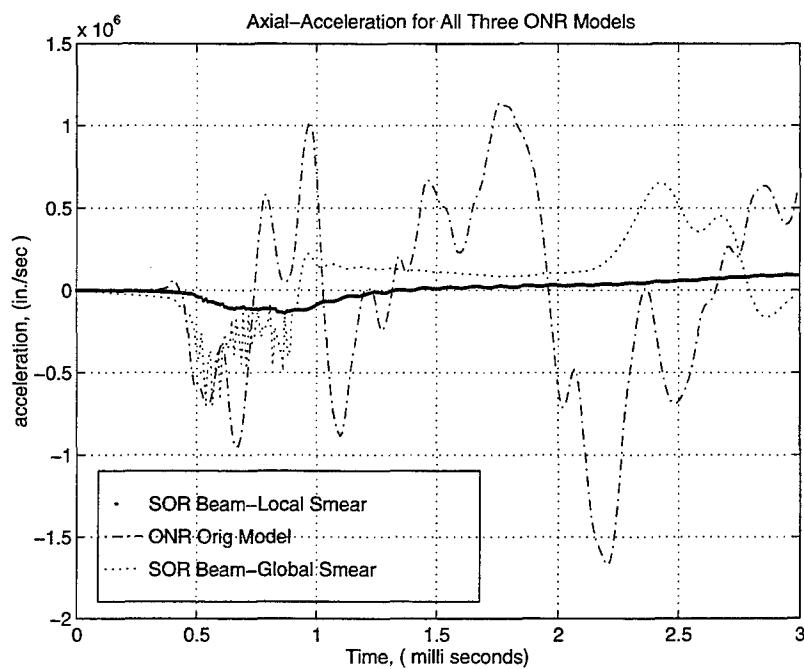
Figure 42. Axial Acceleration Response Comparing Local to Global Mass Density Smearing of SOR Beam Model

70

D.   INTEGRATED SOR BEAM/SHELL MODEL

The integrated SOR beam/shell model incorporates all simplification techniques discussed in this paper. The interface will be modeled using the rigid body material option and local smearing will be done for the beam elements to take into account the mass distribution of the deep frames and endplates. Since it was desired to examine the dynamic responses at one of the deep frames, a beam/shell model was produced with fewer shell elements as shown in Figure 43.   The model contains a total of 450 shell elements and 29 SOR beam elements.   The shell section has the shallow frames and deep frames discretely modeled to produce the fastest computational time. The beam section has the cross-section and second moment of inertia values adjusted to account for the shallow and deep frame stiffeners.   This model will be tested with a charge located off-center as shown in Figure 44. The symmetric test on beam/shell model would have only produced a larger model and hence it was not tested.
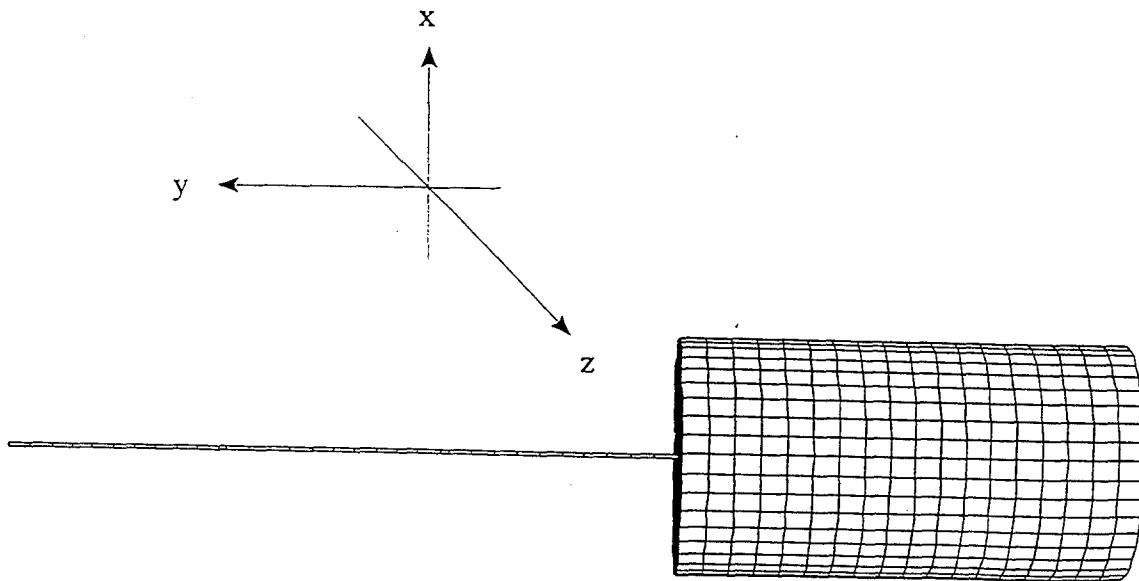
Figure 43. SOR Beam/Shell Model of Stiffened ONR Cylinder

71
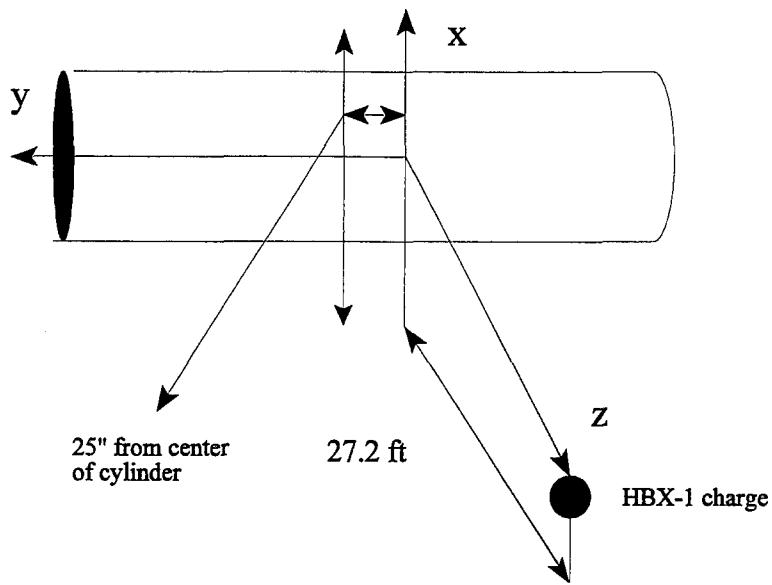
Figure 44. Offcenter Shot Geometry for Integrated Beam/shell Model

The global deformation plots are provided in Figure 45. The deformation plot shows local pinching at deep frames and endplates which is consistent with the discrete model. The rigid body model of the dry endplate produces larger local deformation at the endplate. The overall global deformation appears to be in good agreement with the other three models.

The computational time for the model was about 1/3 of the discrete model which clearly supports using this type of model. It is highly recommended to use as many SOR Beam elements as possible in the model design to reduce the computational time. Detailed analysis at various locations on the beam/shell model will be provided later in this chapter.
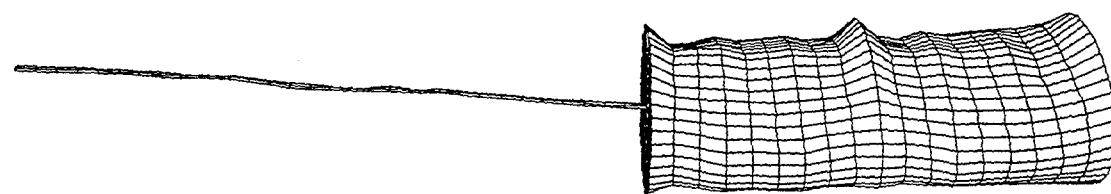
Figure 45a)   State time of 0.5 msec
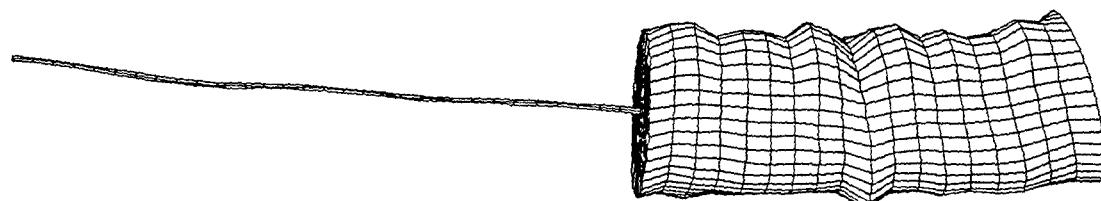
Figure 45b)   State time of 1.0 msec
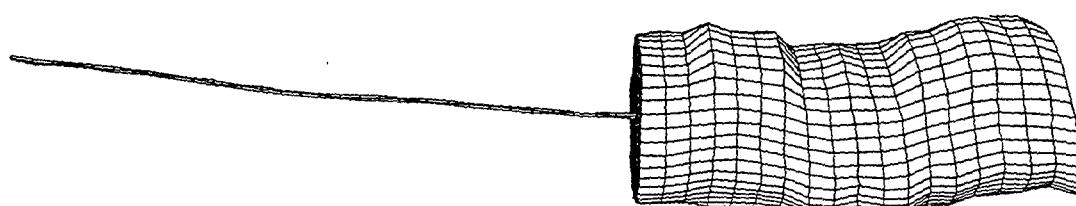
Figure 45c)   State time of 1.5 msec

**Figure 45a,b,c. Deformation Results of Integrated SOR Beam/Shell Model of ONR
Cylinder Model**
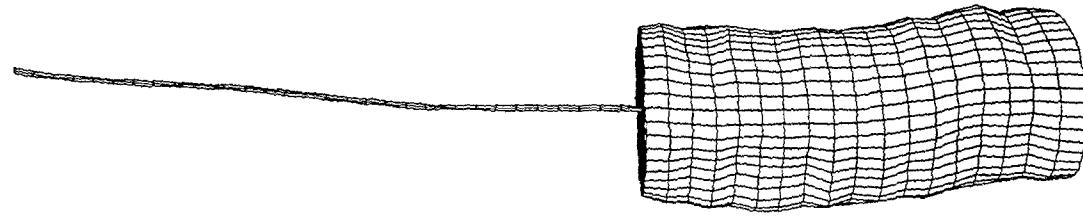
Figure 45d) State time of 2.0 msec
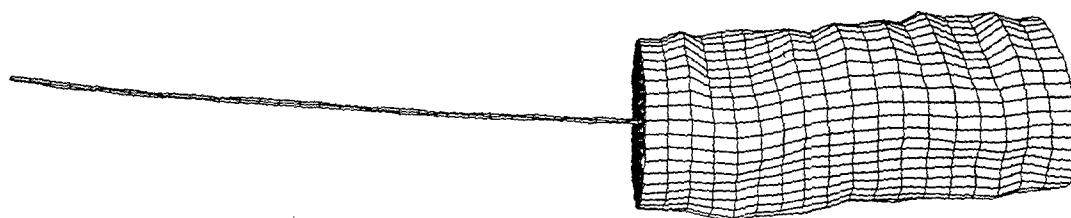
Figure 45e) State time of 2.5 msec
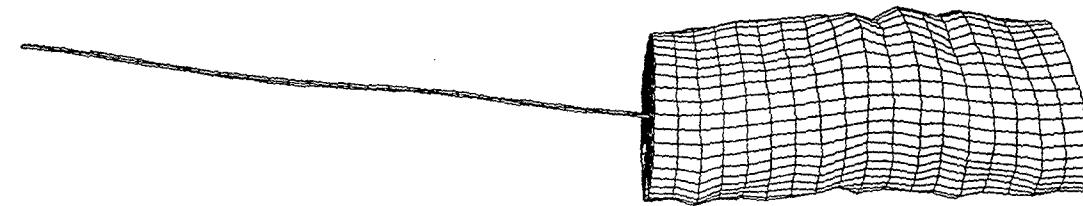
Figure 45f) State time of 3.0 msec

Figure 45d,e,f Deformation Results for Integrated SOR Beam/Shell Model (cont.)

E.   COMPARISON OF DISCRETE TO SIMPLIFIED MODELS

This section will compare the dynamic responses between the fully discretized stiffened ONR cylinder to the simplified models. The analysis will compare both symmetric and off-center geometry for the location of the charge. The displacement, velocity, and acceleration responses will be displayed and discussed.

1.   Comparison Using Symmetric Explosive Testing

The geometry for symmetric testing is the same as Figure 2. The aim of this testing was to simply compare the responses between the orthotropically smeared, beam, and discrete models of the stiffened ONR cylinder. The beam/shell model was not included since more detailed data was taken using off-center shot geometry. The results will aim to compare the responses at a deep frame location, endplates and at the shot location.

Figure 46 compares the overall global longitudinal deformation plots for all four models at state time 0.5 msec and at magnified scale factor of 50. All plots are taken at the same coordinate axis position. There is good agreement except for areas of local deformation at the endplates and deep frames. The deformation plots show that both the smeared stiffener technique and SOR beam element modeling are effective in producing similar global responses. However, it is recommended that use of large numbers of orthotropic shell elements should be avoided since longer computational times occur when using these types of elements due to the decreased critical time step.
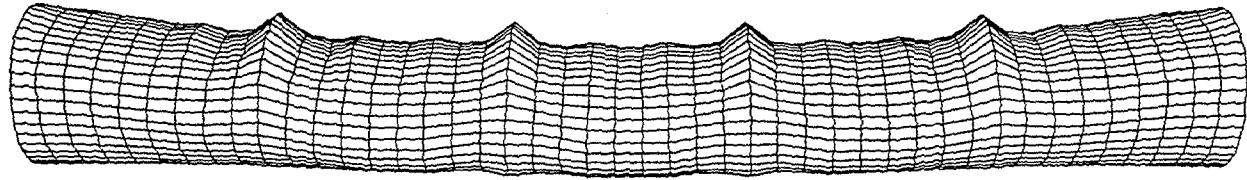
Figure 46a)   ONR Stiffened Cylinder at 0.5 msec
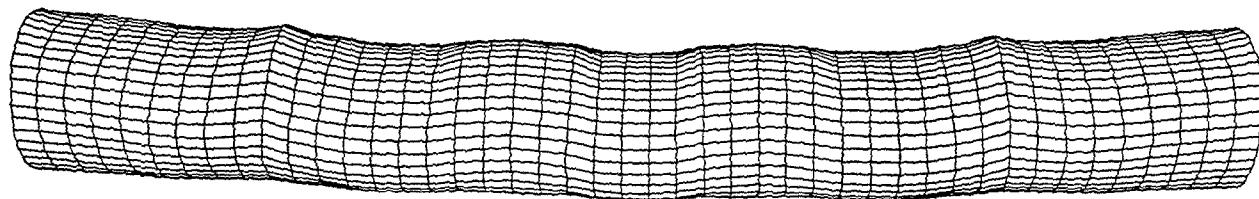
Figure 46b)   Orthotropically Smeared ONR Cylinder at 0.5 msec
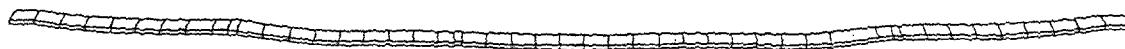
Figure 46c)   SOR Beam Model of ONR Cylinder at 0.5 msec

Figure 46a,b,c Deformation Results for Discrete vs. Simplified Models for ONR
Stiffened Cylinder with Symmetric Underwater Explosion Testing

Next, the axial displacement, velocity, and acceleration plots were made at the left

and right endplate areas to check global motion at the ends. Figures 47-49 shows the

displacement, acceleration of all four models at the left endplate. There is a shift in the

frequency between the SOR beam and discrete model, however the beam's peak magnitude

is very close to the shell's first oscillation peak magnitude. There is significantly less

vibration and acceleration experienced in the beam model as compared to the shell model

which is expected. The orthotropic model compares favorably to the discrete model in shape

but is slightly off in magnitude.
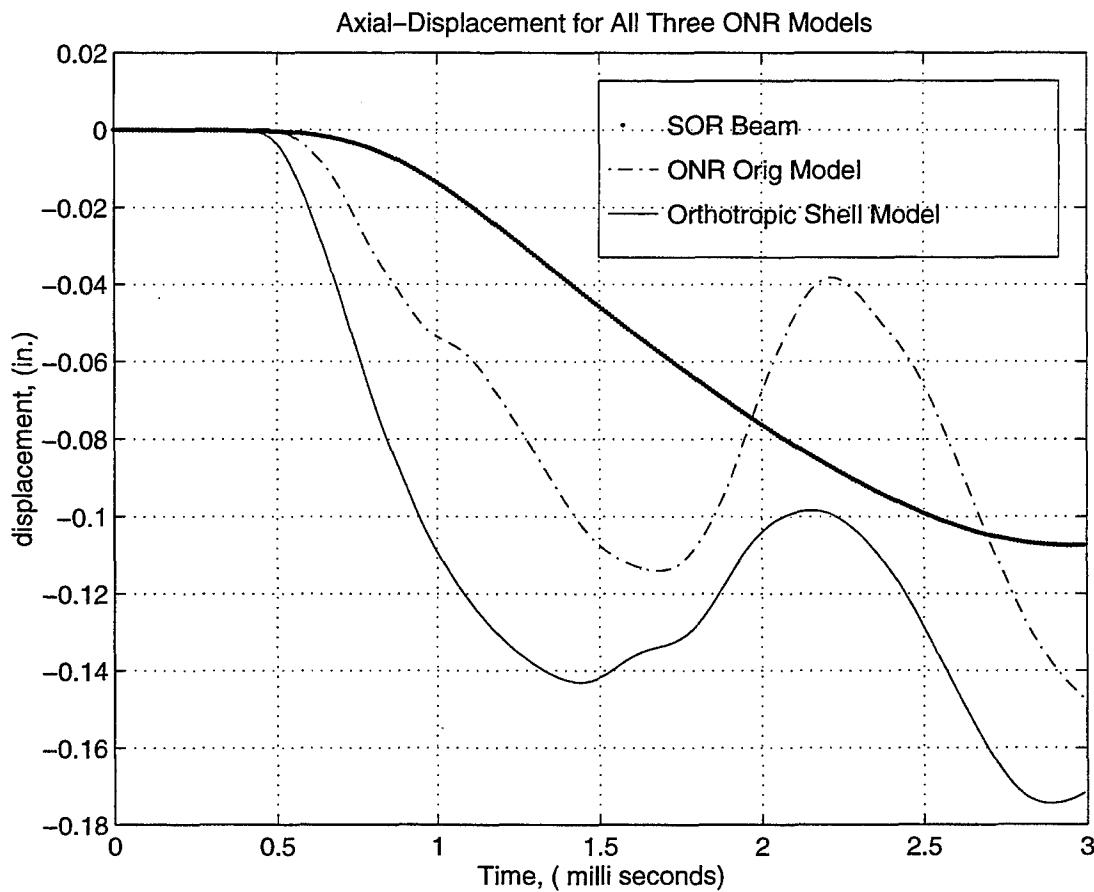
Figure 47. Axial Displacement Comparison at Left Endplate
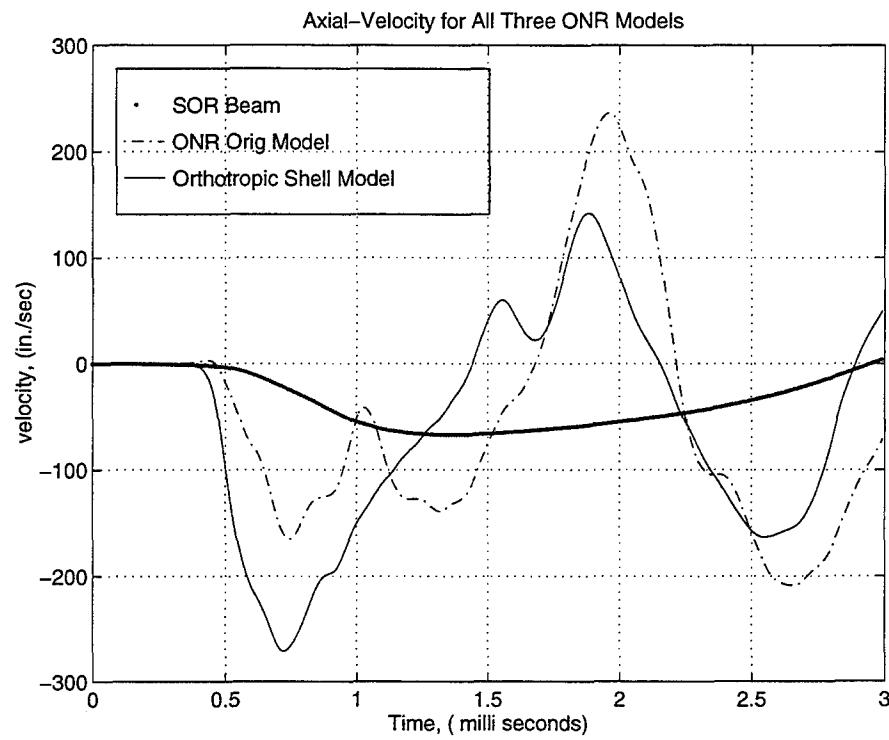
Figure 48. Axial Velocity Comparison At Left Endplate
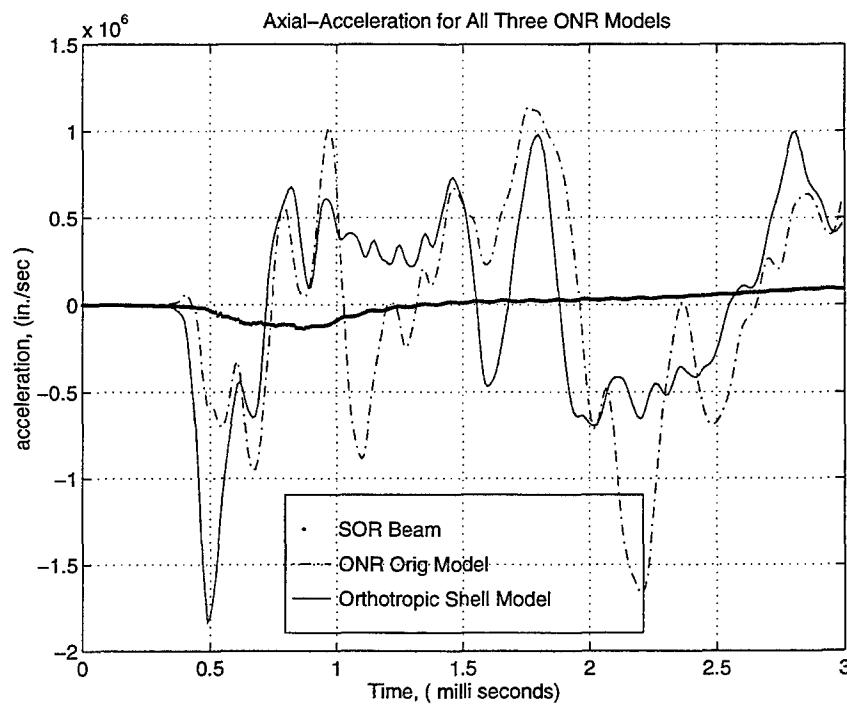
Figure 49. Axial Acceleration Comparison at Left Endplate

78

Figure 50-52 shows the whipping responses for all three models at the shock point (nearest structure point from the charge). The orthotropic shell model and discrete model are very similar in magnitude and shape and have an average error of less than 15%. There is less velocity and acceleration in the SOR Beam model because the local smearing represents the average stiffness which produce fewer oscillations than the original model. The cylindrical models have radial deformation which produce more velocity and acceleration responses as the shock wave progresses through the shell.

Z–Direction Displacement for all Three ONR Models

- SOR Beam
- – – ONR Orig Model
- —— Orthotropic Shell Model

displacement, (in.)

Time, (milli seconds)
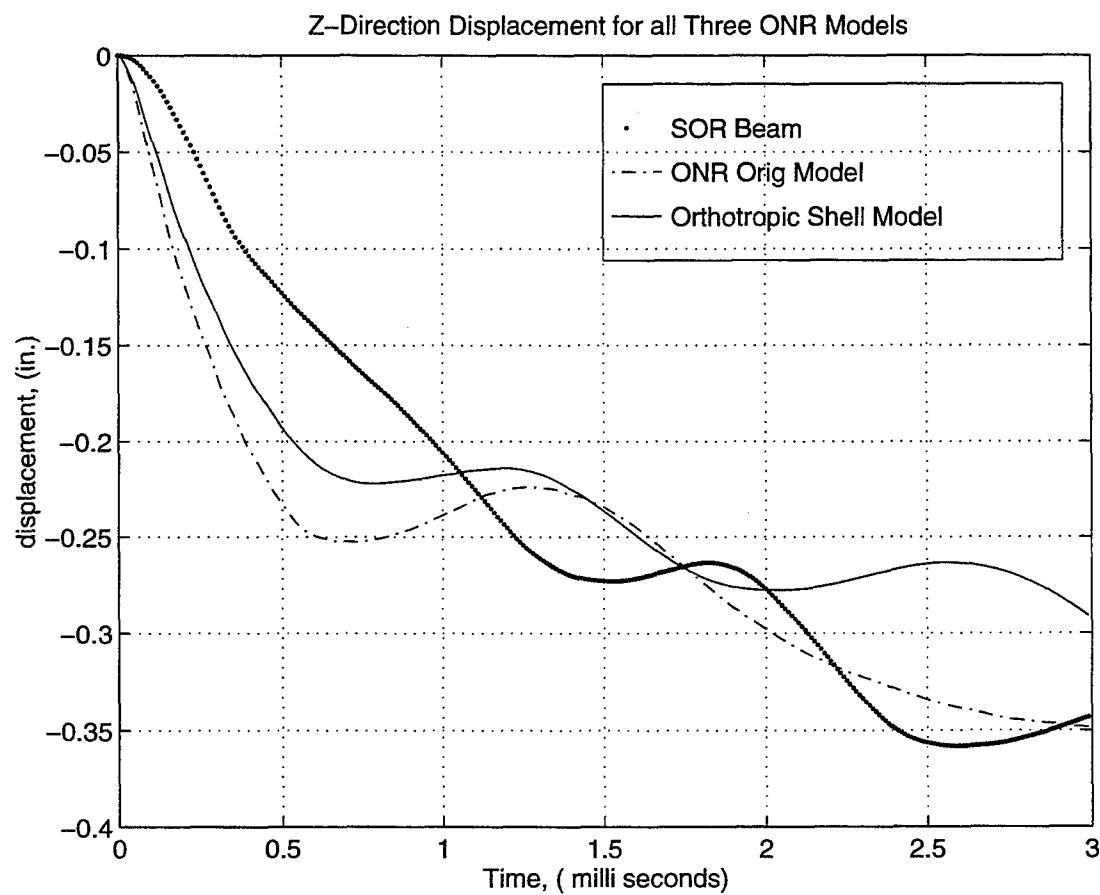
Figure 50. Whipping Displacement Comparison at Shock Point
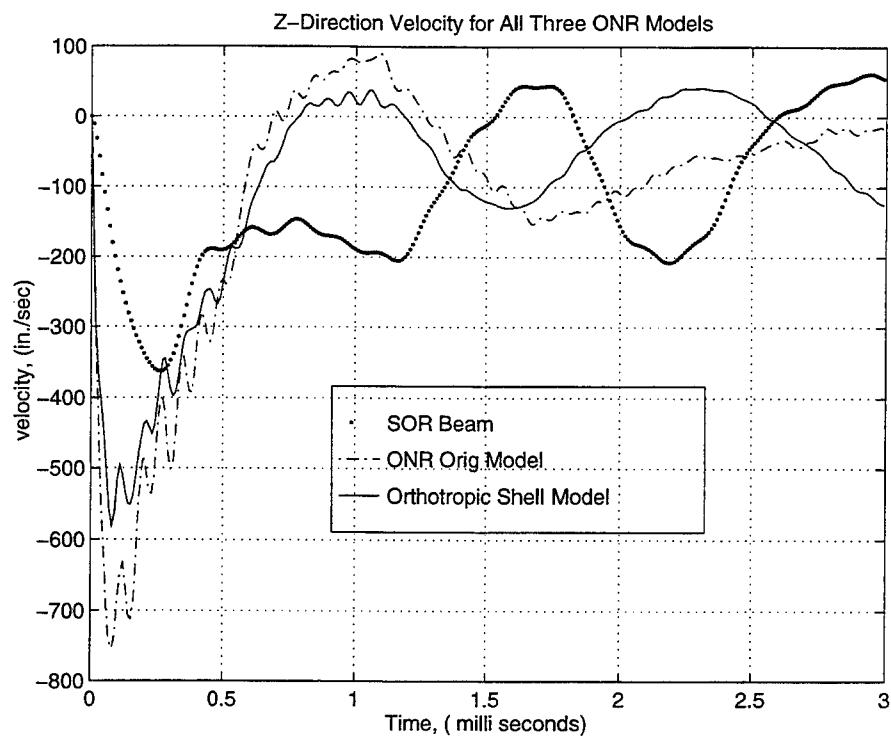
Figure 51. Whipping Velocity Comparison at Shock Point of All Three Models
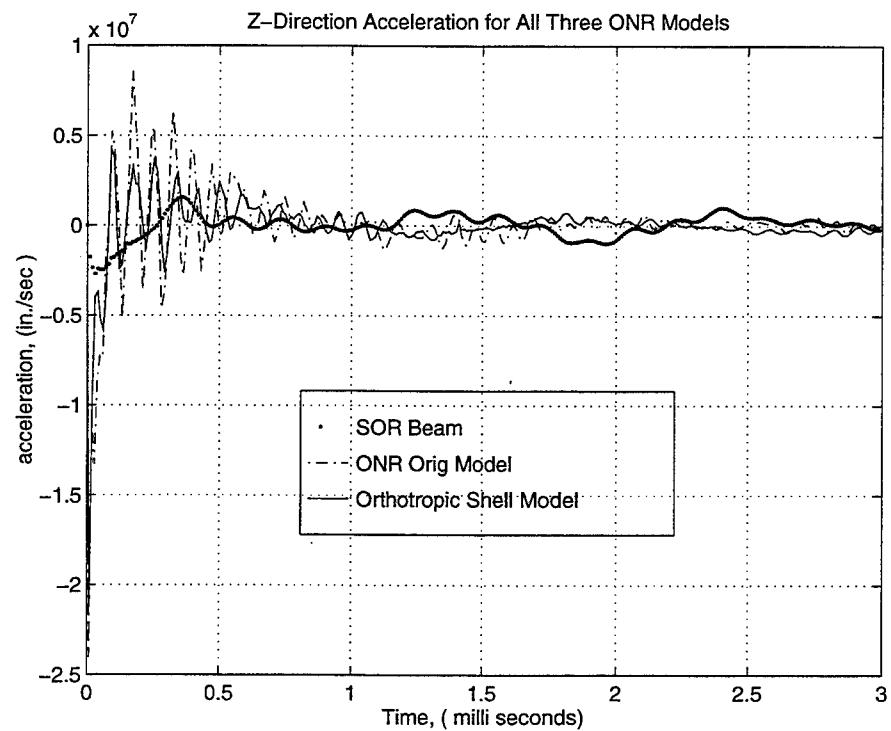
Figure 52. Whipping Acceleration Comparison at Shock Point For All Three Models

80

And finally, the dynamic responses are analyzed at a deep frame on the three models. This location is 75 inches from the center of the cylinder (see Figure 1). Only the whipping motion responses will be presented, however there was good agreement in the axial direction at the deep frame. There was reduced velocity and acceleration in axial direction which was consistent with the endplate responses. Figures 53-55 show the whipping responses at the deep frame. The results show excellent agreement between the discrete and SOR beam model with only slight differences in velocity and acceleartion for reasons previously noted.
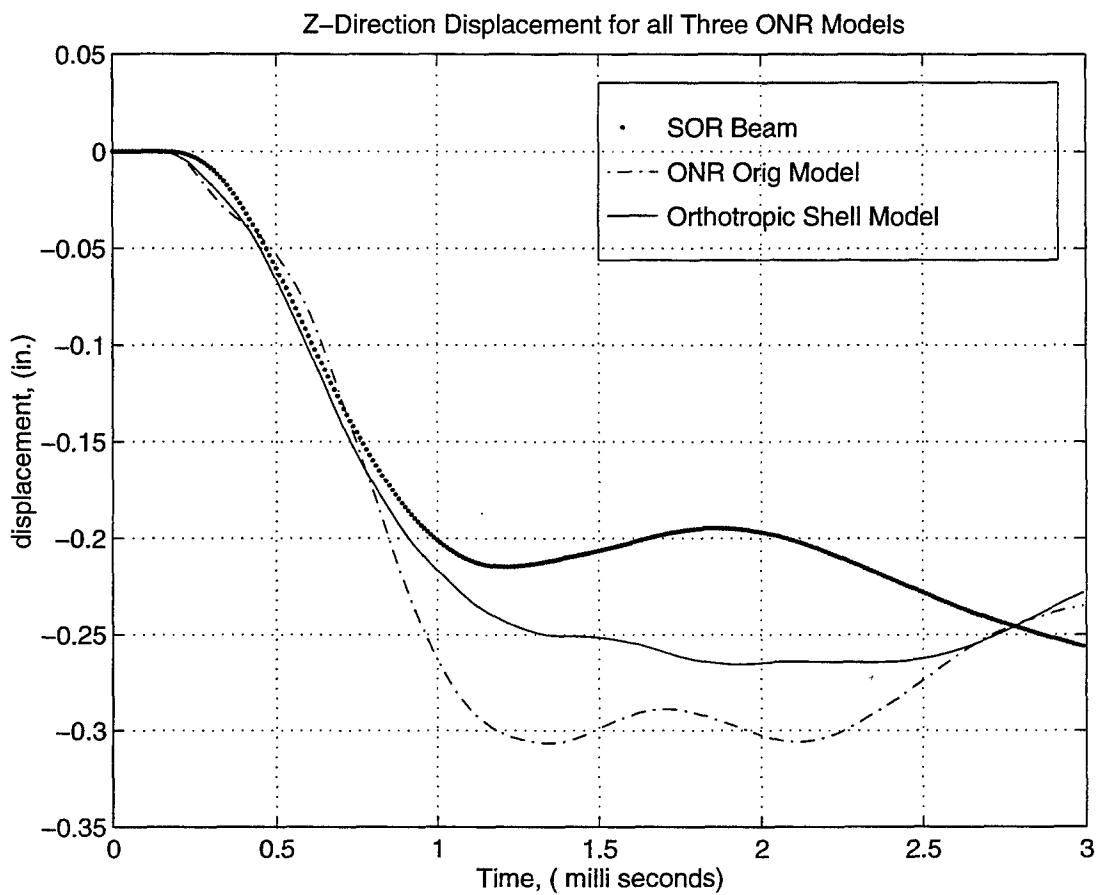
Figure 53. Whipping Displacement Comparison at Deep Frame

81
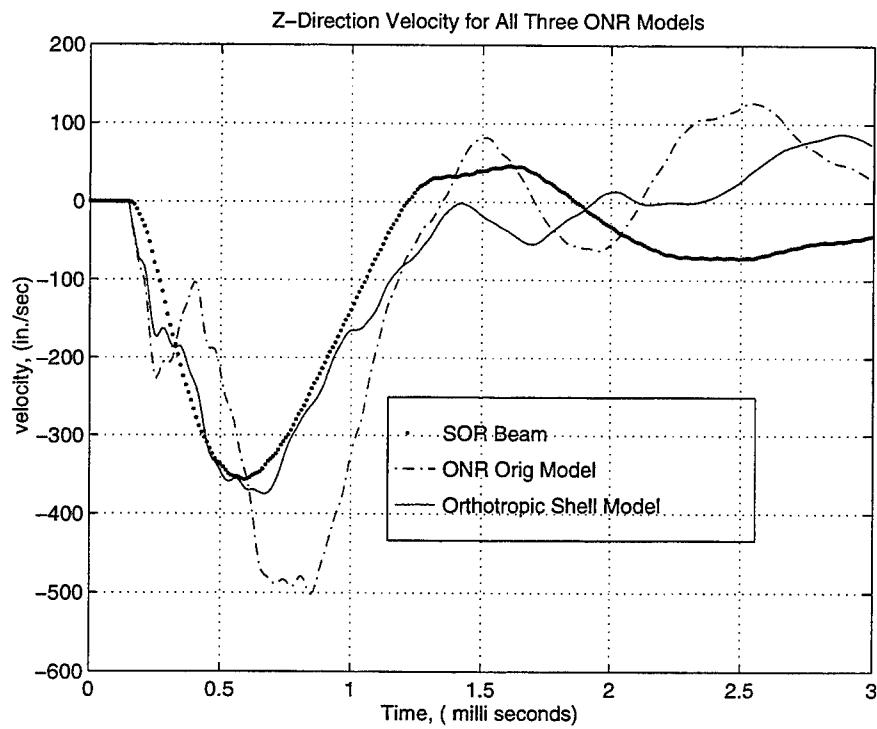
Figure 54. Whipping Velocity Comparison at Deep Frame Location
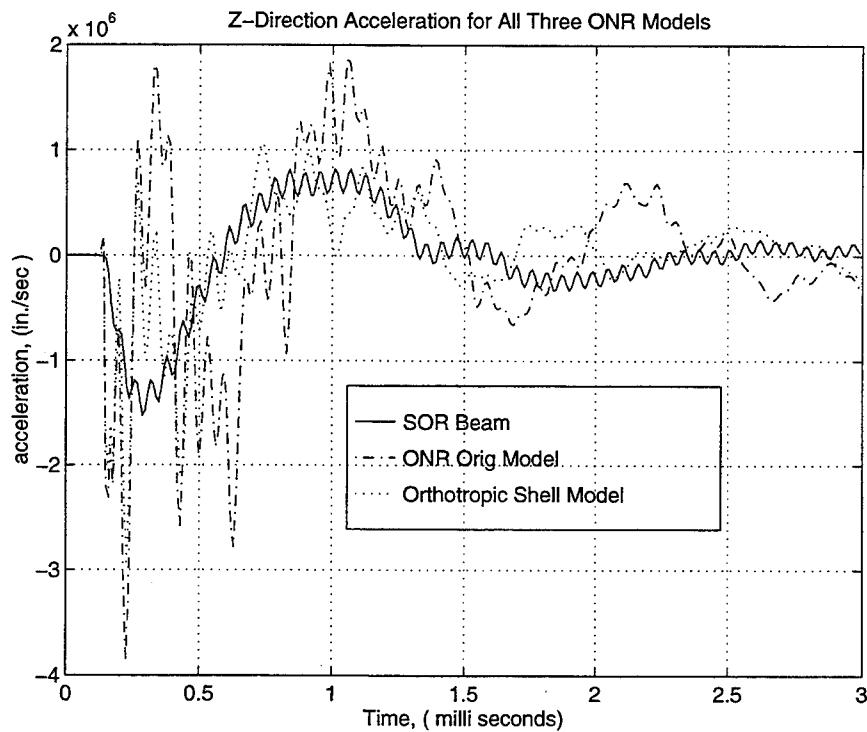
Figure 55. Whipping Acceleration Comparison At Deep Frame

82

Overall, the dynamic responses can support using either SOR beam elements, or orthotropic shell elements. There are tradeoffs to be considered for choosing which technique to use. The orthotropic shell element produces more accurate responses than the SOR beam element, however the SOR beam element's computational time is about 20 times faster than an orthotropic shell elements. When only 49 elements are used for SOR beam model vice 1080 for the orthotropic shell model, there is a big reduction in computational time, but with the reduced accuracy. So both techniques should be considered for analyzing, then if time is the more important factor in the solution, use of SOR beam elements are recommended. Table 4 provides a comparison based on size of model and overall computational time for all three models subjected to symmetrci shock testing.

	Stiffened ONR Cylinder	SOR Beam Model	Orthotropic Smeared Model
Number of Nodes	2064	51	1224
Number of Wet Elements	1080	49	1080
Computational Time (sec)	2070	95	12200

Table 4. Comparison Data For all Three Models of Stiffened ONR Cylinder

2. Comparison Using Off-center Explosive Testing

This section will compare the dynamic responses between the fully discretized stiffened ONR cylinder to the SOR Beam and integrated beam/shell model for an off-center shot geometry. The ONR stiffened model was subjected to the underwater explosion at a location 25 inches to the right of the center of the cylinder (See Figures 1 &44). The SOR beam model was the same model used in the symmetric analysis but subjected to the off-center shock wave. Finally, the integrated beam/shell model was subjected to the same testing. The integrated beam/shell model used the rigid body material option for the endplate and locally smeared the mass distribution and cross-sectional properties of the deep frames and endplates. The orthotropic shell model was not considered due to its lengthy computational time.

Figure 56 is a global deformation plot of all three models at 0.5 msec. The models appear to be in good agreement except for some local pinching at the dry endplate on the integrated beam/shell model. There is however some difference in shape between the SOR beam model and discrete model which is mainly due to applying the average stiffness and mass distribution at the deep frames and endplates. This approximation produces similar results but will not exactly match the discrete model.

Since the main objective in this study was to simplify the original model, it is important to select an area on the shell section of the integrated beam/shell model and compare the responses between discrete and the simplified model. If the responses are in good agreement at this selected area, then further internal structures could be placed inside the shell section of the beam/shell model. Thus, only a small portion of the original model

x

y

z
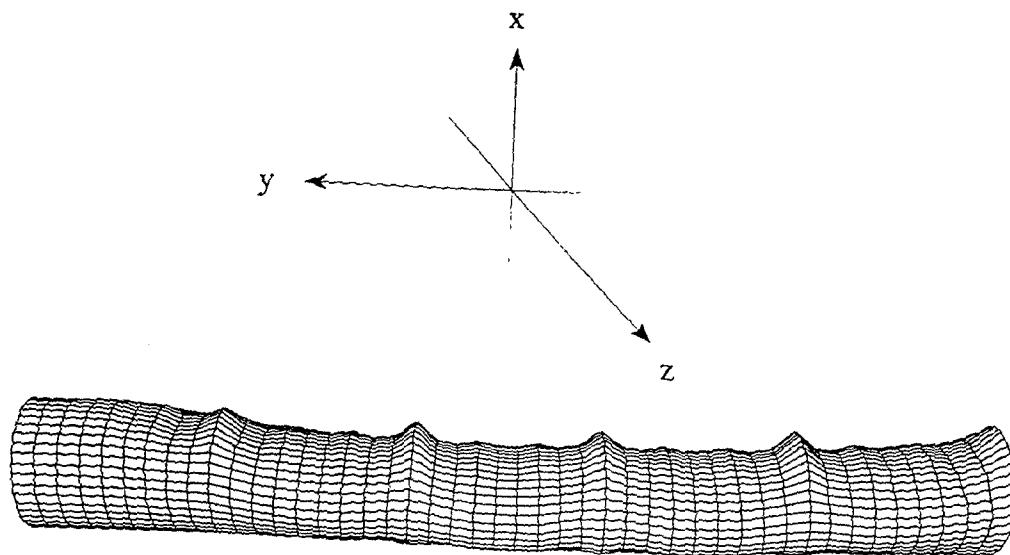
Figure 56a)   ONR Stiffened Cylinder at 0.5 msec
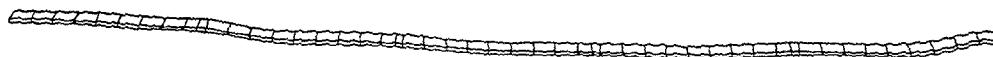
Figure 56b)   SOR Beam Model of ONR Cylinder at 0.5 msec
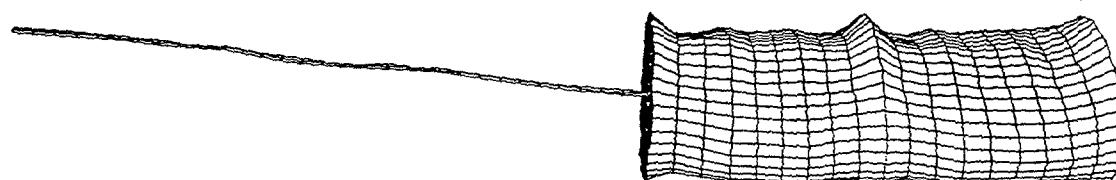
Figure 56c)   Integrated SOR Beam/Shell Model of ONR Cylinder at 0.5 msec

Figure 56a,b,c. Global Deformation Plots - Off-center Explosion Testing for Stiffened
ONR Cylinder

would need to be modeled discretely, and the rest of the model could be modeled with SOR beam elements. The selected area for comparison purposes was the deep frames which is located 75 inches right of the center of the original cylinder and is discretely modeled inside the shell section of the beam/shell model. Both axial and whipping responses were analyzed. Figures 57-59 show the axial responses and Figure 60-62 show the whipping responses at the deep frame. Since the integrated beam/shell model used SOR beam elements for 60% of the longitudinal length of the original cylinder, slightly higher inaccuracies were experienced. The integrated beam/shell model responses are in closer agreement to the discrete model. The whipping responses are very similar in shape and only differ in magnitude due to the use of SOR beam elements. Table 5 is provided for comparing the size and computational time for all three models.

	Stiffened ONR Cylinder	SOR Beam Model	Integrated Beam/shell Model
Number of Nodes	2064	51	942
Number of Wet Elements	1080	49	479
Computational Time (sec)	2070	95	719

Table 5. Comparison Data For all Three Models of Stiffened ONR Cylinder
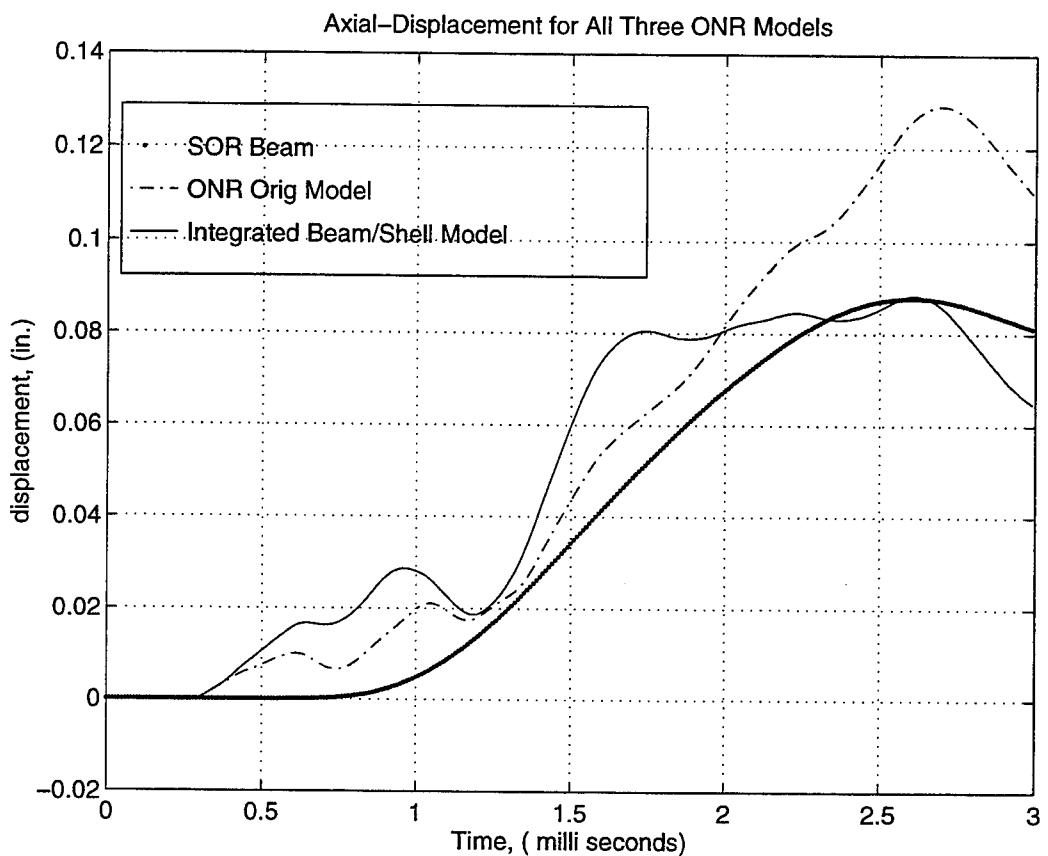
Figure 57. Axial Displacement Comparison At Deep Frame Location

87
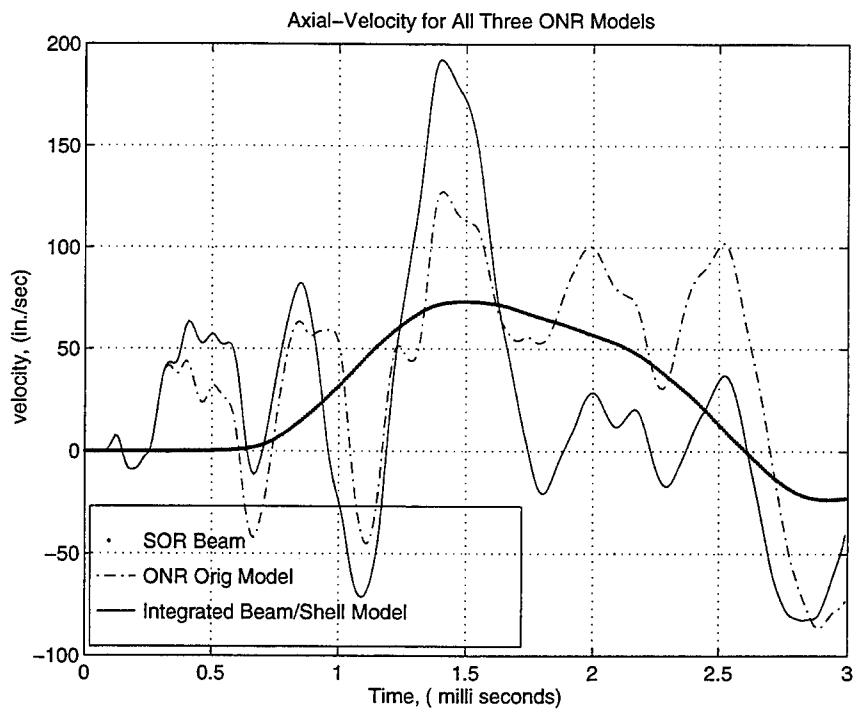
Figure 58. Axial Velocity Comparison At Deep Frame Location
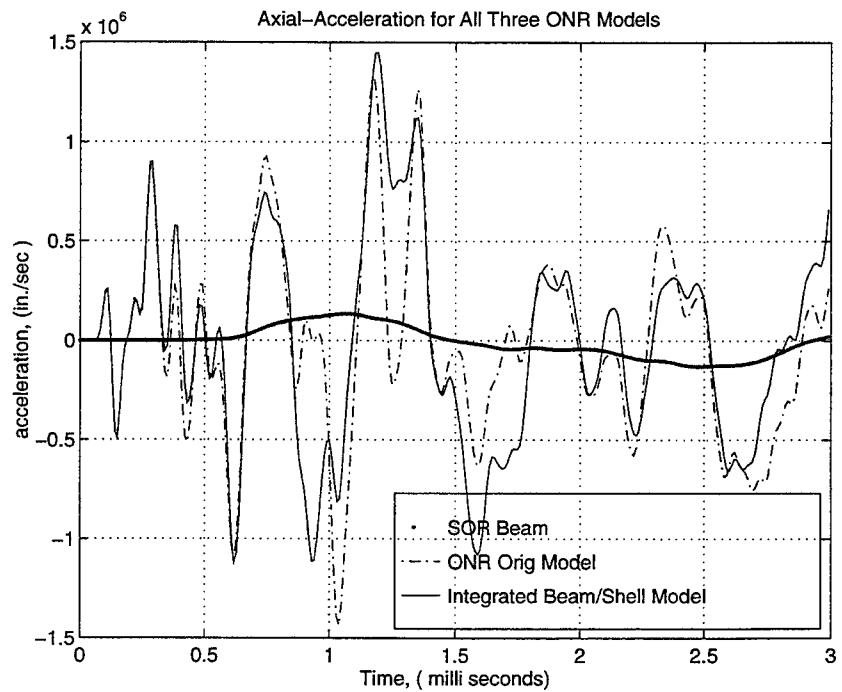
Figure 59. Axial Acceleration Comparison At Deep Frame Location

88
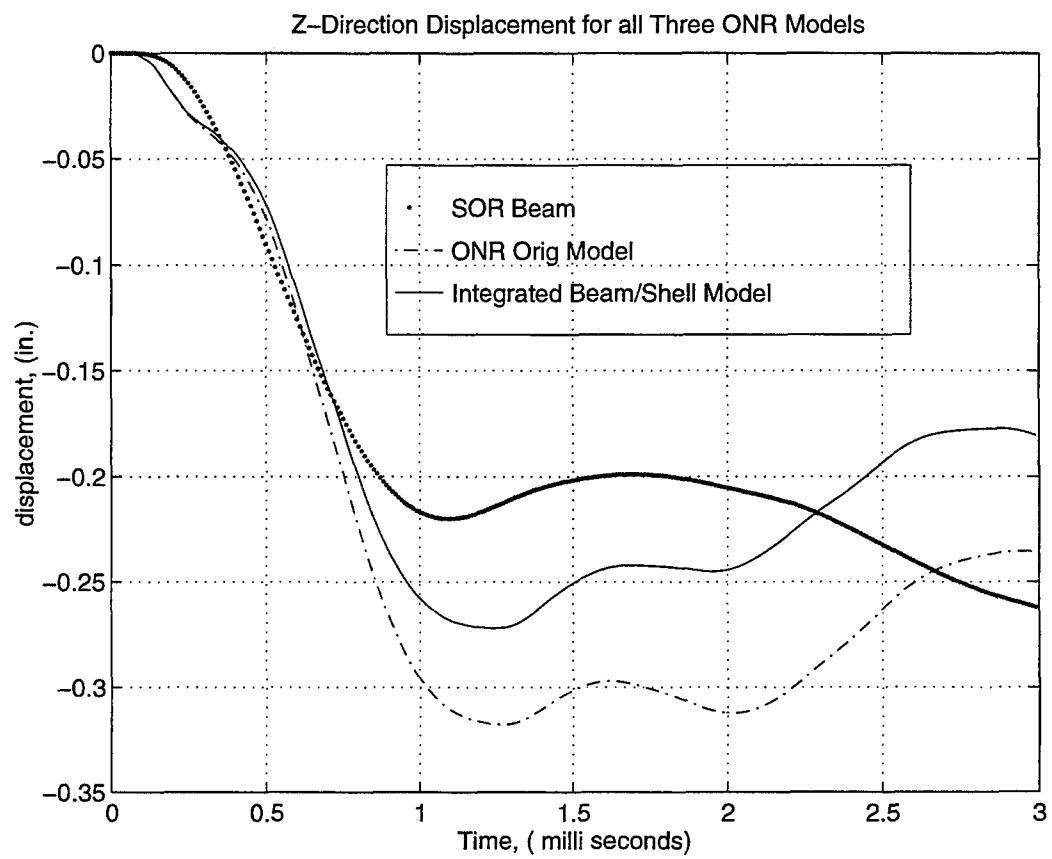
Figure 60. Whipping Motion Comparison At Deep Frame Location

89
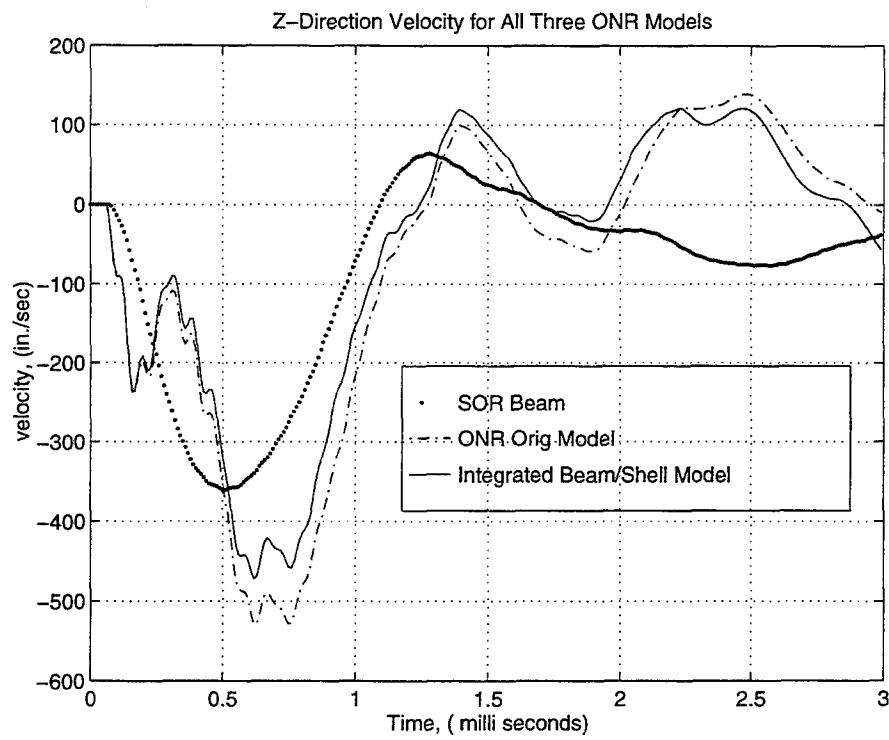
Figure 61. Whipping Motion Comparison At Deep Frame Location
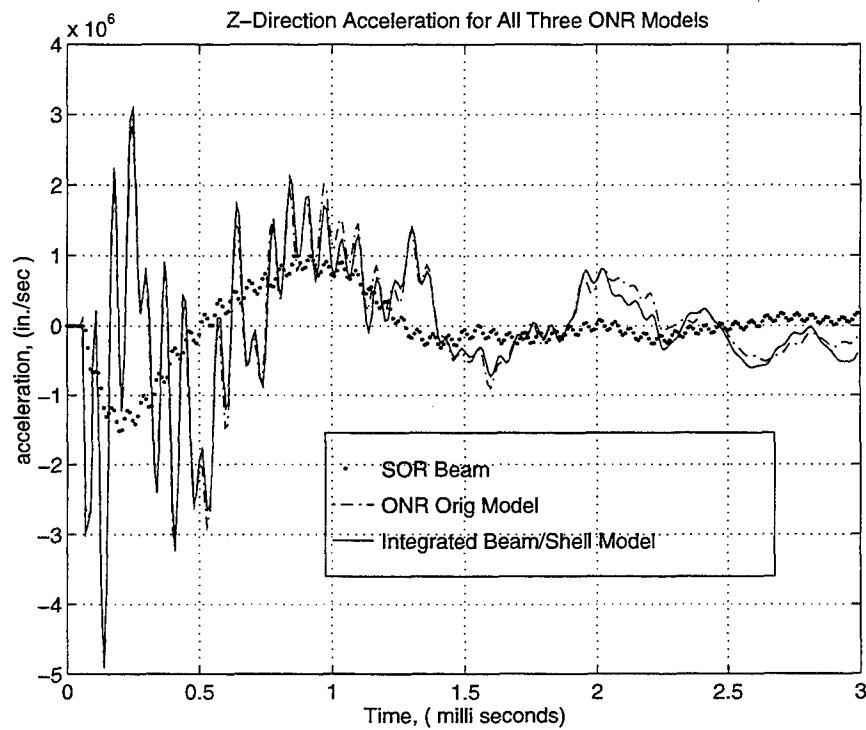
Figure 62. Whipping Motion Comparison At Deep Frame Location

90

Overall, the responses favor using an integrated beam/shell model if additional internal structures require modeling. This model provides both quicker computational time and required accuracy of dynamic responses.

VI. CONCLUSIONS AND RECOMMENDATIONS

Simplified finite element modeling of a stiffened structure is an effective means by which both the design effort and the computational time can be reduced. When the discrete and simplified models are subjected to underwater explosions and closely examined, the results show that either smearing orthotropically or using the SOR beam element produces similar global results. When examining the two models at very discrete points, the results are similar but differ. The orthotropically smeared cylindrical model produces more accurate comparisons, but has a very lengthy computational time. There is more inaccuracy using SOR beam element modeling, however the computational time and design effort is significantly reduced.

Incorporating the advantages of both techniques into an integrated beam/shell model provides the best means of simplifying the discrete model. The results are more favorable and the computational time is still significantly reduced. The interface between the beam and shell section can be modeled as either a dry endplate with smeared properties or by using the rigid body material option within DYNA3D code. It is recommended that the rigid body material option be used since the critical time step is not changed when this material is selected for modeling the interface. The use of the beam/shell model allows further internal structures to be modeled without dramatically increasing both design effort and computational time for numerical solution. If a quick but less accurate solution is needed for a particular problem, then the SOR beam model is recommended.

93

Since no physical experimental data was used in this study, it is highly recommended that a scaled down experimental model be built and tested against the numerical data collected in this study. The present numerical analysis involved using an explicit time integration scheme adopted in DYNA3D code. An additional comparison of the results could be accomplished by using an unconditionally stable implicit time integration technique with another finite element program.

LIST OF REFERENCES

1. Fox, P.K., Shin, Y.S., Kwon, Y.W., "Nonlinear response of Cylindrical Shells to Underwater Explosion: Testing and Numerical Prediction Using VEC/DYNA3D," Report NPS-ME-92-002, Naval Postgraduate School, Monterey, Ca, March 1992.

2. Chisum, J.E. , "Response Prediction for Double Hull Cylinders Subjected to Underwater Shock Loading ," Master's Thesis, Naval Postgraduate School, Monterey, Ca, 1992.

3. Raftenberg, M.N. , "Smearing In An Axisymmetric Finite Element Structural Analysis Application To The GCFR Steam Generator Cavity Closure Plug ," *Nuclear Engineering and Design,* Vol. 40, pp. 215-224, 1977.

4. Pitarresi, J. M., Caletka, D.V., Caldwell, R., Smith, D.E., "The "Smeared" Property Technique for the FE Vibration Analysis of Printed Circuit Cards," *Journal of Electronic Packaging,* Vol. 113, pp. 250-257, September, 1991.

5. Hallquist, J.O., and Stillman, D.W., "VEC/DYNA3D users Manual (Nonlinear Dynamic Analysis of Structures in Three Dimensions)." Livermore Software Technology Corporation Report 1018, 1990.

6. Deruntz, J.A. Jr., "The Underwater Shock Analysis Code and its Applications," Paper Presented at the 60th Shock and Vibration Symposium, Virginia Beach, Va., 1989.

7. Geers, T.L., "Residual Potential and Approximate Methods for Three-Dimensional Fluid-Structure Interaction Problem," *Journal of the Acoustic Society of America,* Vol. 49, pp. 1505-1510, 1971.

8. Shin, Y.S., Geers, T.L. "Response of Marine Structures to Underwater Explosion," Course Notes For Underwater Shock Analysis, Naval Postgraduate School, Monterey, Ca, 1993.

9. Timoshenko, S., Woinowsky-Kreiger, S., "Theory of Plate and Shells", McGraw-Hill Book Company, New York, NY., 1959.

APPENDIX A

INPUT FILES FOR SOR BEAM MODEL

The following input files consist of ingrid which creates the geometric model

for DYNA3D, flumas, augmat, and timint. The flumas, augmat and timint files

provide input for the USA program. These files are for SOR Beam Model Only.

```
model.beam                                                        88 large
      3          51            0          49        0         0            0
      0    0     0     0      0
                  0            0       e20.9                    51
      1    0     0     0      0     0      0    0    0    0    0    0   0   0   0   0
  3.006E-03 1.000E+03 1.000E-05              .000E+00  .000E+00    0         .000E+00
      0    0     0     0      0     1      0    0         0         0    0    0   0
      0    0  .000E+00
      0    0     0
      1   19.5710E-04     0     0 .0000E+00    0 .0000E+00 .0000E+00     1     0     2
material type # 1  (elastic)
  2.900E+07  .000E+00   .000E+00   .000E+00   .000E+00   .000E+00   .000E+00   .000E+00
  3.000E-01  .000E+00   .000E+00   .000E+00   .000E+00   .000E+00   .000E+00   .000E+00
   .000E+00  .000E+00   .000E+00   .000E+00   .000E+00   .000E+00   .000E+00   .000E+00
   .000E+00  .000E+00   .000E+00   .000E+00   .000E+00   .000E+00   .000E+00   .000E+00
   .000E+00  .000E+00   .000E+00   .000E+00   .000E+00   .000E+00   .000E+00   .000E+00
   .000E+00  .000E+00   .000E+00   .000E+00   .000E+00   .000E+00   .000E+00   .000E+00
section properties
              0
  1.970E+01 4.541E+03 4.541E+03 9.082E+03 1.970E+01   .000E+00
      2   18.2692E-04     0     0 .0000E+00    0 .0000E+00 .0000E+00     1     0     2
material type # 1  (elastic)
  2.900E+00  .000E+00   .000E+00   .000E+00   .000E+00   .000E+00   .000E+00   .000E+00
  3.000E-01  .000E+00   .000E+00   .000E+00   .000E+00   .000E+00   .000E+00   .000E+00
   .000E+00  .000E+00   .000E+00   .000E+00   .000E+00   .000E+00   .000E+00   .000E+00
   .000E+00  .000E+00   .000E+00   .000E+00   .000E+00   .000E+00   .000E+00   .000E+00
   .000E+00  .000E+00   .000E+00   .000E+00   .000E+00   .000E+00   .000E+00   .000E+00
   .000E+00  .000E+00   .000E+00   .000E+00   .000E+00   .000E+00   .000E+00   .000E+00
section properties
              0
  3.970E+02 3.614E+03 3.614E+03 7.227E+03 3.970E+02   .000E+00
      3   11.0473E-03     0     0 .0000E+00    0 .0000E+00 .0000E+00     1     0     2
material type # 1  (elastic)
  2.900E+07  .000E+00   .000E+00   .000E+00   .000E+00   .000E+00   .000E+00   .000E+00
  3.000E-01  .000E+00   .000E+00   .000E+00   .000E+00   .000E+00   .000E+00   .000E+00
   .000E+00  .000E+00   .000E+00   .000E+00   .000E+00   .000E+00   .000E+00   .000E+00
   .000E+00  .000E+00   .000E+00   .000E+00   .000E+00   .000E+00   .000E+00   .000E+00
   .000E+00  .000E+00   .000E+00   .000E+00   .000E+00   .000E+00   .000E+00   .000E+00
   .000E+00  .000E+00   .000E+00   .000E+00   .000E+00   .000E+00   .000E+00   .000E+00
section properties
              0
  8.880E+02 6.275E+04 6.275E+04 1.255E+05 8.880E+02   .000E+00
            1    0.  .0000000000000E+00  .1265625000000E+03  .0000000000000E+00    0.
            2    0.  .0000000000000E+00  .1209375000000E+03  .0000000000000E+00    0.
            3    0.  .0000000000000E+00  .1153125000000E+03  .0000000000000E+00    0.
            4    0.  .0000000000000E+00  .1096875000000E+03  .0000000000000E+00    0.
            5    0.  .0000000000000E+00  .1040625000000E+03  .0000000000000E+00    0.
            6    0.  .0000000000000E+00  .9843750000000E+02  .0000000000000E+00    0.
            7    0.  .0000000000000E+00  .9281250000000E+02  .0000000000000E+00    0.
            8    0.  .0000000000000E+00  .8718750000000E+02  .0000000000000E+00    0.
            9    0.  .0000000000000E+00  .8156250000000E+02  .0000000000000E+00    0.
           10    0.  .0000000000000E+00  .7793750000000E+02  .0000000000000E+00    0.
           11    0.  .0000000000000E+00  .7593750000000E+02  .0000000000000E+00    0.
           12    0.  .0000000000000E+00  .7031250000000E+02  .0000000000000E+00    0.
           13    0.  .0000000000000E+00  .6468750000000E+02  .0000000000000E+00    0.
           14    0.  .0000000000000E+00  .5906250000000E+02  .0000000000000E+00    0.
           15    0.  .0000000000000E+00  .5343750000000E+02  .0000000000000E+00    0.
           16    0.  .0000000000000E+00  .4781250000000E+02  .0000000000000E+00    0.
           17    0.  .0000000000000E+00  .4218750000000E+02  .0000000000000E+00    0.
           18    0.  .0000000000000E+00  .3656250000000E+02  .0000000000000E+00    0.
```

97

```
19    0.    .0000000000000E+00    .3093750000000E+02    .0000000000000E+00    0.
20    0.    .0000000000000E+00    .2731250000000E+02    .0000000000000E+00    0.
21    0.    .0000000000000E+00    .2531250000000E+02    .0000000000000E+00    0.
22    0.    .0000000000000E+00    .1968750000000E+02    .0000000000000E+00    0.
23    0.    .0000000000000E+00    .1406250000000E+02    .0000000000000E+00    0.
24    0.    .0000000000000E+00    .0843750000000E+02    .0000000000000E+00    0.
25    0.    .0000000000000E+00    .0281250000000E+02    .0000000000000E+00    0.
26    0.    .0000000000000E+00   -.0281250000000E+02    .0000000000000E+00    0.
27    0.    .0000000000000E+00   -.0843750000000E+02    .0000000000000E+00    0.
28    0.    .0000000000000E+00   -.1406250000000E+02    .0000000000000E+00    0.
29    0.    .0000000000000E+00   -.1968750000000E+02    .0000000000000E+00    0.
30    0.    .0000000000000E+00   -.2331250000000E+02    .0000000000000E+00    0.
31    0.    .0000000000000E+00   -.2531250000000E+02    .0000000000000E+00    0.
32    0.    .0000000000000E+00   -.3093750000000E+02    .0000000000000E+00    0.
33    0.    .0000000000000E+00   -.3656250000000E+02    .0000000000000E+00    0.
34    0.    .0000000000000E+00   -.4218750000000E+02    .0000000000000E+00    0.
35    0.    .0000000000000E+00   -.4781250000000E+02    .0000000000000E+00    0.
36    0.    .0000000000000E+00   -.5343750000000E+02    .0000000000000E+00    0.
37    0.    .0000000000000E+00   -.5906250000000E+02    .0000000000000E+00    0.
38    0.    .0000000000000E+00   -.6468750000000E+02    .0000000000000E+00    0.
39    0.    .0000000000000E+00   -.7031250000000E+02    .0000000000000E+00    0.
40    0.    .0000000000000E+00   -.7393750000000E+02    .0000000000000E+00    0.
41    0.    .0000000000000E+00   -.7593750000000E+02    .0000000000000E+00    0.
42    0.    .0000000000000E+00   -.8156250000000E+02    .0000000000000E+00    0.
43    0.    .0000000000000E+00   -.8718750000000E+02    .0000000000000E+00    0.
44    0.    .0000000000000E+00   -.9281250000000E+02    .0000000000000E+00    0.
45    0.    .0000000000000E+00   -.9843750000000E+02    .0000000000000E+00    0.
46    0.    .0000000000000E+00   -.1040625000000E+03    .0000000000000E+00    0.
47    0.    .0000000000000E+00   -.1096875000000E+03    .0000000000000E+00    0.
48    0.    .0000000000000E+00   -.1153125000000E+03    .0000000000000E+00    0.
49    0.    .0000000000000E+00   -.1209375000000E+03    .0000000000000E+00    0.
50    0.    .0000000000000E+00   -.1265625060000E+03    .0000000000000E+00    0.
51    7.    .1000000000000E+02    .1265625000000E+03    .0000000000000E+00    7.
*
*---------------- ELEMENT CARDS FOR BEAM ELEMENTS ----------------*
*
 1    3    1     2    51
 2    1    2     3    51
 3    1    3     4    51
 4    1    4     5    51
 5    1    5     6    51
 6    1    6     7    51
 7    1    7     8    51
 8    1    8     9    51
 9    1    9    10    51
10    2   10    11    51
11    1   11    12    51
12    1   12    13    51
13    1   13    14    51
14    1   14    15    51
15    1   15    16    51
16    1   16    17    51
17    1   17    18    51
18    1   18    19    51
19    1   19    20    51
20    2   20    21    51
21    1   21    22    51
22    1   22    23    51
23    1   23    24    51
24    1   24    25    51
```

98

```
25    1    25    26    51
26    1    26    27    51
27    1    27    28    51
28    1    28    29    51
29    1    29    30    51
30    2    30    31    51
31    1    31    32    51
32    1    32    33    51
33    1    33    34    51
34    1    34    35    51
35    1    35    36    51
36    1    36    37    51
37    1    37    38    51
38    1    38    39    51
39    1    39    40    51
40    2    40    41    51
41    1    41    42    51
42    1    42    43    51
43    1    43    44    51
44    1    44    45    51
45    1    45    46    51
46    1    46    47    51
47    1    47    48    51
48    1    48    49    51
49    3    49    50    51
*
*---------------------- LOAD CURVE DEFINITIONS ----------------------*
*
     1     2
  .000E+00 2.000E-06
 1.000E+00 2.000E-06
```

```
FLUMAS DATA FOR MODEL BEAMONR
beam.flu beam.geo strnam.dat beam.daa  $  FLUNAM  GEONAM  GRDNAM  DAANAM
T T T T                                $  PRTGMT  PRTTRN  PRTAMF  CALCAM
T F F F                                $  EIGMAF  TWODIM  HAFMOD  QUAMOD
F F F T                                $  PCHCDS  NASTAM  STOMAS  STOINV
F F F F       .                        $  FRWTFL  FRWTGE  FRWTGR  FRESUR
F T F F                                $  RENUMB  STOGMT  ROTGEO  ROTQUA
F F F F                                $  PRTCOE  STRMAS  SPHERE  ROTSYM
F F F F                                $  OCTMOD  CAVFLU  FRWTFV  INTCAV
DYNA                                   $  MAINKY
0 51 0 0                               $  NSTRC   NSTRF   NGEN    NGENF
1  0  0                                $  NBRA    NCYL    NCAV
0  1  1  2  0                          $  NHAS    NHAF    NHAI    NFUN
51                                     $  NSEG
0                       .              $  NCIR
9.356E-05   57600.0                    $  RHO     CEE
5                                      $  NVEC
1    50  16.8   16.8  3                $  N1      N2      R1    R2    NSET
1     1   0.    16.8  1
1    50  16.8   16.8 49
50   50  16.8    0.   1
```

99

```
AUGMAT DATA FOR MODEL.BEAMONR
strnam.dat beam.daa beam.geo beam.pre    $  STRNAM  FLUNAM  GEONAM  PRENAM
F F F F                                  $  FRWTGE  FRWTST  FRWTFL  PLNWAV
F T F T                                $  FLUSKY  DAAFRM  SYMCON  DOFTAB
F F F T                                $  PRTGMT  PRTTRN  PRTSTF  PRTAUG
F F F F                                $  MODTRN  STRLCL  INTWAT  CFADYN
F
DYNA                                   $  MAINKY
0.0                                     $  NTYPDA
51 153 3 3
```

```
r≈d3dump
TIME INTEGRATION DATA FOR MODEL BEAMONR
beam.pre beam.pos        $  PRENAM  POSNAM
beam.rst                 $  RESNAM
F F F                    $  BUBPUL  REFSEC  FLUMEN
T F F F                  $  EXPWAV  SPLINE  VARLIN  PACKET
F T F F                  $  HYPERB  EXPLOS  DOUBDC  VELIMP
1                        $  NCHARG
0.0                      $  HYDPRE
0.0 -25.3125 326.4       $  XC   YC    ZC
0.0 -25.3125  16.813     $  SX   SY    SZ
101                      $  JPHIST
1.0                      $  PNORM
14.0E-06                 $  DTHIST
1                        $  CHGTYP
60.0   25.8  10.0        $  WEIGHT  SLANT   CHGDEP
1 0                      $  NTINT   NCHGAL
0.0   2.00E-06           $  STRTIM  DELTIM
5000   5000              $  NSAVER  NRESET
0 0 0 0                  $  LOCBEG  LOGRES  LOCWRT  NSTART
F F                      $  FORWRT  STBDA2
F                        $  DISPLA
```

100

APPENDIX B

INPUT FILES FOR SOR BEAM/SHELL MODEL

The following input files are for the integrated SOR Beam/shell model.

```
bsmodel.half                                                                88 large
       9         942            0         32         860            0                      0
       0      0      0       0      0
              0               0      e20.9                      450      33
       2      0    450      0      0      0      0      0      0      0      0      0      0
3.000E-03 1.000E+03 1.000E-05            .000E+00  .000E+00      0      .000E+00
       0      0      0      0      0      2      0      0      1      0         0      0      0      0 ·
       0      0  .000E+00
       0      0      0
       1     37.3560E-04      0      0 .0000E+00      0 .0000E+00 .0000E+00      2      0      0
material type # 3  (elastic-plastic)
2.900E+07  .000E+00  .000E+00  .000E+00  .000E+00  .000E+00  .000E+00  .000E+00
3.000E-01  .000E+00  .000E+00  .000E+00  .000E+00  .000E+00  .000E+00  .000E+00
2.000E+10  .000E+00  .000E+00  .000E+00  .000E+00  .000E+00  .000E+00  .000E+00
5.020E+04  .000E+00  .000E+00  .000E+00  .000E+00  .000E+00  .000E+00  .000E+00
 .000E+00  .000E+00  .000E+00  .000E+00  .000E+00  .000E+00  .000E+00  .000E+00
 .000E+00  .000E+00  .000E+00  .000E+00  .000E+00  .000E+00  .000E+00  .000E+00
section properties
              5
1.880E-01 1.880E-01 1.880E-01 1.880E-01  .000E+00
       2     17.3560E-04      0      0 .0000E+00      0 .0000E+00 .0000E+00      1      0      2
material type # 1  (elastic)
2.900E+07  .000E+00  .000E+00  .000E+00  .000E+00  .000E+00  .000E+00  .000E+00
3.000E-01  .000E+00  .000E+00  .000E+00  .000E+00  .000E+00  .000E+00  .000E+00
 .000E+00  .000E+00  .000E+00  .000E+00  .000E+00  .000E+00  .000E+00  .000E+00
 .000E+00  .000E+00  .000E+00  .000E+00  .000E+00  .000E+00  .000E+00  .000E+00
 .000E+00  .000E+00 · .000E+00  .000E+00  .000E+00  .000E+00  .000E+00  .000E+00
 .000E+00  .000E+00  .000E+00  .000E+00  .000E+00  .000E+00  .000E+00  .000E+00
section properties
              0
1.970E+01 5.402E+03 5.402E+03 1.081E+04 1.970E+01  .000E+00
       3    209.5710E-04      0      0 .0000E+00      0 .0000E+00 '.0000E+00      2      0      C
material type # 20  (rigid body)
2.900E+07  .000E+00  .000E+00  .000E+00  .000E+00  .000E+00  .000E+00  .000E+00
3.000E-01  .000E+00  .000E+00  .000E+00  .000E+00  .000E+00  .000E+00  .000E+00
 .000E+00  .000E+00  .000E+00  .000E+00  .000E+00  .000E+00  .000E+00  .000E+00
 .000E+00  .000E+00  .000E+00  .000E+00  .000E+00  .000E+00  .000E+00  .000E+00
 .000E+00  .000E+00  .000E+00  .000E+00  .000E+00  .000E+00  .000E+00  .000E+00
 .000E+00  .000E+00  .000E+00  .000E+00  .000E+00  .000E+00  .000E+00  .000E+00
section properties
              5
1.880E-01 1.880E-01 1.880E-01 1.880E-01  .000E+00
       4     37.3560E-04      0      0 .0000E+00      0 .0000E+00 .0000E+00      2      0      0
material type # 3  (elastic-plastic)
2.900E+07  .000E+00  .000E+00  .000E+00  .000E+00  .000E+00  .000E+00  .000E+00
3.000E-01  .000E+00  .000E+00  .000E+00  .000E+00  .000E+90  .000E+00  .000E+00
2.000E+05  .000E+00  .000E+00  .000E+00  .000E+00  .000E+00  .000E+00  .000E+00
5.100E+04  .000E+00  .000E+00  .000E+00  .000E+00  .000E+00  .000E+00  .000E+00
 .000E+00  .000E+00  .000E+00  .000E+00  .000E+00  .000E+00  .000E+00  .000E+00
 .000E+00  .000E+00  .000E+00  .000E+00  .000E+00  .000E+00  .000E+00  .000E+00
section properties
              5
2.500E+00 2.500E+00 2.500E+00 2.500E+00  .000E+00
       5     37.3560E-04      0      0 .0000E+00      0 .0000E+00 .0000E+00      2      0      0
material type # 3  (elastic-plastic)
2.900E+07  .000E+00  .000E+00  .000E+00  .000E+00  .000E+00  .000E+00  .000E+00
3.000E-01  .000E+00  .000E+00  .000E+00  .000E+00  .000E+00  .000E+00  .000E+00
2.000E+05  .000E+00  .000E+00  .000E+00  .000E+00  .000E+00  .000E+00  .000E+00
5.100E+04  .000E+00  .000E+00  .000E+00  .000E+00  .000E+00  .000E+00  .000E+00
 .000E+00  .000E+00  .000E+00  .000E+00  .000E+00  .000E+00  .000E+00  .000E+00
```

101

```
 .000E+00  .000E+00   .000E+00   .000E+00   .000E+00   .000E+00   .000E+00   .000E+00
section properties
             5
3.250E+00 3.250E+00 3.250E+00 3.250E+00  .000E+00
    6    37.3560E-04    0    0 .0000E+00    0 .0000E+00 .0000E+00    2    0    0
material type # 3   (elastic-plastic)
2.900E+07  .000E+00   .000E+00   .000E+00   .000E+00   .000E+00   .000E+00   .000E+00
3.000E-01  .000E+00   .000E+00   .000E+00   .000E+00   .000E+00   .000E+00   .000E+00
2.000E+05  .000E+00   .000E+00   .000E+00   .000E+00   .000E+00   .000E+00   .000E+00
5.100E+04  .000E+00   .000E+00   .000E+00   .000E+00   .000E+00   .000E+00   .000E+00
 .000E+00  .000E+00   .000E+00   .000E+00   .000E+00   .000E+00   .000E+00   .000E+00
 .000E+00  .000E+00   .000E+00   .000E+00   .000E+00   .000E+00   .000E+00   .000E+00
section properties
             5
2.000E+00 2.000E+00 2.000E+00 2.000E+00  .000E+00
    7    37.3560E-04    0    0 .0000E+00    0 .0000E+00 .0000E+00    2    0    C
material type # 3   (elastic-plastic)
2.900E+07  .000E+00   .000E+00   .000E+00   .000E+00   .000E+00   .000E+00   .000E+00
3.000E-01  .000E+00   .000E+00   .000E+00   .000E+00   .000E+00   .000E+00   .000E+00
2.000E+05  .000E+00   .000E+00   .000E+00   .000E+00   .000E+00   .000E+00   .000E+00
5.100E+04  .000E+00   .000E+00   .000E+00   .000E+00   .000E+00   .000E+00   .000E+00
 .000E+00  .000E+00   .000E+00   .000E+00   .000E+00   .000E+00   .000E+00   .000E+00
 .000E+00  .000E+00   .000E+00   .000E+00   .000E+00   .000E+00   .000E+00   .000E+00
section properties
             5
2.500E-01 2.500E-01 2.500E-01 2.500E-01  .000E+00
    8    18.2692E-04    0    0 .0000E+00    0 .0000E+00 .0000E+00    1    0    2
material type # 1   (elastic)
2.900E+07  .000E+00   .000E+00   .000E+00   .000E+00   .000E+00   .000E+00   .000E+0C
3.000E-01  .000E+00   .000E+00   .000E+00   .000E+00   .000E+00   .000E+00   .000E+0C
 .000E+00  .000E+00   .000E+00   .000E+00   .000E+00   .000E+00   .000E+00   .000E+0C
 .000E+00  .000E+00   .000E+00   .000E+00   .000E+00   .000E+00   .000E+00   .000E+0C
 .000E+00  .000E+00   .000E+00   .000E+00   .000E+00   .000E+00   .000E+00   .000E+0C
 .000E+00  .000E+00   .000E+00   .000E+00   .000E+00   .000E+00   .000E+00   .000E+0C
section properties
             0
3.970E+02 3.614E+03 3.614E+03 7.227E+03 3.970E+02  .000E+00
    9    11.0470E-03    0    0 .0000E+00    0 .0000E+00 .0000E+00    1    0    2
material type # 1   (elastic)
2.900E+07  .000E+00   .000E+00   .000E+00   .000E+00   .000E+00   .000E+00   .000E+00
3.000E-01  .000E+00   .000E+00   .000E+00   .000E+00   .000E+00   .000E+00   .000E+00
 .000E+00  .000E+00   .000E+00   .000E+00   .000E+00   .000E+00   .000E+00   .000E+00
 .000E+00  .000E+00   .000E+00   .000E+00   .000E+00   .000E+00   .000E+00   .000E+00
 .000E+00  .000E+00   .000E+00   .000E+00   .000E+00   .000E+00   .000E+00   .000E+00
 .000E+00  .000E+00   .000E+00   .000E+00   .000E+00   .000E+00   .000E+00   .000E+00
section properties
             0
8.880E+02 6.275E+04 6.275E+04 1.255E+05 8.880E+02  .000E+00
         1   1.   .0000000000000E+00 -.1265625000000E+03 -.1681300163269E+02    5.
         2   0.   .2630132913589E+01 -.1265625000000E+03 -.1660600662231E+02    0.
         3   0.   .5195503234863E+01 -.1265625000000E+03 -.1599011611938E+02    0.
         4   0.   .7632943153381E+01 -.1265625000000E+03 -.1498049640656E+02    0.
         5   0.   .9882434844971E+01 -.1265625000000E+03 -.1360200595856E+02    0.
         6   0.   .1188858795166E+02 -.1265625000000E+03 -.1188858795166E+02    0.
         7   1.   .0000000000000E+00 -.1209375000000E+03 -.1681300163269E+02    5.
         8   0.   .2630133152008E+01 -.1209375000000E+03 -.1660600852966E+02    0.
         9   0.   .5195504188538E+01 -.1209375000000E+03 -.1599011707306E+02    0.
        10   0.   .7632942199707E+01 -.1209375000000E+03 -.1498049640656E+02    0.
        11   0.   .9882434844971E+01 -.1209375000000E+03 -.1360200691223E+02    0.
        12   0.   .1188858795166E+02 -.1209375000000E+03 -.1188858795166E+02    0.
```

102

```
913   0.    .1259073257446E+02  -.1153125000000E+03  -.9147703170776E+01   0.
914   0.    .1386673641205E+02  -.1153125000000E+03  -.7065455436707E+01   0.
915   0.    .1480129528046E+02  -.1153125000000E+03  -.4809232711792E+01   0.
916   0.    .1537139701843E+02  -.1153125000000E+03  -.2434590816498E+01   0.
917   0.    .1556300067902E+02  -.1153125000000E+03   .0000000000000E+00   0.
918   0.    .1537139511108E+02  -.1153125000000E+03   .2434589624405E+01   0.
919   0.    .1480129432678E+02  -.1153125000000E+03   .4809231758118E+01   0.
920   0.    .1386673641205E+02  -.1153125000000E+03   .7065454959869E+01   0.
921   0.    .1259073352814E+02  -.1153125000000E+03   .9147703170776E+01   0.
922   1.    .0000000000000E+00  -.1209375000000E+03  -.1556300067902E+02   5.
923   0.    .2434589624405E+01  -.1209375000000E+03  -.1537139511108E+02   0.
924   0.    .4809231758118E+01  -.1209375000000E+03  -.1480129432678E+02   0.
925   0.    .7065454959869E+01  -.1209375000000E+03  -.1386673641205E+02   0.
926   0.    .9147703170776E+01  -.1209375000000E+03  -.1259073352814E+02   0.
927   0.    .1100470352173E+02  -.1209375000000E+03  -.1100470352173E+02   0.
928   1.    .0000000000000E+00  -.1209375000000E+03   .1556300067902E+02   5.
929   0.    .2434589624405E+01  -.1209375000000E+03   .1537139511108E+02   0.
930   0.    .4809231758118E+01  -.1209375000000E+03   .1480129432678E+02   0.
931   0.    .7065454959869E+01  -.1209375000000E+03   .1386673641205E+02   0.
932   0.    .9147703170776E+01  -.1209375000000E+03   .1259073352814E+02   0.
933   0.    .1100470352173E+02  -.1209375000000E+03   .1100470352173E+02   0.
934   0.    .1259073257446E+02  -.1209375000000E+03  -.9147703170776E+01   0.
935   0.    .1386673641205E+02  -.1209375000000E+03  -.7065455436707E+01   0.
936   0.    .1480129528046E+02  -.1209375000000E+03  -.4809232711792E+01   0.
937   0.    .1537139701843E+02  -.1209375000000E+03  -.2434590816498E+01   0.
938   0.    .1556300067902E+02  -.1209375000000E+03   .0000000000000E+00   0.
939   0.    .1537139511108E+02  -.1209375000000E+03   .2434589624405E+01   0.
940   0.    .1480129432678E+02  -.1209375000000E+03   .4809231758118E+01   0.
941   0.    .1386673641205E+02  -.1209375000000E+03   .7065454959869E+01   0.
942   0.    .1259073352814E+02  -.1209375000000E+03   .9147703170776E+01   0.
*
*---------------- ELEMENT CARDS FOR BEAM ELEMENTS ------------------*
*
    1    9    553    554    552
    2    2    554    555    552
    3    2    555    556    552
    4    2    556    557    552
    5    2    557    558    552
    6    2    558    559    552
    7    2    559    560    552
    8    2    560    561    552
    9    2    561    562    552
   10    2    562    563    552
   11    8    563    564    552
   12    2    564    565    552
   13    2    565    566    552
   14    2    566    567    552
   15    2    567    568    552
   16    2    568    569    552
   17    2    569    570    552
   18    2    570    571    552
   19    2    571    572    552
   20    2    572    573    552
   21    2    573    574    552
   22    8    574    575    552
   23    2    575    576    552
   24    2    576    577    552
   25    2    577    578    552
   26    2    578    579    552
   27    2    579    580    552
```

103

```
2.500E-01 2.500E-01 2.500E-01 2.500E-01
     839      7      920      921      383      364
2.500E-01 2.500E-01 2.500E-01 2.500E-01
     840      7      921      912      132      383
2.500E-01 2.500E-01 2.500E-01 2.500E-01
     841      7        7      922      923        8
2.500E-01 2.500E-01 2.500E-01 2.500E-01
     842      7        8      923      924        9
2.500E-01 2.500E-01 2.500E-01 2.500E-01
     843      7        9      924      925       10
2.500E-01 2.500E-01 2.500E-01 2.500E-01
     844      7       10      925      926       11
2.500E-01 2.500E-01 2.500E-01 2.500E-01
     845      7       11      926      927       12
2.500E-01 2.500E-01 2.500E-01 2.500E-01
     846      7      928      121      122      929
2.500E-01 2.500E-01 2.500E-01 2.500E-01
     847      7      929      122      123      930
2.500E-01 2.500E-01 2.500E-01 2.500E-01
     848      7      930      123      124      931
2.500E-01 2.500E-01 2.500E-01 2.500E-01
     849      7      931      124      125      932
2.500E-01 2.500E-01 2.500E-01 2.500E-01
     850      7      932      125      126      933
2.500E-01 2.500E-01 2.500E-01 2.500E-01
     851      7      927      934      230       12
2.500E-01 2.500E-01 2.500E-01 2.500E-01
     852      7      934      935      249      230
2.500E-01 2.500E-01 2.500E-01 2.500E-01
     853      7      935      936      268      249
2.500E-01 2.500E-01 2.500E-01 2.500E-01
     854      7      936      937      287      268
2.500E-01 2.500E-01 2.500E-01 2.500E-01
     855      7      937      938      306      287
2.500E-01 2.500E-01 2.500E-01 2.500E-01
     856      7      938      939      325      306
2.500E-01 2.500E-01 2.500E-01 2.500E-01
     857      7      939      940      344      325
2.500E-01 2.500E-01 2.500E-01 2.500E-01
     858      7      940      941      363      344
2.500E-01 2.500E-01 2.500E-01 2.500E-01
     859      7      941      942      382      363
2.500E-01 2.500E-01 2.500E-01 2.500E-01
     860      7      942      933      126      382
2.500E-01 2.500E-01 2.500E-01 2.500E-01
*
*--------------------- LOAD CURVE DEFINITIONS ----------------------*
*
     1      2
 .000E+00   .000E+00
1.000E+00   .000E+00
     2      2
 .000E+00  2.000E-06
1.000E+00  2.000E-06
*
*---------------- PRESSURE BOUNDARY CONDITION CARDS -----------------*
*
     1      1      7      8     2-1.000E+00-1.000E+00-1.000E+00-1.000E+00
     1      7     13     14     8-1.000E+00-1.000E+00-1.000E+00-1.000E+00
     1     13     19     20    14-1.000E+00-1.000E+00-1.000E+00-1.000E+00
```

```
FLUMAS DATA FOR BEAMSHELL MODEL
beam.flu beam.geo strnam.dat beam.daa  $  FLUNAM  GEONAM  GRDNAM  DAANAM
T T F T                                $  PRTGMT  PRTTRN  PRTAMF  CALCAM
T F T F                                $  EIGMAF  TWODIM  HAFMOD  QUAMOD
F F T T                                $  PCHCDS  NASTAM  STOMAS  STOINV
F F F F                                $  FRWTFL  FRWTGE  FRWTGR  FRESUR
F T F F                                $  RENUMB  STOGMT  ROTGEO  ROTQUA
F F F F                                $  PRTCOE  STRMAS  SPHERE  ROTSYM
F F F F                                $  OCTMOD  CAVFLU  FRWTFV  INTCAV
DYNA                                   $  MAINKY
0 942 0 450                            $  NSTRC   NSTRF   NGEN    NGENF
1 0 0                                  $  NBRA    NCYL    NCAV
0 1 1 2 0                              $  NHAS    NHAF    NHAI    NFUN
33                                     $  NSEG
0                                      $  NCIR
9.356E-05   57600.0                    $  RHO     CEE
5                                      $  NVEC
1.  1.                                 $  CQ(I)
0.  -1.   0.   0.                      $  DHALF   CXHF    CYHF    CZHF
3                                      $  NSRADI
  0.0   16.813     1   180  1          $  RAD1    RAD2    JBEG    JEND    JINC
16.813  0.0      181   360  1
  0.0    0.0      431   520  1
0                                      $  NSORDER
553 585  16.813  16.813  2             $  N1      N2      R1      R2      NSET
553 553   0.0    16.813  1
553 585  16.813  16.813  32
```

```
AUGMAT DATA FOR BEAMSHELL.MODEL
strnam.dat beam.flu beam.geo beam.pre   $   STRNAM  FLUNAM  GEONAM  PRENAM
F F F F                                 $  FRWTGE  FRWTST  FRWTFL  PLNWAV
F F F T                                 $  FLUSKY  DAAFRM  SYMCON  DOFTAB
F F F T                                 $  PRTGMT  PRTTRN  PRTSTF  PRTAUG
F F F F                                 $  MODTRN  STRLCL  INTWAT  CFADYN
F                                       $  LUMPFM
DYNA                                    $  MAINKY
0.50                                    $  DAA2
942 2826 3 3                            $  NSTR    NSFR    NFRE    NFTR
1                                       $  NSETLC
0 1 450 1                               $  NDICOS  JSTART  JSTOP   JINC
3                                       $  NUMCON
0  1  86  5                             $  ICON    NSTART  NSTOP   NINC
0  91 176  5
0 400 472  6
```

```
r=d3dump
TIME INTEGRATION DATA FOR MODEL BEAMSHELL
beam.pre beam.pos      $  PRENAM  POSNAM
beam.rst               $  RESNAM
F F F                  $  BUBPUL  REFSEC  FLUMEN
T F F F                $  EXPWAV  SPLINE  VARLIN  PACKET
F T F F                $  HYPERB  EXPLOS  DOUBDC  VELIMP
1                      $  NCHARG
0.0                    $  HYDPRE
0.0 -25.3125 326.4     $  XC   YC   ZC
0.0 -25.3125  16.813   $  SX   SY   S2
101                    $  JPHIST
1.0                    $  PNORM
14.0E-06               $  DTHIST
1                      $  CHGTYP
60.0  25.8  10.0       $  WEIGHT  SLANT   CHGDEP
1 0                    $  NTINT   NCHGAL
0.0  2.0000E-06        $  STRTIM  DELTIM
5000  5000             $  NSAVER  NRESET
0 0 0 0                $  LOCBEG  LOGRES  LOCWRT  NSTART
F F                    $  FORWRT  STBDA2
F                      $  DISPLA
```

INITIAL DISTRIBUTION LIST

No. of Copies

1. Defense Technical Information Center 2
    8725 John J. Kingman Rd., STE 0944
    Ft. Belvoir, Va 22060-6218

2. Dudley Knox Library 2
    Naval Postgraduate School
    411 Dyer rd.
    Monterey, CA 93943-5101

3. Professor Young W. Kwon, Code ME/Kw 1
    Department of Mechanical Engineering
    Naval Postgraduate School
    Monterey, CA 93943-5002

4. Mr. Byron Rose 1
    Naval Surface Warfare Center
    Submarine Protection & Weapons Effects Department
    Code 67
    Carderock Division
    Bethesda, MD 20084

5. Mr. Erik A. Rasmussen 1
    Naval Surface Warfare Center
    Submarine Protection & Weapons Effects Department
    Carderock Division
    Bethesda, MD 20084

6. Mr. Charles D. Milligan 1
    Naval Surface Warfare Center
    Submarine Protection & Weapons Effects Department
    Carderock Division
    Bethesda, MD 20084